STUDIES ON INFILTRATION OF POROUS FORMATIONS BY DRILLING FLUIDS IN RELATION TO THE QUANTITATIVE ANALYSIS OF ELECTROLOGS IN DRILL HOLES

Thesis by

Leendert de Witte

In partial fulfillment of the requirements
for the degree of
Doctor of Philosophy

California Institute of Technology
Pasadena, California
1950

ACKNOWLEDGMENTS

The author wishes to make acknowledgments to:

Dr. G. W. Potapenko under whose supervision the research was carried out.

Dr. W. R. Smythe and Dr. W. Magnus with whom some theoretical aspects of the problems were discussed.

Dr. F. W. Maxstadt and Mr. R. C. Serviss for valuable advice on construction of the measuring circuits.

Mr. R. von Huene and Mr. W. J. P. Otto for aid in the preparation of the samples.

Mr. E. Offeman of the Baroid Sales Division in Los Angeles, for furnishing several pieces of Baroid equipment used in the experimental investigations.

ABSTRACT

This thesis presents a discussion of a method, by which certain characteristics of the infiltrated zones around bore holes can be made to good use in determining the fluid content and the formation factor, of the horizons in which we are interested.

To obtain the necessary field data a new combination of electrode spacings is proposed, namely a short latteral spacing, with two normal spacings. It is shown that apparent resistivities, obtained with these spacings, enable us to obtain the true resistivity, the resistivity of the invaded zone and the diameter of the latter.

To be able to use the invaded zone resistivity in the determination of the formation factor and fluid contents a group of laboratory experiments were carried out, using consolidated sandstone samples and drilling muds or liquids having the properties of the mud filtrate. The sandstones were invaded by the muds or their equivalent filtrates for different conditions of initial fuild contents. Then the resistivity changes were measured by a four electrode arrangement coupled to an amplifier-rectifier circuit and a sensitive test meter.

For the case of oil and gas sands the displacement of the non-wetting phase by water is treated analytically using the concept of relative permeabilities of the reservoir rocks and the results are compared with the experimental data.

From measurements on coresamples the actual resistivity profiles in the infiltrated zones of formations were computed. These showed that in all cases the resistivity of the invaded zone may be approximated by a constant.

The relations between resistivities of rocks and their fluid contents are considered in the light of experimental results and several new formulae are introduced, governing these relations.

Finally the water saturations of the invaded zones of oil and gas horizons are correlated with the water saturations of the undisturbed formations.

A brief outline is given of the computation of fluid contents and formation factors of porous rocks from the measured values of infiltrated zone- and true resistivities, using the new resistivity formulae and data obtained from analysis of the self potential curve of electrologs.

TABLE OF CONTENTS

INTRODUCTION

Quantitative analysis of electric well logs, or electrologs, has as its main purpose the determination of the relative saturation of the fluids, contained in the formations traversed. The fluids in which we are mainly interested are oil and gas.

To be able to interpret the resistivity measurements given on electrologs into terms of fluid content of the formations, we must know the basic relations between the content and character of interstitial fluids and the resistivity of the rock. Important factors in these relations are the effect of the solid framework of the rock on the electrolytic conduction of current by its interstitial water and the amount of "conductive solids" present in the rock. This means that essentially there are four unknown parameters governing the formation resistivities, namely: The saturation of oil or gas, the conductivity of the interstitial water, the "cell constant" due to the inert framework, and the amount of conductive solids present.

In order to attempt to solve for these quantities, we must first of all determine the true resistivity of the formations in question. Additional information can be obtained from determination of the true resistivity of the zones of porous formations immediately surrounding the drill holes which have been invaded by the filtrate of the drilling fluids, displacing part or all of the initially present interstitial fluids. Finally, important information can be gained from analysis of the self potential measurements which are made simultaneously with the resistivity measurements in electrologging practice.

This thesis outlines a method of computing the true resistivities of the undisturbed formations and the invaded zones from the apparent resistivities measured on the electrolog.

Furthermore, experimental studies were made on the basic relations between the resistivities, the fluid content, and the rock characteristics of the formations.

Finally, the displacement of the interstitial fluids by the mud filtrate upon invasion and the resulting relations between resistivities of the infiltrated zones and those of the undisturbed formations are studied both theoretically and experimentally.

No attempt is made to outline all of the work done and literature published on the subject of electrolog interpretation. Previous work by other investigators is only quoted where it has a direct bearing on the experiments and analyses reported in this thesis.

Because of the many factors involved in the interpretation of resistivity measurements in drill holes, the research was limited in most cases to the bare essentials and therefore this work should be regarded strictly as a reconnaissance type investigation of the problems involved in quantitative analyses of electrologs.

PART I

Derivation of Relations Between Actual Resistivities and Apparent Resistivities*

Nomenclature

R_a = apparent resistivity

R_m = mud resistivity

R_i = resistivity of infiltrated zone

R_t = true resistivity of formation

R_w = resistivity of interstitial water

ρ_w = resistivity of infiltrating liquid

r_o = radius of drill hole

d_o = diameter of drill hole

r_i = radius of infiltrated zone

d_i = diameter of infiltrated zone

AM = spacing of electrodes in normal arrangement (See Fig. I-1)

AO = spacing of electrodes in lateral arrangement (See Fig. I-1)

S_w = water saturation as a fraction of porespace

S_o = oil saturation as a fraction of porespace

S_g = gas saturation as a fraction of porespace

I = modified bessel function of first kind, of order zero ($I \equiv I_o$)

K = modified bessel function of second kind, of order zero ($K \equiv K_o$)

I_n = modified bessel function of first kind, of order n

K_n = modified bessel function of second kind, of order n

---

* A historical review of the development of these relations is given on Pages 5 and 6.

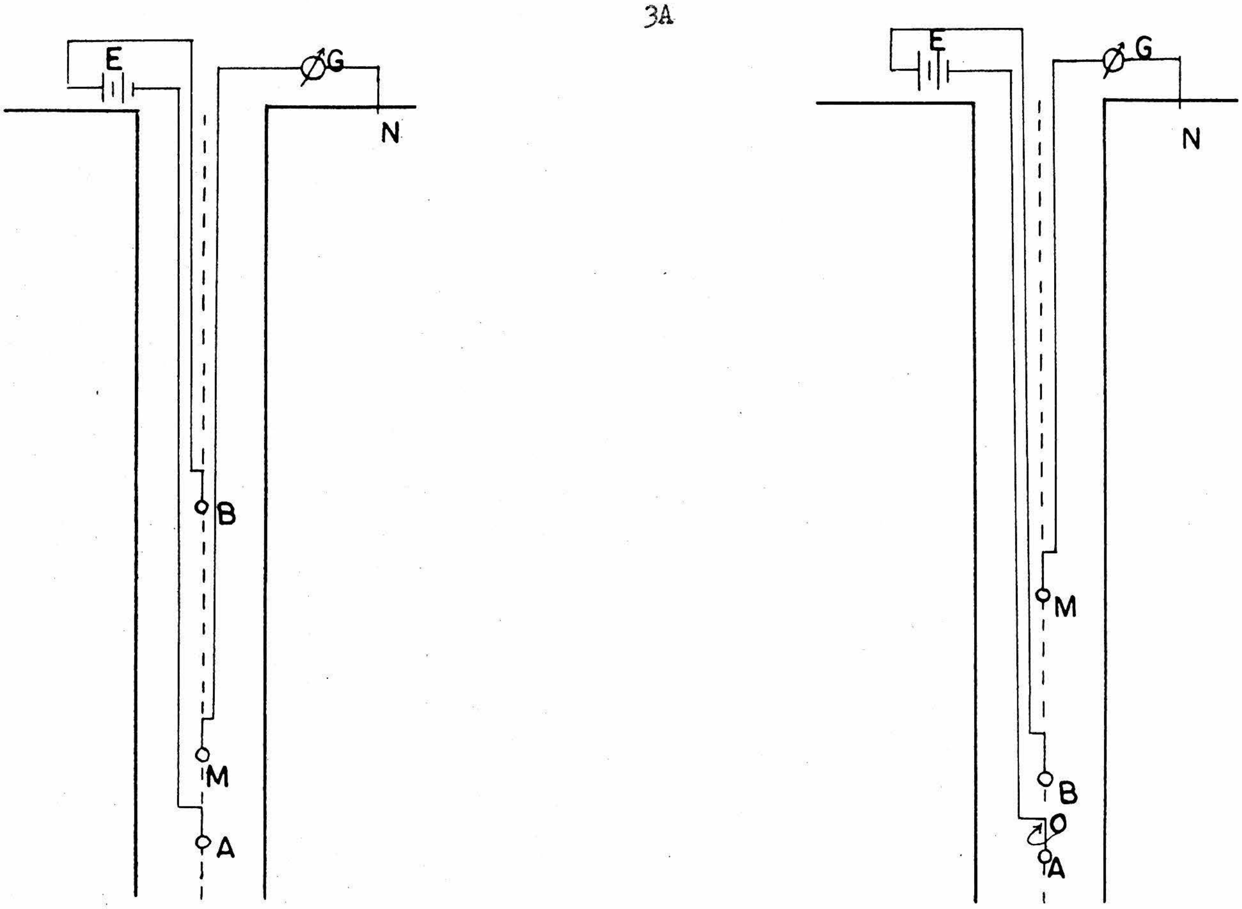

NORMAL-ELECTRODE ARRANGEMENT-LATERAL

Fig. I-1

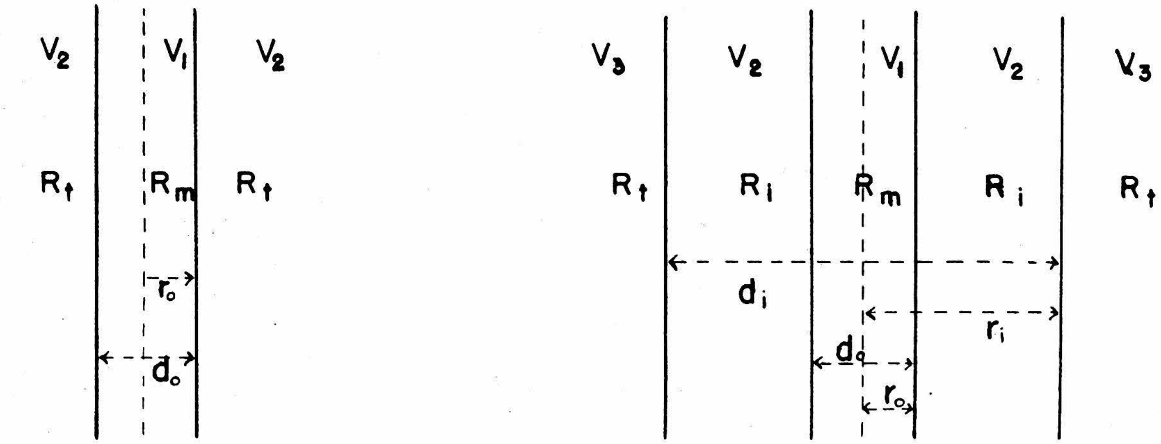

NO INVASION

INVASION

Fig. I-2

r = distance from origin

s = $\frac{AM}{r_0}$ for normal arrangement of electrodes

s_1 = $\frac{AM}{r_0}$ for lateral arrangement of electrodes

s_2 = $\frac{BM}{r_0}$ for lateral arrangement of electrodes

Physical Description of the Problem

When measuring resistivity in a drill hole (see Fig. I-1) the current is sent between two current electrodes and the potential difference is measured between two potential electrodes. For the normal arrangement one current electrode and one potential electrode are at the surface, which for theoretical purposes is considered to be at infinity. For the lateral arrangement, two current electrodes and one potential electrode are in the hole and the second potential electrode is at infinity (zero potential) or two potential electrodes and one current electrode are in the hole and the other current electrode at the surface.

To calculate the potential distribution due to the current between the current electrodes, all electrodes in the hole are assumed to be dimensionless (point electrodes) and located on the central axis of the drill hole.

Further assumptions are that the wall of the hole is cylindrical, and that invasion if present is equal in all radial directions.

This means that in the case of no invasion we have two media of constant resistivity and with cylindrical boundaries. In the case of invasion we have three media with two cylindrical boundaries and it is normally assumed that the resistivity of the invaded zone is also a constant. We will later inspect the limitations of this latter assumption and see that the behavior of the resistivity in the infiltrated zone is of primary importance to our interpretation.

Fig. I-2 represents schematically the conditions for which we want to calculate the potential distribution caused by axial point electrodes.

If we calculate the potential distribution due to one electrode, we can find the distribution for any number of axial current electrodes by mere superposition, so we will limit our derivations to the case of one electrode on the axis.

Historical Review of the Development of the Theory of Resistivity Logging

The theory of resistivity logging as outlined above was largely developed in Russia.

In 1933, only shortly after electrologging became generally accepted as commercially useful, V. A. Fock (3) worked out the basic theory of the relations between apparent and true resistivities. However, his treatment was limited to the case of no invasion.

Some years later the research department of the Schlumberger Corporation, in Paris, extended the theory to include the effects of invasion and started the computation of master curves (7). The results of this work were not published until 1947. In 1938 the complete theory with many examples of computation procedures was published in a book by L. M. Alpin (4), written in the Russian language.*

Another book, by V. N. Dakhnov (5), also in Russian, was published

---

* The dielectric analogy of the case of no invasion is treated by Smythe in his book on static and dynamic electricity. (1)

in 1941. Dakhnov's work is based mostly on the theory as outlined by Alpin, and describes several methods of the use of these theories in the interpretation of electrologs.

Some of the more important conclusions of Dakhnov's work were reviewed by Hubert Guyod in a series of articles in the Oil Weekly of 1947 and 1948.

The most complete set of data on the apparent resistivity relationships was published in 1947 by the Schlumberger Corporation (7) in the form of a booklet containing assemblies of resistivity departure curves for use in quantitative interpretation of electrologs.

In this thesis no attempt is made to outline the previous work done on the theory of electrologging. Only the parts that are necessary to understand the proposed method of obtaining additional data from electrologging are described.

Derivation of the Potential Distribution in the Case of No Invasion

The primary condition on which all following derivations are based is that at no point of the system under consideration there can be accumulation of charge. This means that for any volume element the total current coming in must equal the total outgoing current.

If we consider such volume element, enveloped by a surface A (see Fig. I-3) we can express the above condition analytically by:

$$\iint_A y \cdot n dA = 0$$

where $y \cdot n$ is the component of the current density y normal to the surface.

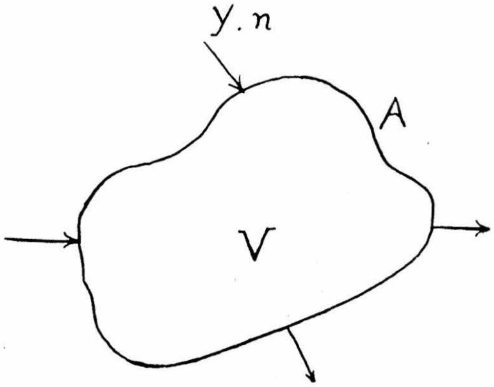

Fig. I-3

By Green's theorem:

$$\iint_A y \cdot n dA = \iiint_V \nabla \cdot y dv = 0 \qquad (1\text{-}1)$$

This holds for any volume so that $\nabla \cdot y$ must be zero.

By Ohm's law:

$$y = \sigma E = \frac{1}{R} E \qquad (1\text{-}2)$$

where σ is the conductivity, R is the resistivity and E is the field strength. The field strength, E, can be expressed as:

$$E = - \nabla V$$

where V is the potential. Substituting into (1-2) gives:

$$\nabla \cdot y = \nabla \cdot (\frac{1}{R} E) = - \nabla \cdot (\frac{1}{R} \nabla V) \qquad (1\text{-}3)$$

When R is a constant we can write:

$$\nabla \cdot y = - \frac{1}{R} \nabla^2 V = 0 \qquad \text{or} \qquad \nabla^2 V = 0 \qquad (1\text{-}4)$$

which is Laplace's equation.

We know that for no invasion R is a constant in both media and in the case of invasion that R_1 is also a constant, so that we may use Laplace's equation for the potential distribution in both cases.

As all the boundaries in our system have cylindrical symmetry, we want to use cylindrical coordinates. Equation (1-4) then becomes:

$$\frac{1}{r} \frac{\partial}{\partial r} (R \frac{\partial V}{\partial r}) + \frac{1}{r^2} \frac{\partial^2 V}{\partial \varphi^2} + \frac{\partial^2 V}{\partial z^2} = 0$$

$$\frac{\partial^2 V}{\partial r^2} + \frac{1}{r} \frac{\partial V}{\partial r} + \frac{1}{r^2} \frac{\partial^2 V}{\partial \varphi^2} + \frac{\partial^2 V}{\partial z^2} = 0$$

Let $V = R(r) \; \Phi(\varphi) \; Z(z)$

Then we have:

$$\Phi Z \left(\frac{d^2R}{dr^2} + \frac{1}{r}\frac{dR}{dr}\right) + \frac{RZ}{r^2}\frac{d^2\Phi}{d\varphi^2} + R\Phi\frac{d^2Z}{dz^2} = 0$$

Dividing by V and multiplying by r^2:

$$\frac{r^2}{R}\left(\frac{d^2R}{dr^2} + \frac{1}{r}\frac{dR}{dr}\right) + \frac{1}{\Phi}\frac{d^2\Phi}{d\varphi^2} + \frac{r^2}{Z}\frac{d^2Z}{dz^2} = 0 \qquad (1\text{-}5)$$

Here $\frac{1}{\Phi}\frac{d^2\Phi}{d\varphi^2} = 0$, as V is independent of φ, and hence:

$$-\frac{1}{Z}\frac{d^2Z}{dz^2} = \frac{1}{R}\left(\frac{d^2R}{dr^2} + \frac{1}{r}\frac{dR}{dr}\right)$$

This holds for all values of z and r so that obviously both sides must be equal to the same constant.

Let $\frac{1}{Z}\frac{d^2Z}{dz^2} = -k^2$

This gives $\frac{d^2Z}{dz^2} \ k^2Z = 0$, so that $Z = A \sin kz + B \cos kz$.

Equation (1-5) now becomes:

$$\frac{r^2}{R}\left(\frac{d^2R}{dr^2} - \frac{1}{r}\frac{dR}{dr}\right) - k^2r^2 = 0.$$

or $$r^2\frac{d^2R}{dr} + r\frac{dR}{dr} - (k^2r^2 + 0^2)R = 0$$

Let $kr = v$ then:

$$v^2\frac{d^2R}{dv} + v\frac{dR}{dv} - (v^2 - 0^2)\,R = 0 \qquad (1\text{-}6)$$

This is the modified Bessel equation of zero order.

Its solutions are the modified Bessel functions of zero order:

$$R(v) = C\,I_0(v) + D\,K_0(v)$$

The general solution of (1-5) then becomes:

$$V = (A \sin kz + B \cos kz) \left[CI_o (kr) + DK_o (kr) \right] \qquad (1\text{-}7)$$

Before solving the constants by applying the boundary conditions of our system we will list some properties of the modified Bessel functions:

$$I_n (v) = j^{-n} J_n (jv) = \sum_{p=o}^{\infty} \frac{(\frac{1}{2}v)}{p! \; (n-p)!} \qquad (a)$$

$$K_n (v) = -I_n(v) \int \frac{dv}{v \;\; I_n(v)^{\;2}} \qquad (b)$$

From these expressions a series of recurrence formulae have been derived, relating functions of different order and derivatives of the modified Bessel functions. (1)

We will make use of the following:

$$K_o'(v) = -K_1(v) \qquad (c)$$

$$I_o'(v) = I_1(v) \qquad (d)$$

$$I_n' K_n - K_n' I_n = \frac{1}{v} \qquad (e)$$

Also of importance are the extreme values:

$I_o(o) = 1$ $\qquad$ $I_o(\infty) = \infty$

$K_o(o) = \infty$ $\qquad$ $K_o(\infty) = 0$

Finally we will use an expression for the inverse distance from the origin in terms of modified Bessel functions, namely:

$$\frac{1}{r} = \frac{2}{\pi} \int_o^{\infty} \cos kz \, K_o(kr) \, dk$$

For the derivation of this expression see appendix (A).

With the aid of the outlined properties of the modified Bessel functions we will now proceed to determine the constants of our general solution for the potential distribution. We will call the potential in the drill hole V_1 and in the surrounding formation V_2.

Furthermore we can write $V_1 = V_0 - V'$, where V_0 is due directly to the point source and V' represents the effect of the boundary. As V_1 and V_0 satisfy Laplace's equation, V' necessarily does so too.

We know that V is of the form $A/\bar{r}$ (from the analogy of the potential around a point charge in the dielectric case).

The r-component of the field strength is given by:

$$E_r = -\frac{\partial V}{\partial r} \qquad \text{so that} \qquad \gamma_r = -\frac{1}{R}\frac{\partial V}{\partial r} =$$

= current density in r direction.

Assuming a small sphere around the electrode with radius ϵ and surface S, we have for the total current:

$$\mathcal{I} = -\iint_S \frac{1}{R}\frac{\partial V}{\partial r}\,dS = -\frac{1}{R}\left(-\frac{A}{\epsilon^2}\right)4\pi\epsilon^2 = \frac{4\pi A}{R} \quad \left(\text{as } \frac{\partial V}{\partial r} = \frac{-A}{\bar{r}^2}\right)$$

Therefore $A = \frac{R\mathcal{I}}{4\pi}$ and $V_0 = \frac{R\mathcal{I}}{4\pi\bar{r}}$ (1-8)

With $R = R_m$ and substituting the expression for $1/\bar{r}$ this becomes:

$$V_0 = \frac{\mathcal{I}R_m}{4\pi\bar{r}} = \frac{\mathcal{I}R_m}{4\pi} \times \frac{2}{\pi}\int_0^\infty K_0(kr)\cos(kz)\,dk$$

V', satisfying Laplace's equation must be of the form:

$$(A\,K_0 + B\,I_0)\quad(C\cos kz + D\sin kz)$$

As the potential on the axis is finite and $K_0(0) = \infty$, A must be zero. This makes $V' = B\,I_0\,(C\cos kz + D\sin kz)$, or in its most general form:

$$V' = \frac{\mathcal{I}R_m}{2\pi^2}\int_0^\infty \psi(k)\,I_0(kr)\,(\cos kz + D'\sin kz)\,dk$$

The constant $\frac{J R_m}{2\pi^2}$ can be included in $\psi(k)$, but is placed before the integral sign in order to obtain the same type of formula as for V_o. For V_2 we must consider that the potential at infinity must be zero so that the I_o term cancels out and V_2 becomes:

$$V_2 = \frac{J R_m}{2\pi^2} \int_0^\infty \varphi(k)\, K_o(kr) \quad (\cos kz - E \sin kz)\, dk$$

For both V_1 and V_2 the additional condition: $V(r,z) = V(r,-z)$ exists. This means that the coefficients of the sine terms must be zero.

The final expressions for V_1 and V_2 therefore are:

$$V_1 = \frac{J R_m}{2\pi^2} \int_0^\infty \left[K_o(kr) + \psi(k)\, I_o(kr) \right] \cos kz\, dk$$

and $$V_2 = \frac{J R_m}{2\pi^2} \int_0^\infty \varphi(k)\, K_o(kr) \cos kz\, dk.$$

We are primarily interested in the potential distribution in the bore hole and therefore we want to find the value of $\psi(k)$. To do this we must make use of the boundary conditions.

First Boundary Condition:

At the bore face, the potential must be continuous, or $(V_1)_{r=r_o} = (V_2)_{r=r_o}$. Using the properties of the Fourrier-Bessel integrals we can show that in this case we may equate the integrands directly. This gives:

$$K_o(kr_o) + \psi(k)\, I_o(kr_o) = \varphi(k)\, K_o(kr_o) \tag{1-9}$$

Second Boundary Condition:

The r-component of the current density must be continuous. Since $j_r = \frac{1}{R}\frac{\partial V}{\partial r}$ we have:

$$\frac{1}{R_m}\left(\frac{\partial V_1}{\partial r}\right)_{r=r_0} = \frac{1}{R_t}\left(\frac{\partial V_2}{\partial r}\right)_{r=r_0}$$

or with $\frac{R_m}{R_t} = T$:

$$\left(\frac{\partial V_1}{\partial r}\right)_{r=r_0} = T\left(\frac{\partial V_2}{\partial r}\right)_{r=r_0} \qquad (1\text{-}10)$$

Differentiating the expressions for V_1 and V_2 under the integral sign, substituting into (1-10) and equating the integrands gives:

$$K'(kr_0) + \psi(k)\, I'(kr_0) = T\,\varphi(k)\, K'(kr_0) \qquad (1\text{-}11)$$

From (1-9) we have

$$\psi(k) = \frac{\varphi(k)\, K(kr_0) - K(kr_0)}{I(kr_0)}$$

Substituting into (1-11):

$$K'(kr_0) + \frac{I'(kr_0)K(kr_0)\,(\varphi(k)-1)}{I(kr_0)} = T\varphi(k)\, K'(kr_0) \qquad (1\text{-}11a)$$

We now use property (e):

$$I'K - K'I = \frac{1}{kr_0}$$

Rearranging (1-11a) and substituting gives:

$$T\varphi(k)\, K'(kr_0)\, I(kr_0) = \varphi(k)\left[\frac{1}{kr_0} + K'(kr_0)I(kr_0)\right] - \frac{1}{kr_0}$$

or

$$\varphi(k) = \frac{1}{1 - kr_0\,(T-1)\, I(kr_0)\, K'(kr_0)} \qquad (1\text{-}12)$$

Substituting (1-12) in (1-9):

$$\psi(k) = \frac{kr_0\,(T-1)\, K(kr_0)\, K'(kr_0)}{1 - kr_0\,(T-1)\, I(kr_0)\, K'(kr_0)}$$

This gives for points on the axis ($I_0(0) = 1$)

$$V_1 = \frac{J R_m}{4\pi r} + \frac{J R_m}{2\pi^2} \int_0^\infty \frac{kr_o(T-1)K(kr_o)K'(kr_o)}{1-kr_o\,(T-1)I(kr_o)K'(kr_o)} \cos kz\, dk$$

A similar formula was worked out in Smythe's book (2) for the dielectric case.

Let $kr_o = x$ and let us make the following abbreviations:

$$x\,K(x)\,K_1(x) = -x\,K(x)\,K'(x) \equiv M$$

$$x\,I(x)\,I_1(x) = x\,I(x)\,I'(x) \equiv N$$

$$x\,I(x)\,K_1(x) = -x\,I(x)\,K'(x) \equiv P$$

$$x\,K(x)\,I_1(x) = x\,K(x)\,I'(x) \equiv Q$$

Obviously $MN = PQ$ and property (e) can now be written as

$$P = 1 - Q \qquad \text{or} \qquad P + Q = 1$$

Substituting the above definitions:

$$V_1 = \frac{J R_m}{2\pi r} + \frac{J R_m}{2\pi^2} \int_0^\infty \left[\frac{-(T-1)\,M \cos\left(\frac{z}{r_o}x\right)}{1 + (T-1)\,(1-Q)} \right] \frac{1}{r_o}\, d\,x$$

The integrand can be reworked to:

$$\frac{1}{r_o}\;\frac{M \cos \frac{z}{r_o}\, d\,x}{-\left(\frac{1}{T-1}\right) + 1-Q} = \frac{1}{r_o}\;\frac{M}{\left(\frac{1}{T-1} - 1\right) + Q}\;\cos\left(\frac{z}{r_o}x\right) d\,x$$

Here $T = \frac{R_m}{R_t}$ so that $\frac{1}{1-T} - 1 = \frac{1}{1-\frac{R_m}{R_t}} - 1 = \frac{R_m}{R_t - R_m} = \frac{1}{\frac{R_t}{R_m} - 1}$

Let $\frac{R_t}{R_m} - 1 = e$ then $\frac{1}{1-T} - 1 = \frac{1}{e}$

The final expression for V_1, substituting the above results, becomes:

$$V_1 = \frac{J R_m}{4\pi r} + \frac{J R_m}{2\pi^2 r_o} \int_0^\infty \frac{M}{\frac{1}{e} + Q} \cos\left(\frac{z}{r_o}x\right) d\,x \qquad (1\text{-}13)$$

For the normal electrode arrangement, electrode N is at zero potential, so that the measured ΔV equals the potential at M. Electrode B is far enough away so that its influence may be neglected, and therefore we have to consider only the potential at M due to a single point electrode.

This means $\Delta V_{MN} = V_1$, where ΔV_{MN} is the potential difference measured by the galvanometer in the resistivity logging circuit, between M and the surface electrode N.

However, the resistivity logs are calibrated to read directly in terms of so-called apparent resistivity, R_a. The apparent resistivity is defined as the resistivity of a homogeneous, infinite medium surrounding the electrodes, that would give the same potential at M, due to the current   between A and B, for the given electrode spacing, as the potential measured by the galvanometer.

We may write therefore $V_1 = \frac{J R_a}{4 \pi \bar{r}}$ with $\bar{r} = \overline{AM}$. This is of the same form as equation (1-8), which was derived for V_o.

The equation for R_a becomes:

$$R_a = \frac{V_1}{J} 4 \pi (\overline{AM})$$

As M is a point on the axis, we also have $z = \overline{AM}$. Let $\frac{z}{r_o} = \frac{\overline{AM}}{r_o} = s$. Then we have from (1-13) and 1-14):

$$R_a = R_m + \frac{2}{\pi} R_m s \int_0^\infty \frac{M}{\frac{1}{e} + Q} \cos (sx) \, dx$$

$$\text{or} \quad \frac{R_a}{R_m} = 1 + \frac{2}{\pi} s \int_0^\infty \frac{M}{\frac{1}{e} + Q} \cos (sx) \, dx \qquad (1\text{-}15)$$

For the lateral arrangement (see Fig. I-1) we have either two current electrodes and one pick-up electrode in the hole or two pick-up electrodes and one current electrode. (The second current electrode may either be at a sufficiently large distance in the hole or at the surface so that its influence can be neglected.)

It can be shown that the resulting voltage differences for similar spacings between the electrodes are the same in both cases.*

We will limit our discussion therefore to the case of two relatively closely spaced current electrodes and one pick-up electrode in the hole and the other pick-up electrode at infinity.

The voltage difference between M and N (N has zero potential) may be expressed in this case as:

$$\Delta V = \frac{J R_a}{4\pi}\left(\frac{1}{AM} - \frac{1}{BM}\right) = (V_1)_A - (V_1)_B$$

Where $(V_1)_A$ and $(V_1)_B$ are respectively the potentials at M due to the point sources A and B.

$$R_a = \frac{(V_1)_A - (V_1)_B}{J} \; \frac{4\pi}{\frac{1}{AM} - \frac{1}{BM}}$$

Let $AM = z_1$, $\overline{BM} = z_2$, $s_1 = \frac{z_1}{r_o}$, $s_2 = \frac{z_2}{r_o}$

$$\overline{OM} = \frac{1}{2}(\overline{AM} - \overline{BM}) = z \qquad \text{while} \quad b = \overline{BM} - \overline{AM}$$

$$(V_1)_i = \frac{J R_m}{4\pi \overline{r}} + \frac{J R_m}{2\pi^2 r_o} \int_0^\infty \frac{M}{\frac{1}{e} + Q} \cos\left(\frac{z_i}{r_o} x\right) dx \qquad \text{with} \quad i = 1,2$$

$$R_a = \left(\frac{J R_m}{4\pi z_1} - \frac{J R_m}{4\pi z_2}\right) \frac{4\pi}{J\left(\frac{1}{z_1} - \frac{1}{z_2}\right)} + \frac{4\pi}{\left(\frac{1}{z_1} - \frac{1}{z_2}\right)} \cdot \frac{J R_m}{2\pi^2 r_o} \int_0^\infty \left[\frac{M}{\frac{1}{e} + Q} (\cos s_1 x - \cos s_2 x)\, dx\right]$$

$$= R_m + \frac{2R_m}{\pi r_o} \cdot \frac{1}{\left(\frac{1}{z_1} - \frac{1}{z_2}\right)} \int_0^\infty \frac{M}{\frac{1}{e} + Q} (\cos s_1 x - \cos s_2 x)\, dx \qquad (1\text{-}16)$$

$$= R_m + \frac{z^2}{b}\left(1 - \frac{b^2}{4z^2}\right) \frac{2R_m}{\pi r_o} \int_0^\infty \frac{M}{\frac{1}{e} + Q} (\cos s_1 x - \cos s_2 x)\, dx \qquad (1\text{-}16a)$$

---

* This statement is known as the reciprocity theorem.

A commonly used approximated formula for the lateral arrangement is derived as follows:*

Given one point electrode as current source, we will designate the potentials at the pick-up electrodes M and N respectively as V_M and V_N. The potential difference measured by the lateral arrangement then is

$$V_\ell = V_M - V_N = \frac{J(R_a)_\ell}{4\pi}\left(\frac{1}{AM} - \frac{1}{AN}\right)$$

where $(R_a)_\ell$ is the apparent resistivity corresponding to the characteristic volume of the lateral spacing in question.

We now assume that M and N are far from the point source A and the distance between them is small compared to $\overline{AO}$ so that in the region between them the potential decreases approximately linearly with the distance and therefore the fieldstrength in the s-direction (E_s) is a constant.

We then have $V_M - V_N = \Delta s \cdot E_s$ where $\overline{MN} = \Delta s$, $V_M > V_N$ and the positive s direction is the direction from M to N.

We make a second approximation by writing:

$$\frac{1}{\overline{AM}} - \frac{1}{\overline{AN}} = \frac{\overline{AN} - \overline{AM}}{\overline{AM} \cdot \overline{AN}} \approx \frac{\overline{MN}}{(\overline{OA})^2} = \frac{\Delta s}{s^2}$$

where $\overline{OA} = \frac{1}{2}(\overline{AN} + \overline{AM}) = s$

This holds true only for $\overline{AM}/\overline{AN} \approx 1$ (or $\overline{OA} \gg \overline{MN}$) and is in general a good approximation for large latteral spacings, e.g. for the conventional 10', 16' or 18' spacings.

---

* As the physical picture is somewhat easier understood for the case of two pick-up electrodes and one current electrode in the hole, we will make the derivation for this arrangement. The results apply equally well, however, to the alternative arrangement.

Combining the above expressions we have:

$$(R_a)_\ell = \frac{4\pi}{J} \cdot E_s \cdot s^2 \qquad \text{with } E_s = -\frac{\partial V}{\partial s} \approx \text{constant.}$$

As $V = \frac{J R_m}{4\pi s} + \frac{J R_m}{2\pi^2 r_0} \int_0^\infty \psi(x) \cos\left(\frac{s}{r_0} x\right) dx$

$$E_s = -\left\{ -\frac{J R_m}{4\pi s^2} - \frac{J R_m}{2\pi^2 r_0} \int_0^\infty \frac{x}{r_0} \psi(x) \sin\left(\frac{s}{r_0} x\right) dx \right\}$$

$$= \frac{J R_m}{4\pi s^2} + \frac{J R_m}{2\pi^2 r_0^2} \int_0^\infty x\psi(x) \sin\left(\frac{s}{r_0} x\right) dx$$

Substitution of this expression gives for $(R_a)_\ell$:

$$(R_a)_\ell = R_m + \frac{2}{\pi} R_m \frac{s^2}{r_0^2} \int_0^\infty x\,\psi(x) \sin\left(\frac{s}{r_0} x\right) dx$$

or replacing $\frac{s}{r_0}$ by s:

$$W = \frac{(R_a)_\ell}{R_m} \quad 1 + \frac{2}{\pi} s^2 \int_0^\infty x\psi(x) \sin(sx)\, dx$$

If we call the apparent resistivity for a normal arrangement with $\frac{\overline{AM}}{r_0}$ equal to the $\frac{\overline{OA}}{r_0}$ of our lateral arrangement (=s), $(R_a)_n$ and write $X = \frac{(R_a)_n}{R_m}$ then we have from equation (1-15):

$$X = \frac{(R_a)_n}{R_m} = 1 + \frac{2}{\pi} s \int_0^\infty \psi(x) \cos sx\, dx$$

and $\frac{dX}{ds} = -2/\pi \; s \int_0^\infty x\;\psi(x) \sin sx\, dx + 2/\pi \int_0^\infty \psi(x) \cos s\, x\, dx$

and therefore $W = X - s\frac{dX}{ds}$

This permits us to plot the departure curves for the lateral arrangement if we have calculated them for the normal arrangement. For small lateral spacings however it is better to use formula (1-16).

Potential Distribution if Invasion has Occurred

In this case it is assumed that there is an infiltrated zone of radius r_1 and of a constant resistivity R_1. We will see later exactly what happens to the resistivity in the invaded zone and in how far the latter assumption is justified.

Using the above assumptions we have a three-layer problem, analogous to the two-layer case of non-invasion, but with two more unknowns and two more boundary conditions.

For the potential in the hole we write again:

$$V_1 = V_0 + V' = \frac{J R_0}{2\pi^2} \int_0^\infty \left[K_0 (kr) + \psi(k) I_0 (kr) \right] \cos kz \, dk \qquad (1\text{-}17)$$

In the infiltrated zone r neither approaches zero nor infinity so that the potential V_2 will be expressed as the general solution containing both K_0 and I_0.

$$V_2 = \frac{J R_0}{2\pi^2} \int_0^\infty \left[\alpha (k) K_0 (kr) + \beta (k) I_0 (kr) \right] \cos (kz) \, dk \qquad (1\text{-}18)$$

Finally the potential in the undisturbed formation, as in the case of non-invasion becomes:

$$V_3 = \frac{J R_0}{2\pi^2} \int_0^\infty \varphi (k) K_0 (kr) \cos kz \, dk \qquad (1\text{-}19)$$

We now have the following boundary conditions:

1) $V_1 = V_2$ for $r = r_0$

or $K_0 (kr_0) + \psi(k) I_0 (kr_0) = \alpha(k) K_0 (kr_0) + \beta(k) I_0 (kr_0)$

$$K_0 (kr_0) \left[\alpha(k) - 1 \right] = \left[\psi(k) - \beta(k) \right] I_0 (kr_0) \qquad (1\text{-}20)$$

2) $V_2 = V_3$ for $r = r_i$

$$\text{or} \quad \alpha(k)\, K_0(kr_i) + \beta(k)\, I_0(kr_i) = \varphi(k)\, K_0(kr_i) \qquad (1\text{-}21)$$

3) Continuity of radial component of current density at first boundary:

$$\frac{1}{R_m}\left(\frac{\partial V_1}{\partial r}\right)_{r=r_0} = \frac{1}{R_i}\left(\frac{\partial V_2}{\partial r}\right)_{r=r_0}$$

which gives:

$$K_0'(kr_0) + \psi(k)\, I_0'(kr_0) = T_1\left[\alpha(k) K_0'(kr_0) + \beta(k) I_0'(kr_0)\right]$$

where:

$$T_1 = \frac{R_m}{R_i} \qquad K_0'(kr_0) = -K_1(kr_0) \quad \text{and} \quad I_0'(kr_0) = I_1(kr_0)$$

so that

$$-K_1(kr_0) + \psi(k) I_1(kr_0) = T_1\left[-\alpha(k) K_1(kr_0) + \beta(k) I_1(kr_0)\right] \qquad (1\text{-}22)$$

4) Continuity of radial component of current density at second boundary:

$$\frac{1}{R_i}\left(\frac{\partial V_2}{\partial r}\right)_{r=r_i} = \frac{1}{R_t}\left(\frac{\partial V_3}{\partial r}\right)_{r=r_i}$$

$$\text{or} \quad -\alpha(k) K_1(kr_i) + \beta(k) I_1(kr_i) = -T_2\, \varphi(k) K_1(kr_i) \qquad (1\text{-}23)$$

where $T_2 = \frac{R_i}{R_t}$.

Thus we have four equations (1-20) through (1-23) with four unknowns, namely $\psi(k)$, $\alpha(k)$, $\beta(k)$, and $\varphi(k)$ which we want to solve for $\psi(k)$, as we are primarily interested in the potential in the hole itself.

We will use the notations:

$kr_0 = x$	$K_0(x) \equiv K$	$I_0(x) = I$
$K_1(x) = K_1$	$I_1(x) \equiv I_1$	$\frac{r_i}{r_0} = n$

$$K(n) \equiv K(nx) \qquad I(n) \equiv I(nx) \qquad M(n) \equiv M(nx) \quad \text{etc.}$$

$$\psi(k) \equiv \psi \qquad \varphi(k) \equiv \varphi \qquad \alpha(k) \equiv \alpha \qquad \beta(k) \equiv \beta$$

From (1-20): $\psi = \dfrac{(\alpha - 1) K + \beta I}{I}$ (a)

From (1-22): $\psi = \dfrac{T_1 (\beta I_1 - \alpha K) + K_1}{I_1}$ (b)

While (1-23) gives: $\varphi = \dfrac{\beta I_1(n) - \alpha K_1(n)}{-T_2 K_1(n)}$ (c)

From (1-22) and (c):

$$\alpha = \frac{\beta I_1(n) - \alpha K_1(n)}{-T_2 K_1(n)} - \frac{\beta I(n)}{K(n)}$$

$$\alpha = \frac{\beta I_1(n) K(n) - \alpha K_1(n) K(n) + \beta I(n) K_1(n) T_2}{-T_2 K_1(n) K(n)}$$

$$\alpha = \frac{\beta Q_n - \alpha M_n + \beta P_n T_2}{-T_2 M_n}$$

or $-T_2 M_n \alpha + \alpha M_n = \beta Q_n + \beta P_n T_2$

$$M_n (1 - T_2) \alpha = \beta (Q_n + P_n T_2)$$

Here we can write:

$$P_n T_2 = Q_n + T_2(1 - Q_n) = T_2 - T_2 Q_n + Q_n = T_2 + Q_n(1 - T_2)$$

so that we have:

$$M_n (1 - T_2) \alpha = \beta \left[T_2 + Q_n (1 - T_2) \right]$$

or $M_n \alpha = \beta \left(\dfrac{T_2}{1 - T_2} + Q_n \right)$

with $\dfrac{T_2}{1 - T_2} = \dfrac{1}{1/T_2 - 1} = \dfrac{1}{R_t/R_1 - 1} = \dfrac{1}{D'}$ where $D' = \dfrac{R_t}{R_1 - 1}$

this gives $\alpha = \dfrac{1/D' + Q_n}{M_n}$ (d)

Equating (a) and (b)

$$\frac{(\alpha - 1)K + \beta I}{I} = \frac{T_1(\beta I_1 - \alpha K_1) + K_1}{I_1}$$

Substituting α from (d):

$$\beta + \frac{1/D' - Q_n}{M_n}\beta - 1 \quad \frac{K}{I} = \frac{T_1 \ \beta\left[I_1 - (1/D' + Q_n)K_1/M_n\right] + K_1}{I_1}$$

or $\beta \dfrac{M_n I \ I_1 + K \ I_1(1/D' + Q_n) - T_1 M_n I \ I_1 + I \ K_1(1/D' + Q_n) \ T_1}{M_n I \ I_1}$

$$= \frac{K_1}{I_1} + \frac{K}{I}$$

$$\beta \frac{M_n N + Q(1/D' + Q_n) - T_1 M_n N + T_1 P(1/D' + Q_n)}{M_n N} = \frac{P + Q}{N}$$

and as $P = 1 - Q$ or $P + Q = 1$ we have

$$\beta = \frac{M_n}{(1 - T_1)M_n N + (1/D', + Q_n) \quad (Q + T_1 P)}$$

$$\beta = \frac{M_n}{M_n N \ (1 - T_1) \quad (1/D' + Q_n) \left[T_1 + Q(1 - T_1)\right]}$$

$$\beta = \frac{M_n}{(1 - T_1)\left[M_n N + (1/D' + Q_n) \quad (1/c + Q)\right]} \tag{e}$$

From (d): $\alpha = \dfrac{1/D' + Q_n}{(1 - T_1)\left[M_n N + (1/D' + Q_n) \quad (1/c + Q)\right]}$ (f)

Substitution of (e) and (f) into (b) gives:

$$\psi = \frac{T_1\left[M_n I_1 - (1/D' + Q_n)K_1\right] + K_1(1 - T_1)\left[M_n N + (1/D' + Q_n) \ (1/c + Q)\right]}{I_1(1 - T_1) \quad M_n N + (1/D' - Q_n) \quad (1/c - Q)}$$

$$= \frac{T_1\left[M_n N - (1/D' + Q_n)P\right] + P(1 - T_1)\left[M_n N - (1/D' - Q_n) \ (1/c - Q)\right]}{N \ (1 - T_1)\left[M_n N + (1/D' + Q_n) \ (1/c + Q)\right]}$$

$$= \frac{1/c\left[M_nN-(1/D'+Q_n)P\right] + P\left[M_nN + (1/D'+Q_n)\ \ (1/c+Q)\right]}{N\left[M_nN + (1/D' + Q_n)\ \ (1/c + Q)\right]}$$

$$\psi = \frac{1/c\ M_nN - P/cD' - PQ_n/c + PM_nN + P/cD' + PQ/D' + PQ_n/c + PQQ_n}{N^2M_n + N/cD' + NQ/D' + NQ_n/c + NQQ_n}$$

Using $MN = PQ$ this becomes

$$\psi = \frac{1/c\ M_nN + PM_nN + MN/D' + MNQ_n}{N^2M_n + N/cD' + NQ/D' + NQ_n/c + NQQ_n}$$

$$\psi = \frac{1/c\ M_n + PM_n + M/D' + MQ_n}{NM_n + 1/cD' + Q/D' + Q_n/c + QQ_n} \qquad (g)$$

This expression can be used directly or can be reworked to take a slightly simpler form:

Letting $D = \frac{R_1}{R_t} - 1$ we have:

$$\frac{1}{D'} = \frac{1}{R_t/R_1-1} = \frac{R_1/R_t}{1 - R_1\ R_t} = \frac{D+1}{-D} = -(1+\frac{1}{D})$$

Also using $Q_n = 1 - P_n$ we obtain for   :

$$\psi = \frac{1/cM_n - M\ (\ 1 + 1/D) + M(1-P_n) + PM_n}{NM_n - 1/c\ (1 + 1/D) - Q(1 + 1/D) + Q(1-P_n) + 1/c(1 - P_n)}$$

$$\psi = \frac{M/D - M_n/c + (MP_n - PM_n)}{1/cD + Q/D + P_n/c + (QP_n - NM_n)} \qquad (1\text{-}24)$$

In the same way as for non-invasion:

$$V_1 = \frac{J R_m}{4\pi\bar{r}} + \frac{J\ R_m}{2\pi^2 r_o}\int_0^\infty \psi(k)\ I_o\ (kr)\ \cos\ (kr\frac{z}{r_o})\ d(kr_o)$$

On the axis $I_o\ (kr) = 1$ and $\bar{r} = z$

So for the normal arrangement with $z = \overline{AM}$ and $s = \frac{\overline{AM}}{r_o}$ we have

$$R_a = \frac{V_1}{J}4\pi z = R_m + \frac{2}{\pi}R_m\ s\int_0^\infty \psi\ (k)\ \cos\ (sx)\ dx$$

or $$\frac{R_a}{R_m} = 1 + \frac{2}{\pi} s \int_0^\infty \psi(k) \cos(s\,x)\, d\,x \qquad (1\text{-}25)$$

where $\psi(k)$ is given by (1-24).

For the lateral arrangement we obtain in the same manner:

$$\frac{R_a}{R_m} = 1 + \frac{2}{\pi} \frac{1}{(1/s_1 - 1/s_2)} \int_0^\infty \psi(k) \left[\cos(s_1\,x) - \cos(s_2 x) \right] d\,x \qquad (1\text{-}26)$$

where $s_1 = \frac{\overline{AM}}{r_o}$ and $s_2 = \frac{\overline{BM}}{r_o}$ and $\psi(k)$ again is given by (1-24).

Values of R_a can be obtained by plotting the integrands and finding the area under the curves by using a planimeter. Both integrands converge very fast.

In this way curves can be plotted for R_a as a function of R_t, s, r_i and R_i. These curves are often called resistivity departure curves, and a large assembly of them is published under that name by the Schlumberger Well Surveying Corporation (7).

PART II

Computation of the True Resistivity of Formations and the Resistivity of the Infiltrated Zone

The conventional way of plotting resistivity departure curves is to give R_a/R_m as a function of s for several values of R_t/R_m and d_i/d_o for a given ratio of R_i/R_m. Instead of using s, the abscissae are mostly in terms of $s/2 = \frac{\overline{AM}}{2r_o} = \frac{\overline{AM}}{d_o}$. Fig. II-1 gives a family of these departure curves for the case of no-invasion, for the normal electrode arrangement. Fig. II-2 gives departure curves for the case of invasion, with $r_i = 2r_o$ and $R_i = 10\ R_m$ also for the normal device. For larger values of r_i the curves will be shifted upward, as indicated by dotted lines. Fig. II-3 gives the departure curves in the case of invasion for the lateral device.

The present use of resistivity departure curves for determination of R_t is as follows: (6)

An experimental curve is plotted in the same way as the resistivity departure curves, using measurements of R_a from electrologs for different electrode spacings. This curve is compared with master curves made up in series as described above (7), and R_t is found by interpolation between the two closest fitting theoretical curves. As can be easily seen from the shape of the curves in Figs. II-1 to II-3, at least four points will be needed to make an accurate plot of such experimental curve. This means that the logs have to be run with four different normal spacings. Though this is possible with the modern seven conductor cables, it is not yet a universally common practice. Some authors have

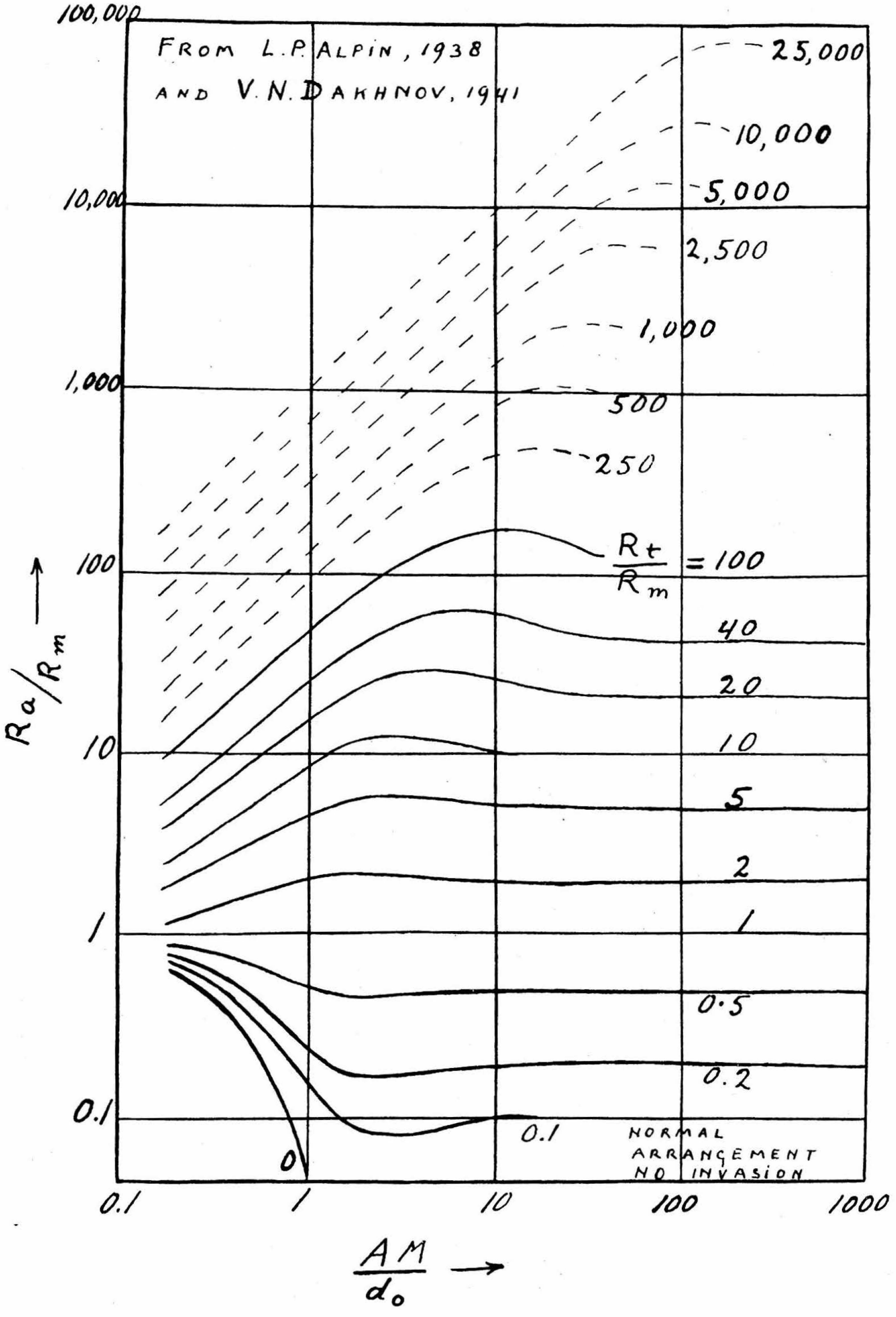
FROM L.P. ALPIN, 1938
AND V.N. DAKHNOV, 1941
25,000
10,000
5,000
2,500
1,000
500
250
$\frac{R_t}{R_m}$ = 100
40
20
10
5
2
1
0.5
0.2
0.1
0
NORMAL
ARRANGEMENT
NO INVASION
100,000
10,000
1,000
100
10
1
0.1
R_a/R_m
0.1
1
10
100
1000
$\frac{AM}{d_o}$

Fig. II-1

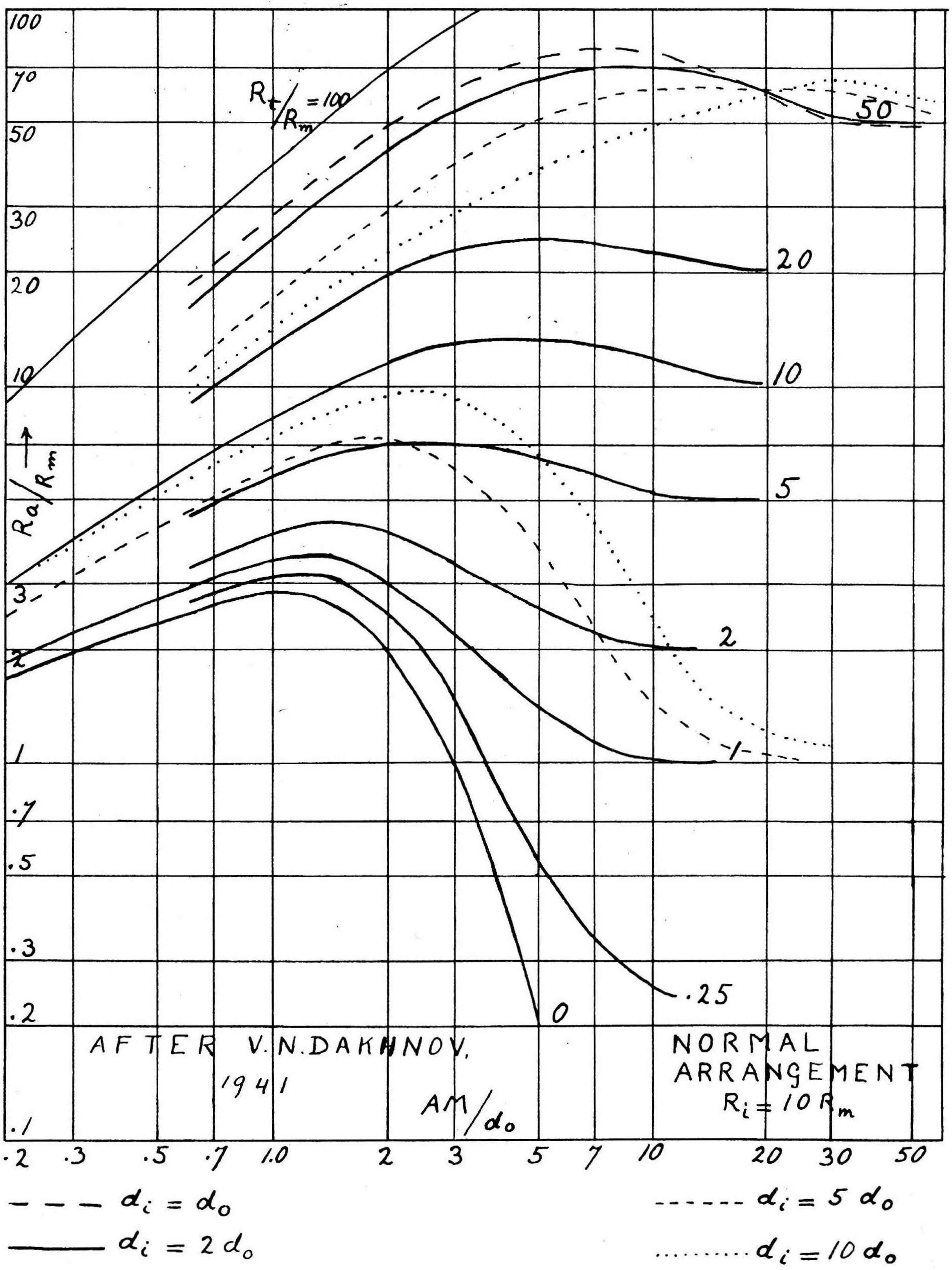
100
70
50
30
20
10
3
2
1
.7
.5
.3
.2
.1
Ra/Rm
Rt/Rm = 100
50
20
10
5
2
1
.25
0
.2
.3
.5
.7
1.0
2
3
5
7
10
20
30
50
AM/do
AFTER V.N.DAKHNOV,
1941
NORMAL
ARRANGEMENT
Ri = 10 Rm
— — — di = do
——— di = 2 do
- - - - - di = 5 do
.... di = 10 do

Fig. II-2

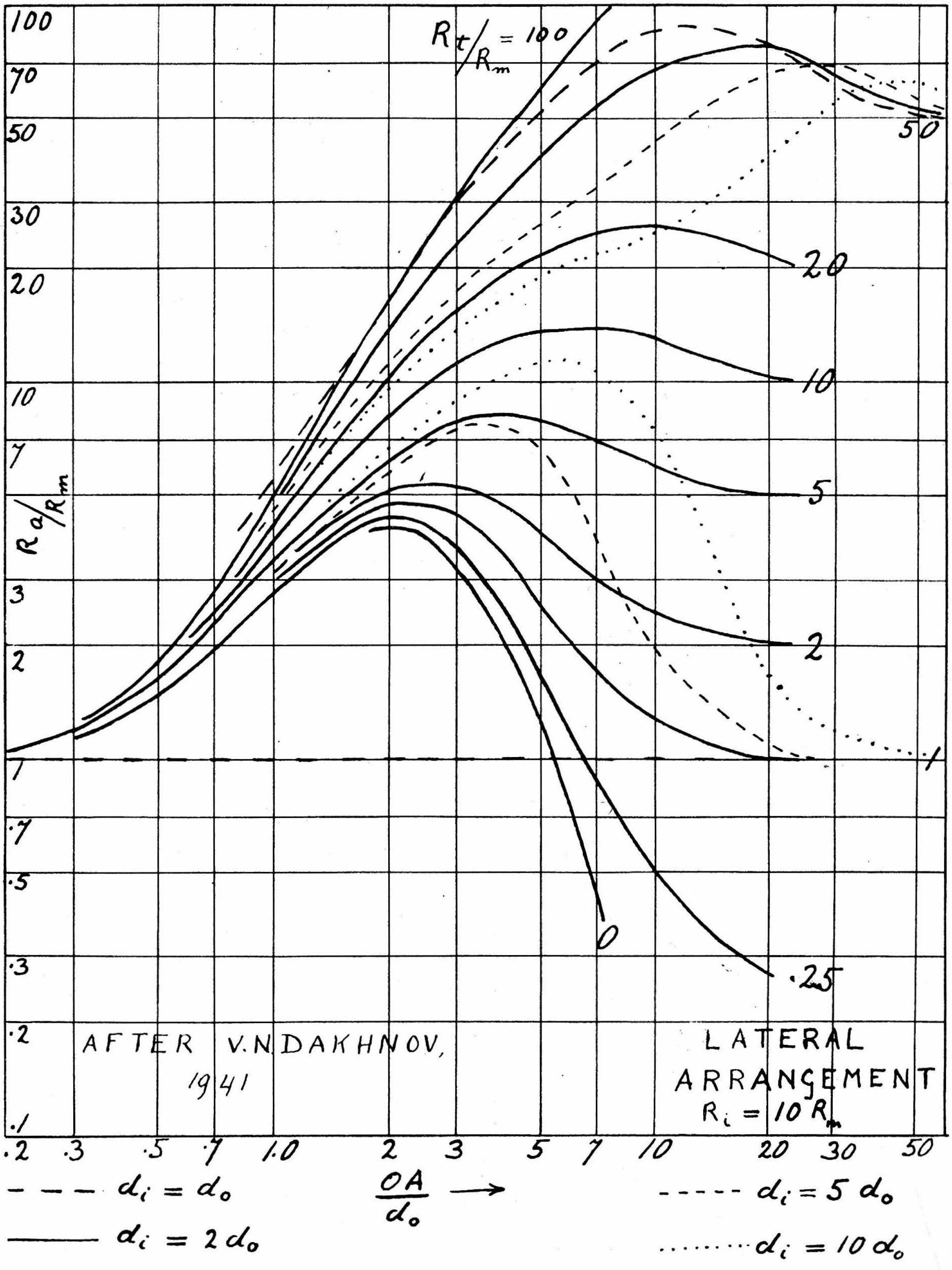
Rt/Rm = 100
50
20
10
5
2
1
0
·25
100
70
50
30
20
10
7
5
3
2
1
·7
·5
·3
·2
·1
Ra/Rm
·2
·3
·5
·7
1.0
2
3
5
7
10
20
30
50
OA/do →
AFTER V.N DAKHNOV, 1941
LATERAL ARRANGEMENT
Ri = 10 Rm
- - - di = do
——— di = 2 do
- - - - - di = 5 do
·········di = 10 do

Fig. II - 3

claimed that a good determination can be made by using an experimental departure curve constructed with the aid of two points only. Obviously it is utterly impossible to construct a curve whose location and shape is of paramount importance, using two points only. The ambiguity of this situation is clearly demonstrated by Fig. II-4 which gives R_t as a function of R_a for different values of R_i and r_i. We see that any R_a gives an infinite number of possible combinations. A second R_a found for another given electrode spacing will eliminate part of the possibilities, but still leave too many to make the method workable, in most cases.

Alternative Method of Finding R_t and R_i

For the reasons described above, it appears to be worth while to find a more direct way of interpretation, and we have therefore worked out a new method, which makes use of one lateral and two normal curves.

In order to evaluate R_t accurately we want a maximum amount of information on the infiltrated zone. More specifically, we want to determine the true resistivity of the infiltrated zone. It is common knowledge that small spacings give information about the resistivities close to the borehole and it has often been stated that the "normal" curve which usually corresponds to a spacing of 10" gives a good approximation of the invaded zone resistivity. However, if we look at Fig. II-2, we see that even for the smallest spacings of the normal arrangement the influence of R_t on the measured R_a is very large. Fig. II-2 shows that for very small spacings of the lateral device, R_a is more independent of the resistivity of the formation beyond the infiltrated zone (R_t).

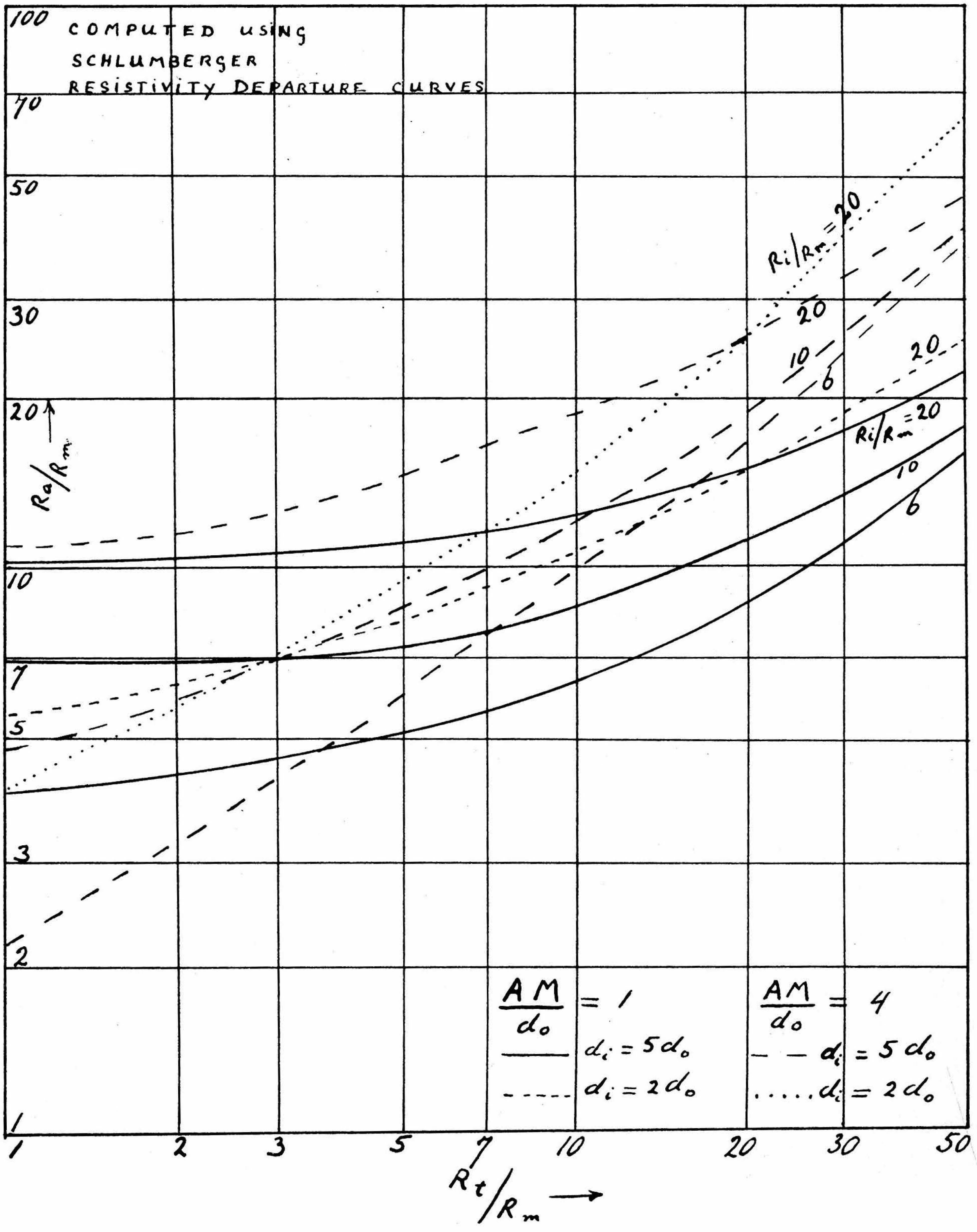
COMPUTED USING
SCHLUMBERGER
RESISTIVITY DEPARTURE CURVES
100
70
50
30
20
10
7
5
3
2
1
R_a/R_m
1
2
3
5
7
10
20
30
50
R_t/R_m
$R_i/R_m = 20$
20
10
6
20
$R_i/R_m = 20$
10
6
$\frac{AM}{d_o} = 1$
$d_i = 5d_o$
$d_i = 2d_o$
$\frac{AM}{d_o} = 4$
$d_i = 5d_o$
$d_i = 2d_o$

Fig. II-4

It seems therefore advisable to use a small lateral spacing, to obtain data on the infiltrated zone and normal spacings to find the true resistivity of the undisturbed formation.

The optimum lateral spacing to be used, will be the one that gives apparent resistivities which are very nearly equal to the true resistivity of the infiltrated zone and which are as little as possible dependent upon R_t.

The second of these conditions is best fulfilled by the smallest possible lateral spacing. However, most of the apparent resistivities for very small spacings have, for usual ranges of R_t, values, which are lower than the infiltrated zone resistivity, because of the large influence of the borehole itself.

In other words the apparent resistivities that would be obtained for a wide range of values of R_t, varying from very small to very large R_t's, will not be distributed symmetrically around the true R_i, but the whole group will be shifted towards lower values.

Also small inaccuracies in the determination of the hole diameter, will give larger errors for the extremely small spacings, than for larger ones.

The optimum spacing therefore will be a compromise between the influence of the borehole and the effect of R_t, on the apparent resistivity.

To determine this optimum spacing, the apparent resistivity was computed for a series of small spacings in the range that appeared most promising, and the most effective one was selected.

The computations were carried out for average invasion diameter, given values of R_i/R_m and values of R_t/R_m which covered most of the conditions that are normally encountered.

As stated before, the approximated formula for R_a cannot be used for small lateral spacings. However it is possible to obtain values for $(R_a)_\ell$ (= apparent resistivity for lateral arrangement) from the departure curves for the normal arrangements using the following method of conversion:

Considering the lateral arrangement as consisting of one current electrode A and two potential electrodes M and N we can write:

$$V_M = \frac{\mathcal{J}(R_a)_1}{4\pi(\overline{AM})} \qquad \text{or} \qquad \frac{V_M}{\mathcal{J}} = \frac{(R_a)_1}{4\pi(\overline{AM})}$$

$$V_N = \frac{\mathcal{J}(R_a)_2}{4\pi(\overline{AN})} \qquad \text{or} \qquad \frac{V_N}{\mathcal{J}} = \frac{(R_a)_2}{4\pi(\overline{AN})}$$

Here $(R_a)_1$ and $(R_a)_2$ are the apparent resistivities corresponding to normal electrode arrangements having respectively the spacing AM and AN.

Denoting the voltage drop between the potential electrodes of the lateral arrangement and the apparent resistivity for this arrangement respectively by V_ℓ and $(R_a)_\ell$ we have:

$$V_\ell = \frac{\mathcal{J}(R_a)_\ell}{4\pi} \quad (1/\overline{AM} - 1/\overline{AN})$$

and as $V_\ell = V_M - V_N$ we can write

$$(R^a)_\ell = 4\pi \frac{V_M - V_N}{\mathcal{J}} \; \frac{1}{(1/\overline{AM} - 1/\overline{AN})}$$

$$= \left[\frac{(R_a)_1}{\overline{AM}} - \frac{(R_a)_2}{\overline{AN}}\right] \frac{1}{(1/\overline{AM} - 1/\overline{AN})}$$

so that

$$\frac{(R_a)_\ell}{R_m} = \left[\frac{(R_a)_1/R_m}{\overline{AM}/d_o} - \frac{(R_a)_2/R_m}{\overline{AN}/d_o}\right]\left(\frac{1}{1/(\overline{AM}/d_o) - 1/(\overline{AN}/d_o)}\right) \tag{2-1}$$

For any given lateral arrangement and hole diameter the factor

$$K_s = \frac{1}{1/(\overline{AM}/d_o) - 1/(\overline{AN}/d_o)}$$

can be calculated directly.

The quantities $(R_a)_1/R_m$ and $(R_a)_2/R_m$ are found from the departure curves for the normal device for any given set of conditions (R_i, d_i and R_t), under consideration, corresponding to the values of $\overline{AM}/d_o$ and $\overline{AN}/d_o$.

Using values of $(R_a)_1/R_m$ and $(R_a)_2/R_m$ obtained from the Schlumberger conventional departure curves (7), $(R_a)_\ell/R_m$ has been computed with the aid of equation(2-1) for three values of R_i/R_m, average invasion diameter and several values of R_t/R_m and are shown in Tables II-A, II-B and II-C.

TABLE II-A

$d_i = 5\ d_o$		$\overline{AM}/d_o = 1.75$		$\overline{AN}/d_o = 2.25$	
$R_i = 6\ R_m$		$R_i = 11\ R_m$		$R_i = 21\ R_m$	
R_t/R_m	$(R_a)_\ell/R_m$	R_t/R_m	$(R_a)_\ell/R_m$	R_t/R_m	$(R_a)_\ell/R_m$
30	6.07	55	9.85	105	18.6
6	5.44	11	9.69	21	11.59
1	5.29	1	7.32	1	11.19
.12	5.08	.11	7.3	.1	10.32

TABLE II-B

$d_i = 5\ d_o$		$\overline{AM}/d_o = 2.75$		$\overline{AN}/d_o = 3.25$	
$R_i = 6\ R_m$		$R_i = 11\ R_m$		$R_i = 21\ R_m$	
R_t/R_m	$(R_a)_\ell/R_m$	R_t/R_m	$(R_a)_\ell/R_m$	R_t/R_m	$(R_a)_\ell/R_m$
30	7.35	55	12.2	105	29.22
6	7.08	11	11.75	21	20.46
1	5.29	1	10.64	1	14.89
.12	4.8	.11	9.12	.1	15.08

TABLE II-C

$d_i = 5\ d_o$		$\overline{AM}/d_o = 3.5$		$\overline{AN}/d_o = 4.0$	
$R_i = 6\ R_m$		$R_i = 11\ R_m$		$R_i = 21\ R_m$	
R_t/R_m	$(R_a)_\ell/R_m$	R_t/R_m	$(R_a)_\ell/R_m$	R_t/R_m	$(R_a)_\ell/R_m$
30	10.0	55	20.8	105	31.6
6	8.34	11	12.87	21	21.4
1	4.86	1	9.18	1	18.8
.12	4.24	.11	9.07	.1	17.7

Similar tables were made up for other small lateral spacings and also for various values of $\overline{MN}/d_o$.

From comparison of eight of these tables it was found that the most satisfactory spacing is:

$$\overline{AM}/d_o = 2.75 \qquad \overline{AN}/d_o = 3.25$$

As shown in Table I-A, for smaller spacings, the average values of

(R_a) $/R_m$ shift below the actual value of R_i/R_m.

For sapcings larger than the optimum spacing, the effect of R_t becomes more and more pronounced and the average values of (R_a) $/R_m$ are found to be larger than the R_i/R_m in question.

For increased $\overline{MN}/d_o$ we find a slightly less regular distribution of (R_a) $/R_m$ with respect to R_i/R_m.

Using the above determined optimum spacing, we can now make up a series of master curves, representing R_a/R_m as a function of R_i/R_m for different values of R_t/R_m and for different ratios of the invasion diameter, d_i, over the hole diameter, d_o.

These master curves will be called "apparent resistivity curves."

To obtain a complete set of these apparent resistivity curves, the use of the heretofore published resistivity departure curves for the normal electrode arrangements, does not suffice, because of scarcity of data in most ranges.

For instance the Schlumberger departure curves, which form the most complete set published to date, give only three values of R_i/R_m and four values of d_i/d_o. For the computation of the vast majority of our curves we have to go back therefore to the formula, which we derived for (R_a) , and is given by equation (1-26) and as direct computation will be more accurate than the semi-graphical method outlined before, it is advisable to obtain the apparent resistivity curves using equation (1-26) exclusively.

Fig. II-5, gives an example of a set of apparent resistivity curves, for the lateral arrangement.

To obtain a set of master curves which will completely cover all or

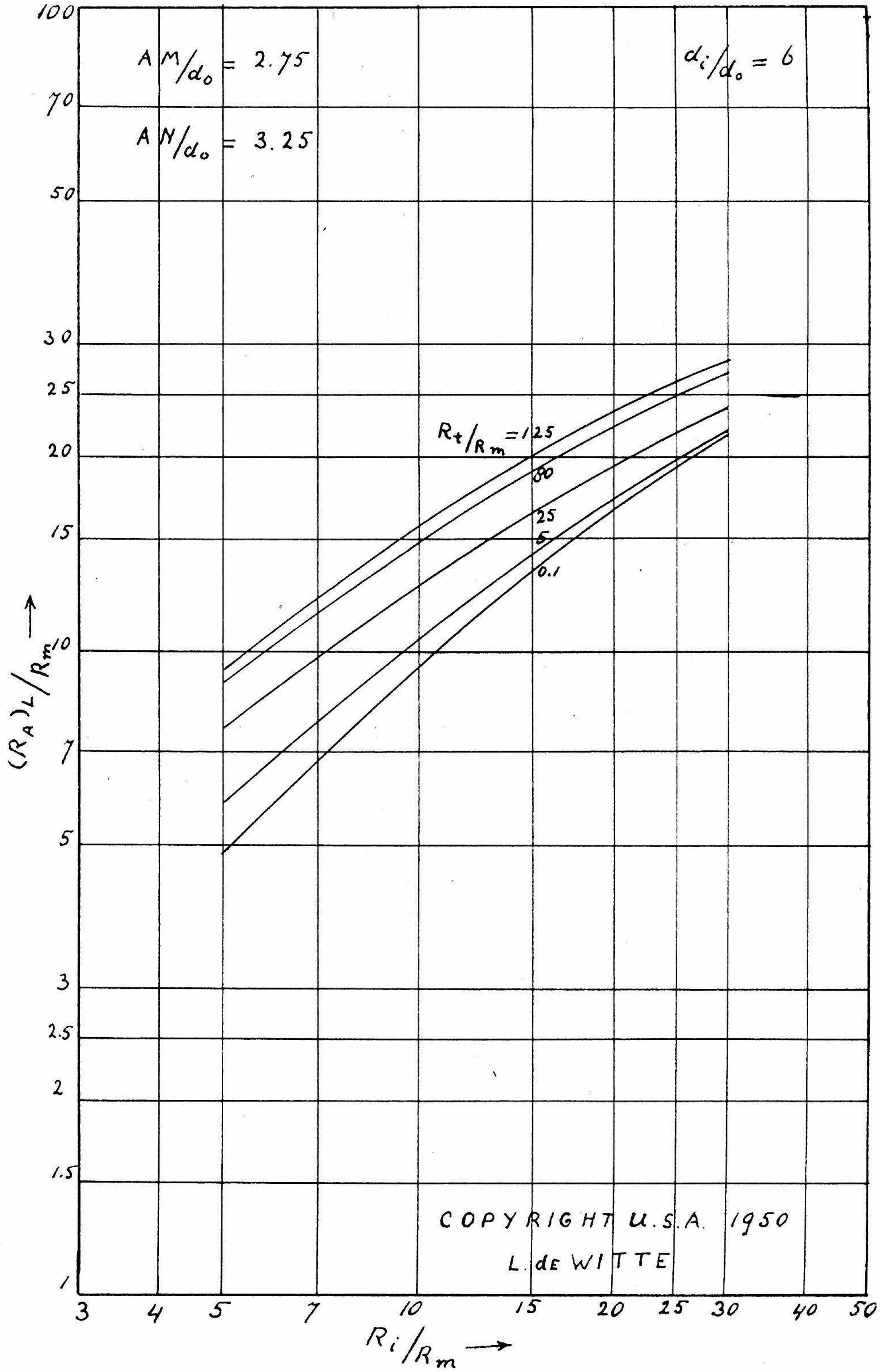
100
70
50
30
25
20
15
10
7
5
3
2.5
2
1.5
1
3
4
5
7
10
15
20
25
30
40
50
$AM/d_o = 2.75$
$AN/d_o = 3.25$
$d_i/d_o = 6$
$R_t/R_m = 125$
80
25
5
0.1
$(R_A)_L/R_m$ →
R_i/R_m →
COPYRIGHT U.S.A. 1950
L. de WITTE

Fig. II - 5

most of the conditions arising in practice, there is one more complication that has to be taken into account, namely the variation in diameter of the drill hole, d_o.

The average drill hole diameter depends upon the size of bit used for drilling. The bit sizes vary from well to well and are often changed several times during the drilling of each single hole.

Apart from the variations due to different bit sizes used, the actual drill hole diameter will also vary with the character of the formations traversed. Hard, well consolidated formations will mostly give a hole of relatively uniform diameter, slightly larger than the bit size. Poorly consolidated formations will often cave in, which results in enlarging of the hole diameter. Clays, shales and slates usually swell, upon coming into contact with the drilling mud, which is mostly less saline than the formation water. This results in decrease of the hole diameter. Fissile shales on the other hand will cave in very often and the swelling may even aid the fracturing as the expansion is restricted in vertical direction and the resulting curvature tends to split off slices of the material. Limestones, and beds of rocksalt, gypsum and anhydrite, loose material due to solution in the drilling mud, which tends to enlarge the hole diameter.

It is obvious therefore that the actual hole diameter is not a constant in any given hole, but is subject to many changes from one depth to the other. Mostly however any given formation which is more or less homogeneous, will show a constant deviation from the average hole diameter, within its boundaries.

To determine the deviations it has become a common practice to run a "calliper log,"* either simultaneous with the electrolog or separately.

The calliper log gives the hole diameter as a function of the depth in the well.

Where no calliper log is available we will have to rely upon the average hole diameter, as estimated from the bit size. This however may introduce very serious errors.

To take into account the various sizes of drill holes, different sets of electrodes should be available to fit the most common hole sizes.

For instance one set of electrodes can be made such that $\overline{AM}/d_o = 2.75$ and $\overline{AN}/d_o = 3.25$ for a hole with a diameter (d_o) of 8". This will give $\overline{AM} = 22"$ and $\overline{AN} = 26"$.

Similarly another set can be made to fit a 12" hole, resulting in $\overline{AM} = 33"$ and $\overline{AN} = 39"$.

The intermediate sizes of drill holes or the extremely small and large ones and also the deviations from the average hole diameter within one well, can then be taken into account by making up "apparent resistivity charts" for the above electrode spacings and deviating values of d_o.

Using for example the arrangement with $\overline{AM} = 22"$ and $\overline{AN} = 26"$, a seven inch hole will give ratios of $\overline{AM}/d_o$ and $\overline{AN}/d_o$ respectively of 3.14 and 3.61 and for these values a set of apparent resistivity charts may be prepared.

In the same way charts can be made up for other ratios of $\overline{AM}/d_o$

---

* The mechanism of the calliper logging device consists of a set of springs which are in contact with the boreface at all times and the expansion or contraction of which acts on a variable resistor or on the motion of an induction coil, which in turn affect changes in a current which are precalibrated in terms of the hole diameter and are registered as such by the logging apparatus.

and $\overline{AN}/d_o$ corresponding to one of the standard size arrangements and a complete range of values of d_o. Approximately 10 sets of charts will be required to cover the range of values of d_o usually encountered in practice. For extreme sizes of drill holes, special arrangements of electrodes should be prepared, to give as nearly as possible: $\overline{AM}/d_o = 2.75$ and $\overline{AN}/d_o = 3.25$.

After having determined the lateral spacing to be used, we will now discuss the requirements for the normal spacing from which we want to obtain an approximate value of R_t.

From the conventional resistivity departure curves we easily observe the fact that very large normal spacings, give apparent resistivities that are good approximations to the true resistivity.

However this holds true only for formations that are thick enough, so that the influence of the boundaries at the top and the bottom of the formations may be neglected.

It can be shown that in order to meet this condition, the thickness of the formation must be at least five times the normal spacing used. (8)

For instance in a drill hole of 8" diameter and using a spacing $\overline{AM}$, equal to 10 d_o, the effect of the boundaries can only be neglected for beds that are 5 x 10 x 8" = 400" or approximately 33 ft. thick.

As many commercially important formations have thicknesses much smaller than 33' we want to use the smallest spacing that will still give an apparent resistivity, which is a fair approximation to the true resistivity.

The best compromise between the two factors described above appears to be obtained, by an electrode spacing ($\overline{AM}$) equal to 5 times the hole diameter.

In the case of an 8" hole, apparent resistivities can be obtained with such spacing, on beds 17 ft. thick or thicker without the necessity of correction for the effect of the formation boundaries. For thinner beds, correction factors may be applied for the boundary effects, as described by Guyod (8).

The lower limit of applicability of such correction factors, is a bed thickness of two times the spacing. In our case this would be a bed of 80" (= 6.7 ft.) thick.

Again standard arrangements may be made up by fitting the actual spacings to the most common hole sizes (8" and 12") and variations of the hole diameters are taken into account by a number of apparent resistivity charts made up for values of $\overline{AM}'/d_o$, smaller and larger than 5.

Fig. II-6 shows a set of apparent resistivity curves for $\overline{AM}/d_o = 5$. R'_a denotes the apparent resistivity as measured with the long normal device.

On the proposed master curves for the lateral device the apparent resistivity is given as a function of the true invaded zone resistivity for various values of the true formation resistivities (see Fig. II-5), while for the long normal device the apparent resistivity is given as a function of R_t for various values of R_i (see Fig. II-6). The reasons for this choice of parameters are that the apparent resistivity for the lateral device in many cases is nearly equal to R_i and varies only little with R_t while for the long normal device, the apparent resistivities are closer to R_t and are influenced to a much lesser degree by R_i. Actually all the variables are given as dimensionless quantities in the forms

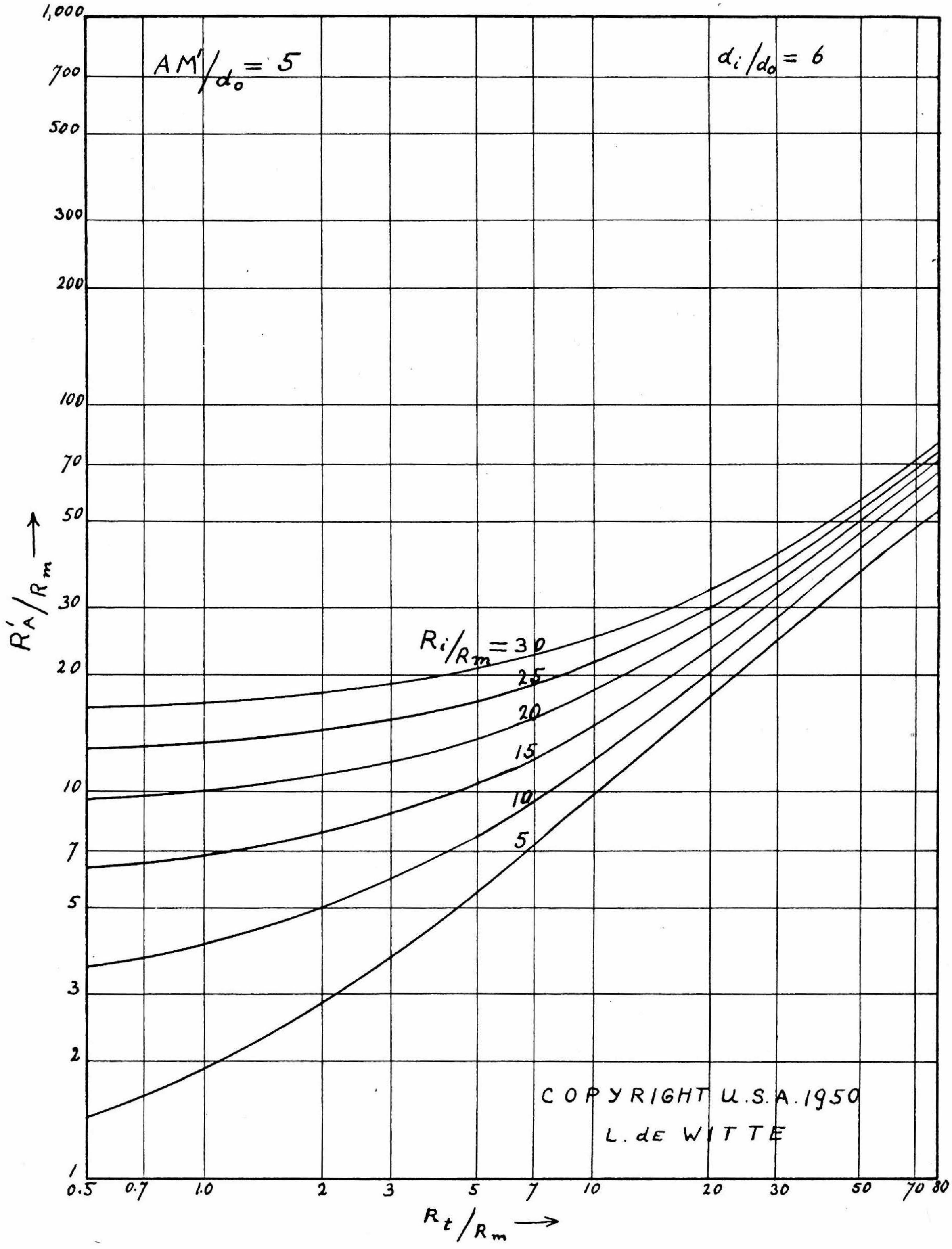
AM'/d_o = 5
d_i/d_o = 6
1,000
700
500
300
200
100
70
50
30
20
10
7
5
3
2
1
R'_A/R_m →
R_i/R_m = 30
25
20
15
10
5
COPYRIGHT U.S.A. 1950
L. dE WITTE
0.5
0.7
1.0
2
3
5
7
10
20
30
50
70
80
R_t/R_m →

Fig. II-6

R_s/R_m, R_i/R_m and R_t/R_m.

The interpretation method to be used with these curves consists basically of the following steps:

1. Take the apparent resistivity obtained with lateral spacing as a first approximation to R_i.

2. For this value of R_i find the R_t corresponding to the apparent resistivity obtained with the long normal device, from the apparent resistivity curves for the ratio of $\overline{AM}'/d_o$ in question.

3. With the obtained value of R_t find a better approximation for R_i using the apparent resistivity curves for the lateral device.

4. This successive approximation is continued till no further substantial changes in the values of R_i and R_t are found.

5. The final values of R_i and R_t thus obtained will be the actual true invaded zone resistivity and true formation resistivity, if the actual invasion diameter equals the invasion diameter given on the set of resistivity charts we used for our determination.

This last condition brings in the necessity for a third curve, for which we have chosen a "short" normal curve.

The spacing for this curve is not critical. Any spacing of either normal or lateral device, that gives an apparent resistivity which is markedly influenced by <u>both</u> the invaded zone resistivity <u>and</u> the true formation resistivity, will suffice.

A good and convenient value is obtained by taking a normal curve of which the spacing $\overline{AM}$ equals the $\overline{AM}$ of the short lateral device already being used. This obviates the necessity for an additional electrode as the apparent resistivity for this normal curve is simply measured between the first pickup electrode of the lateral device and the surface pickup electrode of the long normal device. We will use therefore $(AM) \equiv (AM)_{\ell} = 2.75\ d_o$ for the standard sondes.

In contrast with the long normal spacing described before we will term this spacing the "short normal spacing," although it is considerably larger than the conventional short normal spacing which is only 10" long and in cases even approaches the 38" conventional normal which is often called the "long normal spacing." For the short normal spacing a group of apparent resistivity charts is made up in the same way as for the long normal spacings (see Fig. II-7).

The function of this short normal curve is to check assumptions regarding the invasion diameter.

The interpretation procedure may be started assuming normal invasion ($d_i = 6\ d_o$). Using the apparent resistivity charts made up for $d_i = 6\ d_o$ we then find a value for R_i and another for R_t.

With the aid of these values we can then determine the apparent resistivity that one should obtain for the short normal spacing, using the apparent resistivity charts for that spacing.

If this theoretical value checks with the actually measured value, the assumption regarding the infiltration diameter is right. However if the theoretical and actual values for the short normal apparent resistivity are not equal we must correct our assumption regarding d_i as indicated in Table II-D. Table II-D only shows the direction in which the actual infiltration diameter varies from the assumed diameter, but not the magnitude of the corrections. The correction procedure is best illustrated by an example:

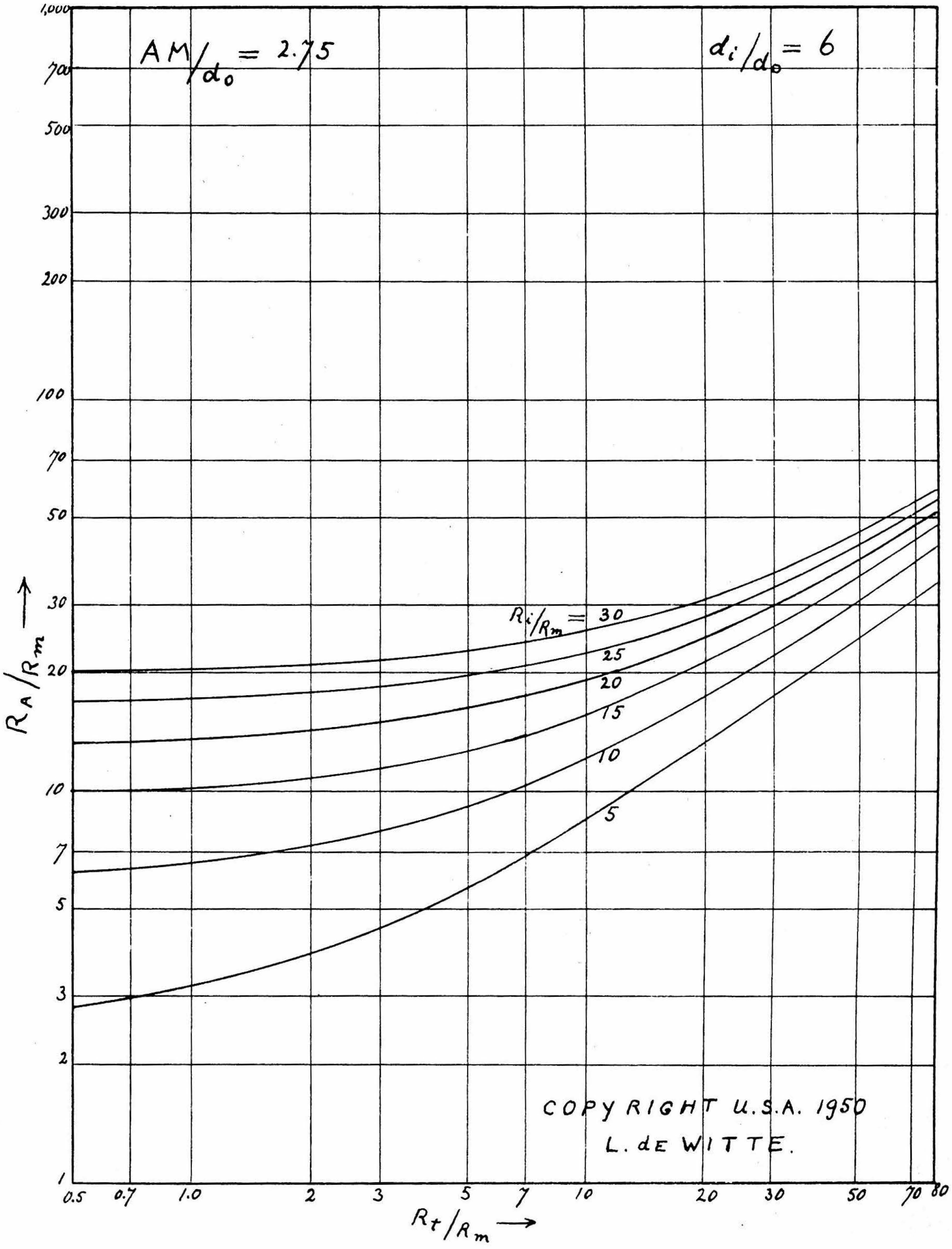

$AM/d_o = 2.75$
$d_i/d_o = 6$
1,000
700
500
300
200
100
70
50
30
20
10
7
5
3
2
1
R_A/R_m →
$R_i/R_m = 30$
25
20
15
10
5
0.5
0.7
1.0
2
3
5
7
10
20
30
50
70
80
R_t/R_m →
COPYRIGHT U.S.A. 1950
L. de WITTE.

Fig. II - 7

Let us first assume $d_i = 6\ d_o$, and suppose that the computed true resistivities, using this assumption, show $R_i < R_t$.

For the values of R_i and R_t as determined we then find the apparent resistivity which the short normal device should register, using the charts for $d_i = 6\ d_o$ made up for the short normal device.

This computed value of R_a is then compared with the apparent resistivity actually measured with the short normal device. Let us assume that we find the computed R_a to be larger than the measured R_a. Table II-D shows that for this case the actual $d_i >$ assumed d_i.

Our next assumption therefore will be $d_i = 8\ d_o$. For this assumption we now repeat the entire interpretation procedure. If this time we find that for the short normal device the computed R_a is smaller than the measured R_a, we know that now the actual $d_i <$ assumed d_i and therefore $6\ d_o < d_i < 8\ d_o$.

If we want great precision in the determination of d_i we may interpolate d_i between the values of $6\ d_o$ and $8\ d_o$ using the differences found in the computed and measured values of R_a as a basis for the interpolation.

The value of d_i thus determined indicates the set of charts to be used for the computation of the final values of R_i and R_t.

Usually we will be able to make a rough first estimate of the amount of filtration from the apparent resistivities of the short normal and the long normal device, especially if R_i and R_t are sufficiently different, as can be judged from the apparent resistivities for the short lateral and the long normal.

Much infiltration will result in larger differences between the short normal and the long normal than little or no infiltration.

If there is no infiltration, the above interpretation procedure will result in $R_i = R_t$ for any assumed invasion diameter.

As will be seen later it is possible that $R_i = R_t$ in cases where invasion is present, as for instance when a water sand is invaded by a mud filtrate of the same resistivity as the connate water, or when in an oil horizon the opposite effects of the oil replaced by water and the saline connate water replaced by the less saline mud filtrate are equal.

In such cases a study of the S.P. curve and (or) the invasion of neighboring formations will often give clues as to whether invasion is present or not.

TABLE II-D

$R_i > R_t$	$R_i < R_t$
computed R_a > measured R_a actual d_i < assumed d_i	computed R_a > measured R_a actual d_i > assumed d_i
computed R_a < measured R_a actual d_i > assumed d_i	computed R_a < measured R_a actual d_i < assumed d_i

The above described method gives us as final answer the quantities R_t, R_i and d_i.

R_t is used directly in the quantitative determination of the fluid content of formations.

In later parts of this thesis it will be outlined how we may use R_i to help solve other unknown factors in fluid content determinations.

PART III

Experimental Equipment

The technique employed in the laboratory investigations on the character of the infiltrated zones around drill holes, in porous reservoir rocks, makes use of two distinct sets of apparatus. The first set is used to saturate, infiltrate or flush sandstone samples, while the second set consists of an arrangement which enables us to measure the resistivity of the cores. The investigations were carried out using sandstone samples from outcrops of formations which are known to be oil-bearing in other parts. These samples were saturated with mixtures of crude oil, gas and water of varying salinity. After saturation, they were infiltrated by fresh water and the changes in resistivity, and relative saturation of the above components were registered.

Also a standard type of drilling mud was filtrated through typical samples and the resistivities of the sample containing the mud filtrate and of the effluent filtrate were measured.

Infiltration Equipment

The equipment used to saturate, infiltrate or flush the sandstone samples employed apparatus as indicated below:

The samples were mounted in the bottom part of a cylinder of a standard 100 pound baroid wall-building tester (9).

The necessary pressure was supplied by a large size nitrogen bottle, equipped with a regulation pressure reducing valve and a 300 pound outlet valve in line with the latter.

To insure accurate measurements of the pressure applied a 160 pound pressure gauge, with 3" dial, was installed near the inlet of the baroid tester.

The filtrate was collected in a 100 cc graduated cylinder, for the flushing experiments on water sands, while for experiments of longer duration a 250 cc bottle with rubber stopper, filter funnel and capillary air vent were used, to minimize evaporation.

The samples were shaped to fit the inside of the baroid tester by cutting them to the approximate proportions with a diamond saw and grinding them to a good cylindrical shape with a rough carborundum grinder and (or) a rotary wire brush. The final size of the cores was approximately 2.8" diameter x 2" height. The inside diameter of the wall building tester is 3", so that sufficient clearance existed for mounting and insulating.

Before mounting the cores they were first coated with castolite, a normally thermo-setting casting plastic, to which a cold-setting promoter had been added. The plastic was allowed to harden at room temperature.

In this way a very firm band with the core was obtained, while the rapidly setting action of the cold-setting promoter limited infiltration to a single granular layer.

After hardening of this first coating the bottom edge of the core was sealed to the inside of the baroid cylinder, with a coldwater putty, in such a way that the lower surface of the core was flush with the lower rim of the cylinder. The cylinder was then placed upright and the annular space between the core and the inner wall of the cylinder was filled with castolite, which was cured for approximately 45 minutes at

175°F.

The drilling muds used were samples of aquagel, zeogel and natural clays, obtained from the Baroid Sales Division of Los Angeles. The proportions were weighed with an ordinary balance (accuracy .05 gram) and mud weight was measured with a baroid mud balance. The muds were mixed with a high speed Hamilton Beach soil dispersion mixer.

To obtain oil or gas saturations in the cores, comparable to those occurring in thick reservoir horizons, the samples were first 100% saturated with water and then oil or gas was forced in, by the capillary pressure method. For this purpose special adapters were machined to hold a porous porcelain diaphragm and to fit the baroid cylinders; details of this equipment and the procedure used, are described in a second thesis by the author (10).

General Circuit for Resistivity Measurements

The resistivity measurements were carried out with a separate set of apparatus.

Fig. III-1 gives the general lay-out of the measuring circuit used. The circuit consists of a four-electrode arrangement, comprising two current electrodes and two potential "pick-up" electrodes and apparatus to measure the current, through the current electrodes, and the corresponding potential difference between the pick-up electrodes, with a minimum of distortion in the potential distribution in the sample.

The current was supplied by a Hewlett-Packard 1 Watt audio oscillator. For reasons, to be outlined later, a frequency of 1000 cycles/sec. was used. In series with the current electrodes a group of standard resistors respectively of 10 Ω , 100 Ω , 1,000 Ω and 10,000 Ω ,

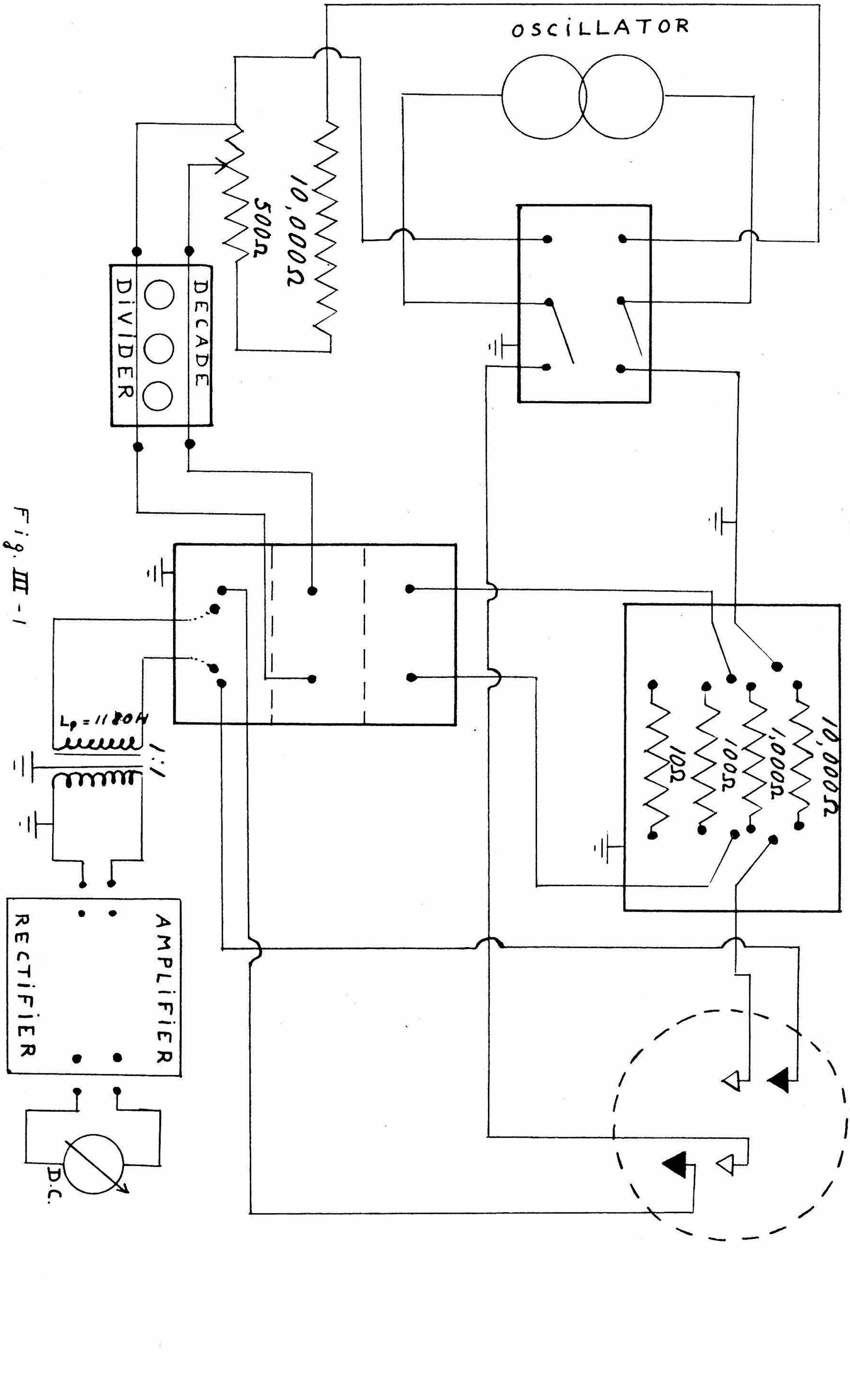
OSCILLATOR
10,000Ω
500Ω
DECADE
DIVIDER
Lp = 1180H
1:1
10,000Ω
1,000Ω
100Ω
10Ω
AMPLIFIER
RECTIFIER
D.C.

Fig. III-1

one of which could be plugged into the circuit at a time. The resistors were all standard A.C., non-inductively wire wound, resistors with an accuracy of 0.25%. The group of resistors were mounted in a grounded chassis and the plugs were shielded chassis plugs. A third plug carrying two separate leads made connections with both ends of the resistors in their respective positions, enabling measurement of the voltage drop across the resistors.

To eliminate spurious affects in the circuit caused by capacitive and inductive coupling, between elements of the circuit and also to avoid pick-up of 60 cycle "noise" all leads had to be carefully shielded, and all shielding connected to a common ground. This however introduced new difficulties as capacitive coupling between wire and its own shielding would cause deviation in part of the current and inaccuracies in the measurements, as well as distortion of the potential distribution between the electrodes. For this reason amphenol polyethylene cables were used for all leads. The cables were of the armoured, single conductor type (RG-62/u). These cables have a capacitive coupling between wire and braid of 13.5 $\mu\mu$F per foot. This was found to be still too high for our requirements and therefore the original wire of the cable was pulled out and replaced by No. 40 wire. This cut the capacitive coupling down to approximately 3 $\mu\mu$F per foot, which was small enough for our purpose.

In order to measure the small voltages across the potential electrodes and the standard resistor in the current circuit, accurately, an amplifier-rectifier combination was used. The input leads to the amplifier could be plugged into one of three positions on a central switch box, thus connecting with the potential electrodes, the resistor in the current circuit, or the output terminals of a decade divider used for calibration.

The voltages to be measured were of the order of 0.01 Volt A.C. They were amplified approximately 800 times and then rectified by a peak voltage rectification arrangement. The amplifier will be discussed in more detail. The final D.C. current was measured with a sensitive research test meter on the 100 A scale.

As, for resistivity measurements, we are only interested in the ratio of the voltage across the potential electrodes (ΔV) and the corresponding current (I). The actual amplification did not have to be determined and only linearity of the test meter reading had to be checked or calibrated.

To calibrate, the output, of the oscillator, was put across a potentiometer consisting of two wire wound resistors of respectively 10,000 ohms and 500 ohms. From the latter one fixed and one variable contact, taking about 1/100 of the total voltage across the potentiometer, were connected with the input terminals of a decade voltage divider. The input impedance of the decade divider was 10,000 ohms while the output impedance varied up to 10,000 ohms. Three dials in series enabled us, to divide the input into one thousandth, one hundredth, and tenth parts. The output was connected with the central switch box as indicated before.

To calibrate, the oscillator output would be varied so as to give a 100 μA reading, with the decade divider shorted out. Then using the different dials the voltage was divided into equal parts of the original and the corresponding test meter readings were noted. Then a table was made up of test meter readings and corresponding proportional parts. The stability of the amplifier with time was very good so that new calibrations were only made every two weeks. All experimental readings were corrected using the above calibration tables.

The Amplifier Rectifier System

Fig. III-2 schematically represents the amplifier and rectification circuit. The amplification circuit consists of three stages. The first stage is a medium μ twin triode (6J6), with a cathode follower arrangement, to provide a high input impedance.

To compute the real input impedance of the cathode follower arrangement we will use notations as indicated in Fig. III-3.

The input impedance is defined as: $R_i = \frac{U}{i}$

$$U = U_1 + U_2 \qquad \text{and} \qquad i = \frac{U_1}{R_1}$$

so that $$R_i = \frac{U}{U_1} \cdot R_1 \qquad (3\text{-}1)$$

If we neglect the influence of R_3 we can write for the plate current:

$$i_p = \frac{\mu U_1}{R_2 + R_p}$$

while $$U_2 = i_p R_2 = \frac{\mu R_2}{R_2 - R_p} \cdot U_1 \qquad (3\text{-}2)$$

From (3-1) and (3-2):

$$R_i = \left[1 + \frac{\mu R_2}{R_2 + R_p}\right] R_1$$

In our case, with $R_p = \frac{7100}{2} = 3550$, $\mu = 38$ and $R = .5$ Meg

we find $R_i = 7.75 R_1 = 5.3$ Meg .

The approximate gain of the first stage is calculated as follows:

$$K_1 = \frac{U_2}{U} = \frac{U_2}{U_1 + U_2} = 0.885$$

The second stage consists of a high mu twin triode (7 F 7). The two stages have a capacitance-resistance coupling.

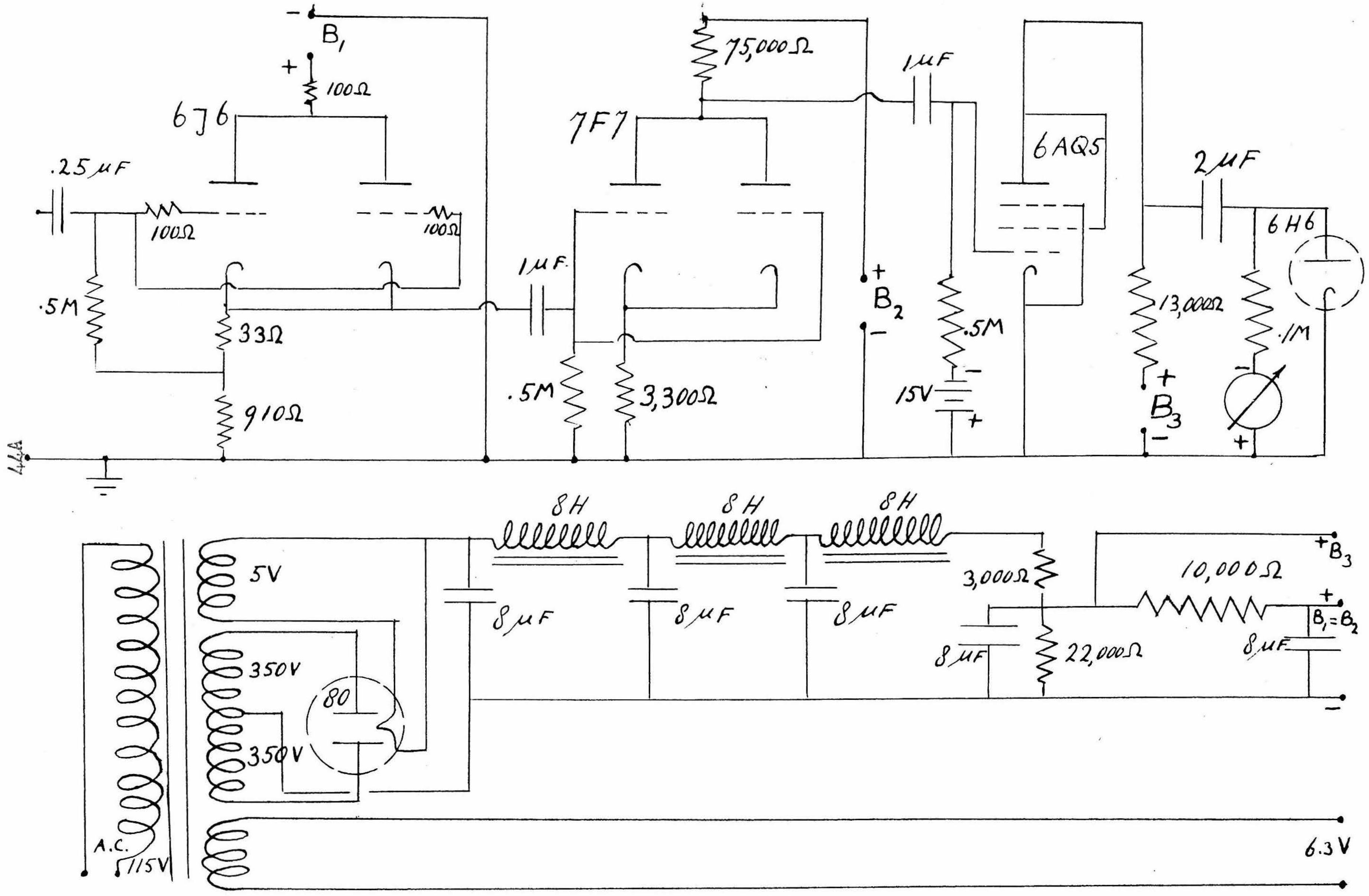

B₁
100Ω
6J6
.25 µF
100Ω
100Ω
.5M
33Ω
910Ω
44A
1µF.
7F7
75,000Ω
.5M
3,300Ω
1µF
B₂
.5M
15V
6AQ5
2µF
6H6
13,000Ω
.1M
B₃
8H
8H
8H
5V
350V
350V
80
8µF
8µF
8µF
3,000Ω
8µF
22,000Ω
10,000Ω
+B₃
B₁=B₂
8µF
A.C.
115V
6.3V

Fig. III - 2

For the two parts of the 7 F 7 coupled in parallel the plate resistance is 22,000 ohms while $\mu = 70$. With a load resistor of 75,000 ohms this would give a gain of $\frac{70 \times 75{,}000}{75{,}000 + 22{,}000} = 54$.

However, the cathode resistor of 3300Ω gives negative feed back, the portion fed back being 0.042. The overall gain therefore is:

$$K_2 = \frac{54}{1 + 54 \times .042} = 16.5$$

The final stage of amplification consists of a 6 AQ 5, beampower amplifier. The suppressor grid is connected to the cathode while the screen grid is connected to the plate. The plate voltage B_3 is approximately 275 V. The load resistor is 13,000 ohms. Under these operating conditions the tube characteristics are approximately:

Plate resistance (r_p)	58,000 ohms
Transconductance g_m	4,000 mhos.

$\mu = g_m \times r_p = 232$

The quiescent grid voltage is maintained at - 15 V by a bias battery. The gain for the third stage is computed as:

$$K_3 = \frac{232 \times 13{,}000}{58{,}000 + 13{,}000} = 42.5$$

The output of the power amplifier is connected to a peak voltage rectification circuit as shown in Fig. III-2. This circuit contains a 6 H 6, twin diode, low voltage rectifier in parallel with a 0.1 Meg. resistor and a sensitive multimeter. The combination is in series with a 2 μF capacitor.

The diode will only conduct current when the plate is positive with respect to the cathode. The electrons going from the cathode to the plate will charge up the capacitor, with the positive and negative sides as indicated in Fig. III-4a. The capacitor then gives a continued slow discharge through the .1 Meg. resistor and the meter.

The charge on the capacitor will keep the anode from becoming positive during most of the A.C. cycle. Only when the positive voltage peak of the A.C. voltage becomes larger than the slowly decreasing negative charge of the capacitor plate, the tube will conduct, recharging the capacitor to the peak voltage level.

The variation of the direct voltage across the meter and the bleeding resistor, will therefore be as indicated on an exaggerated scale in Fig. III-4b. With the capacitor and bleeding resistor sufficiently large, these variations become completely negligible. Fig. III-4a also indicates the direction and path of the D.C. current which of course is opposite to the direction in which the electrons travel.

As indicated by Fig. III-1, the input to the amplifier goes via an input transformer. The transformer has a 1:1 ratio and serves merely to isolate the floating ground of the electrode system from the grounded common level of the amplifier. The amplifier was grounded in order to prevent spurious oscillations generated by the tubes on small fluctuations of the bias voltages, random "noise" picked up by the leads, or induction from the filament connections.

As the impedance between the potential electrodes is in some cases of the order of 50,000 Ω the input impedance of the transformer must be at least several Megohms to keep the error introduced by current drawn by the measuring system, below a few per cent. As the total input impedance of the transformer may be represented by the equivalent

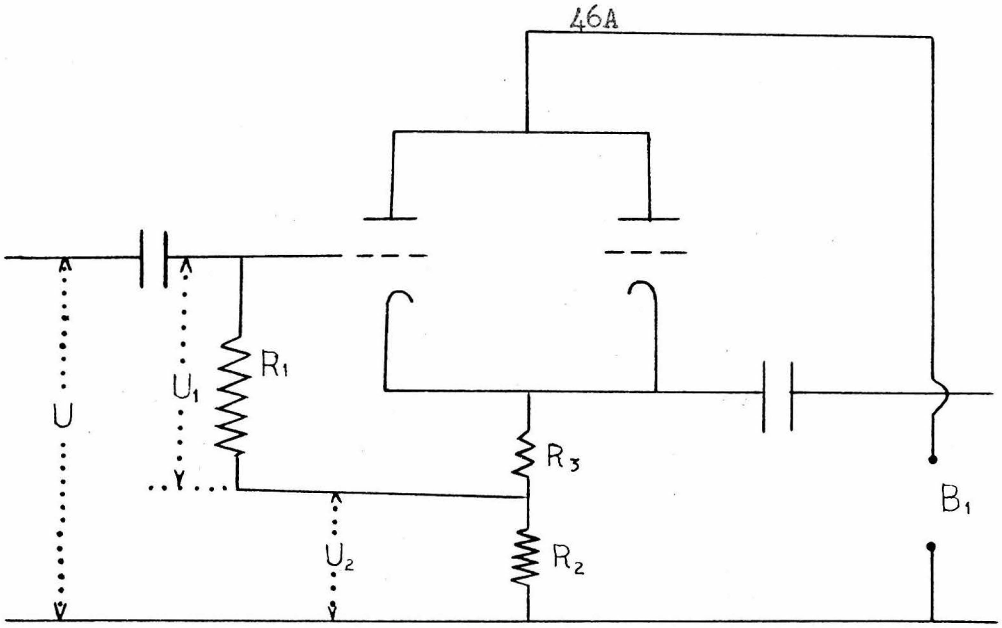

Fig III - 3

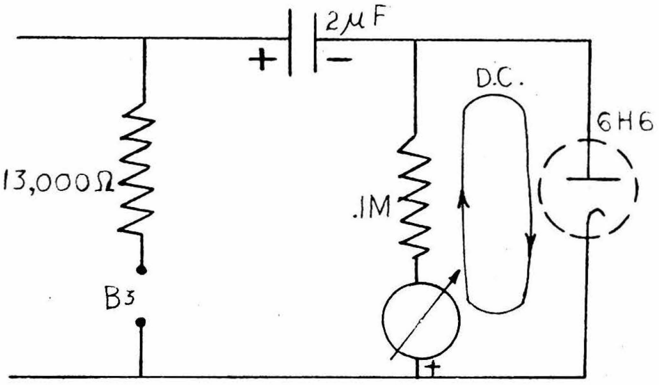

Fig. III - 4a

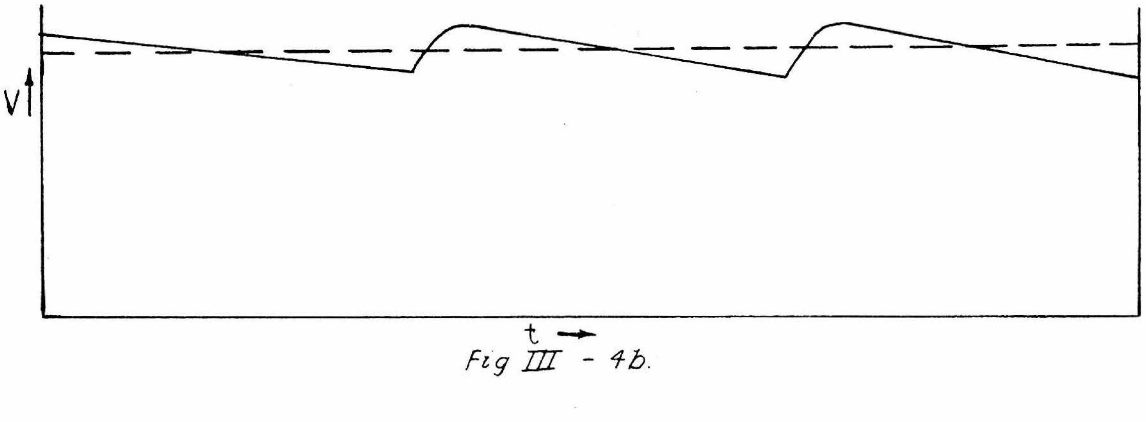

Fig III - 4b.

impedance of the primary with open secondary, in parallel with the load impedance of the secondary, the impedance of the primary must also be several Megohms.

To meet these requirements and also to have sufficient shielding, a special transformer was built by the Pasadena Transformer Engineers Inc. with a primary inductance of 1180 H. For the specifications of this input transformer and the computation of the inductance of the primary see appendix paragraph B. In order to have a sufficiently high primary impedance the frequency used for the measurements was chosen at 1000 cycles. A higher frequency would make capacitive and inductive coupling of some parts of the circuit to ground large enough to cause noticeable inaccuracies. A lower frequency would make the input impedance of the amplifier too small.

At 1000 cycles the primary impedance equals:

$$Z_p = 2\pi f L_p = 7.45 \text{ Megohms}$$

The secondary load impedance was 5.3 Megohms. Therefore the total input impedance for the transformer with its secondary connected to the first stage of the amplifier is:

$$Z_t = \frac{1}{1/Z_p + 1/Z} = 4.5 \text{ Megohms}$$

For an impedance of 50,000 ohms between the potential electrodes the current drawn by the amplifier will be 1% of the total. This is within the permissible limits of accuracy.

The power supply to the amplifier is taken from a power pack of standard design as shown in Fig. III-2.

The transformer has a center tapped main secondary coil giving

350 V on each side. In addition two small coils give 5 V for the filament of the rectifier tube and 6.3 V for the filaments of the amplifier tubes.

The rectifier tube is a No. 80 full-wave rectifier. To insure that the A.C. component in the output will be absolutely negligible, a filter arrangement with three 8H chokes and three 8 μ F capacitors is installed. Each of the three choke-capacitor combinations cuts the A.C. component to about 3% of the value put in.

Finally in order to minimize feedback through the power pack, which might lead to disturbing generations of oscillations in the amplifier, a low impedance path is provided for A.C. across the output terminals, by two 8 μF capacitors.

The voltage B_3 when providing the plate voltage for the 6AQ5 tube, that is, with a 71,000 ohms load across the output, is approximately 300 V, giving an operating plate voltage of 250 V for the beam power amplifier. Similarly B_1 under load conditions is approximately 150 Volts, giving operating plate voltages of 120 V for the 6J6 and 90 Volts for the 7F7.

The supply leads to the amplifier are shielded with 1/2" copper braid.

In order to make the operating conditions as stable as possible the A.C. supply for the power pack and the audio oscillator is obtained via a line voltage stabilizer set at 115 Volts, output voltage, by means of a Variac potentiometer.

While assembling the equipment the behavior of all parts of the circuit was carefully checked with an oscilloscope, to insure that no spurious oscillations were present and that unwanted capacitive and inductive coupling between circuit elements were negligible at all times.

The Electrode Arrangement

As stated before, the resistivity measurements had to be made on the bottom face of cylindrical cores having a diameter of approximately 2.8".

In choosing an electrode arrangement suitable for such measurements the following factors have to be considered:

1. The formulae used for surface measurements of resistivities are all derived for semi-infinite media.

The cores of which the resistivity has to be measured are limited both in depth (or height) and in diameter. The influence of the walls on the potential distribution for a given current are directly dependent upon the spacing and arrangement of the electrodes.

2. In the resistivity formulae it is also assumed that the electrodes are "point electrodes." The error made due to the physical dimensions of the electrodes depends upon the ratio of the distance between current electrodes and potential electrodes and the diameter and amount of penetration of the electrodes.

3. In order to make good contact with the samples the electrodes must be pushed firmly onto the face of the core so that they will penetrate a small amount between the sand grains.

Electrodes of too small a diameter will be flexible and will be bent sidewards by the sand grains. This would continuously change the distance between the points of contact and using predetermined formulae for a supposedly fixed electrode arrangement would give appreciable errors.

The smallest diameter that could be used for firm electrodes that would not be bent by grains of well cemented sandstone was found to be 0.03". Penetration of the electrodes below the surface might be up to 0.05" to make a good contact. For hemispherical electrodes, the error made by assuming the electrodes to be point electrodes will be 1% or less, if the distance at which the measurements are made is larger or equal to 20 times the radius of the electrodes. This gives a lower limit of 0.3" for the distance, the potential electrodes may be separated from the current electrodes.

To estimate the influence of penetration of the electrodes into the medium of which the resistivity is to be measured, on the accuracy of the computation using formulae for point electrodes, the following derivation was made:

Suppose we have a cylindrical electrode of negligible diameter and length B (see Fig. III-5). For an element of length db of the electrode, we may apply the usual formula for point electrodes if db approaches zero. Taking into account the image above the surface we have for a buried point electrode $\varphi = \frac{2I\rho}{4\pi r} = \frac{I\rho}{2\pi r}$ where φ is the potential at a distance r and ρ is the resistivity of the semi-infinite medium.

The potential due to db at a point p, at the surface at a horizontal distance X, from the axis of the electrode, will be:

$$d\varphi_p = \frac{I}{2\pi r} \cdot \frac{db}{B}$$

so that
$$\varphi p = \int_0^B \frac{I\rho}{2\pi B}\,\frac{db}{r} = \frac{I\rho}{2\pi B}\int_0^B \frac{db}{(B^2 + X^2)^{1/2}}$$

$$= \frac{I\rho}{2\pi B}\left[\ln\left\{b + (b^2 + X^2)^{1/2}\right\}\right]_0^B$$

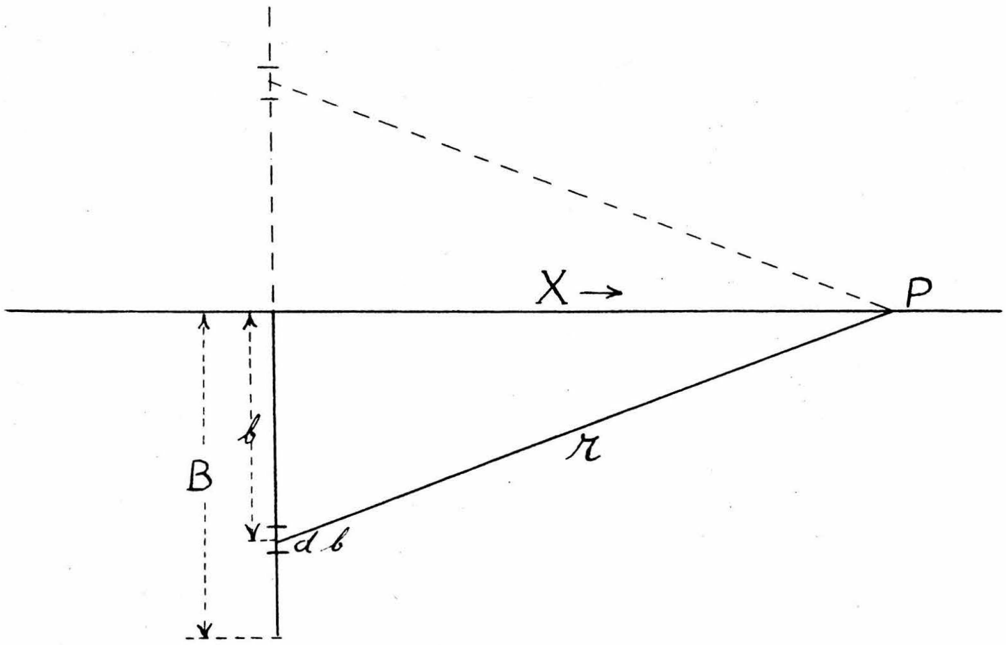

Fig. III-5

$$\varphi_p = \frac{I\rho}{2\pi B}\left[\ln\left\{\frac{B}{X} + \left(\left(\frac{B}{X}\right)^2 + 1\right)^{1/2}\right\}\right]$$

$$= \frac{I\rho}{2\pi X} \cdot \frac{X}{B} \cdot \ln\left\{\frac{B}{X} + \left(\left(\frac{B}{X}\right)^2 + 1\right)^{1/2}\right\}$$

The potential at p due to a point electrode at the surface, emitting the same current would be: $V_p = \frac{I\rho}{2\pi X}$

The error as a percentage of V_p therefore is:

$$\Delta V_p = 100\left[1 - \frac{X}{B}\ln\left\{\frac{B}{X} + \left(\left(\frac{B}{X}\right)^2 + 1\right)^{1/2}\right\}\right]$$

Fig. III-6 represents ΔV_p as a function of B/X. The actual potential is always smaller than the potential due to a point electrode carrying the same current.

We see that for a penetration of 0.05" and X = 0.3", the error is less than 0.3%, so that if we use the lower limit of spacing imposed by the electrode diameter we can neglect the influence of penetration.

The minimum distance between the electrodes being fixed by the above considerations, we must find an arrangement for which the influence of the walls of the cylindrical cores will be as small as possible. It must be pointed out however that the influence of the walls gives a deviation from the formulae used, for which we can make corrections. On the other hand the error due to the deviation from the assumed point electrodes is very difficult to estimate quantitavely, due to the irregularity of the contact. Therefore in compromising between distance from the walls and mutual distance between the electrodes, we will allow a sufficient safety margin above the lower limit, established for the latter theoretically.

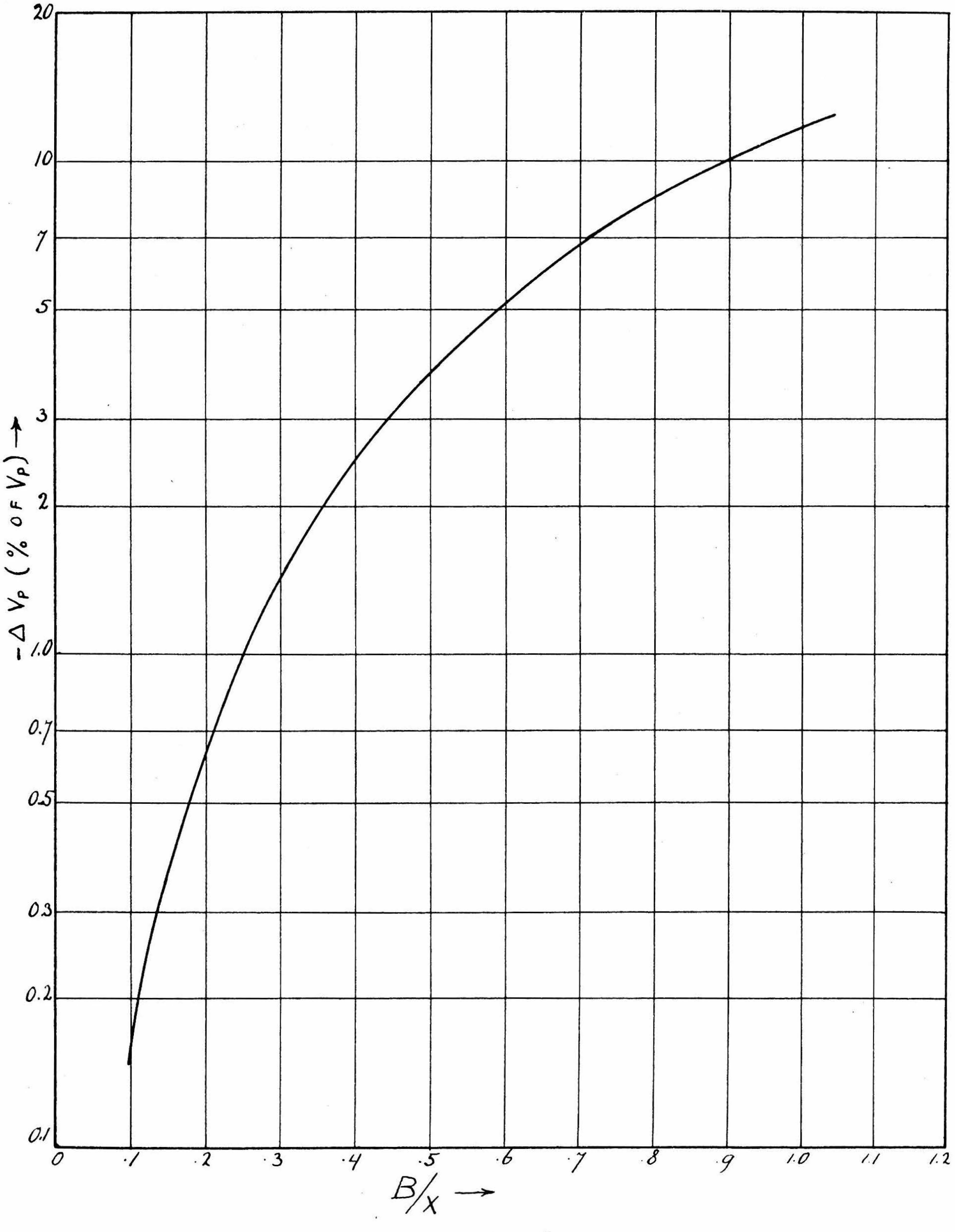

Fig III - 6

Considering possible arrangements that would fit within the circular area of the core-face, it is obvious that the Wenner arrangement, having equally spaced electrodes on a straight line does not make efficient use of the area available.

It seems logical therefore to choose an arrangement in which the current electrodes lie on a diameter of the circular area and the potential electrodes are placed symmetrically above and below that diameter.

In determining the optimum position of the potential electrodes, there is another important factor to be considered, namely the potential gradient in different parts of the field. In general, near the current electrodes the gradient is very steep and small fluctuations of the current or inaccuracies made in the determination of the distances between the electrodes will give relatively large errors in the measured voltages, when the potential electrodes are too close to the current electrodes.

Fig. III-7a gives the potential distribution, on the line connecting the two current electrodes. We see that to minimize the above difficulties the potential electrodes must be located in the central part between 30% and 70% of the distance AB, away from A, where the gradient is less steep.

When the potential electrodes are not located on the line AB we still can determine the zone where the potential gradient is small and about constant by projection of the limiting points P and Q along the equipotential lines through these points. Fig. III-7b shows the equipotential pattern due to two current electrodes and the area in

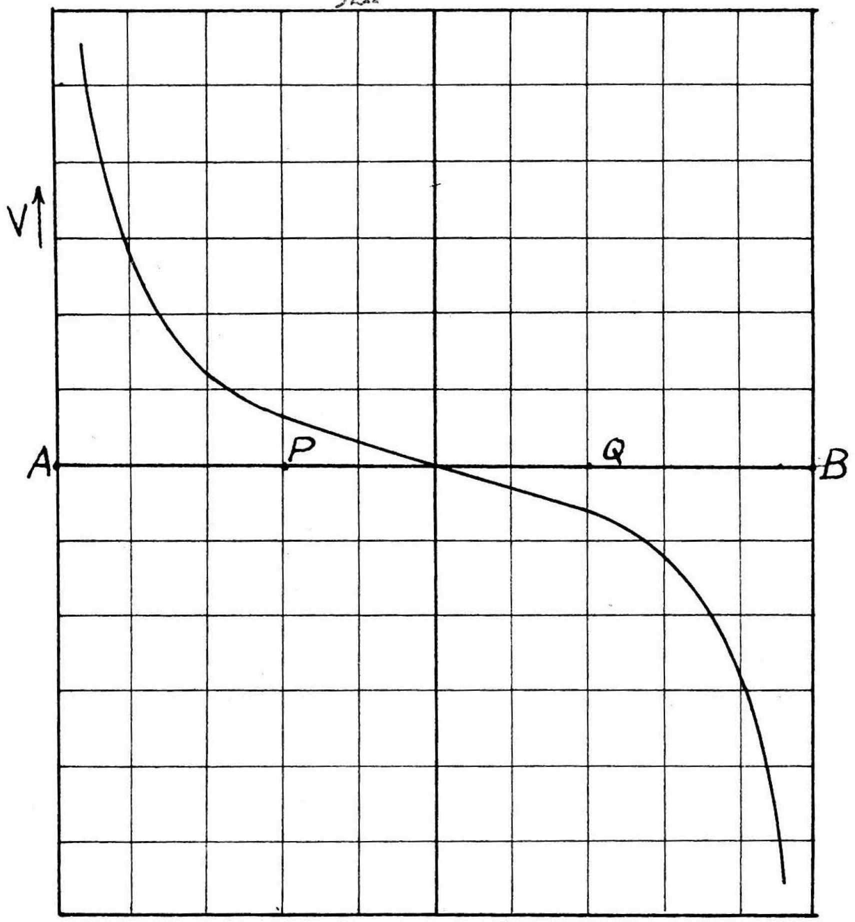

Fig. III - 7a

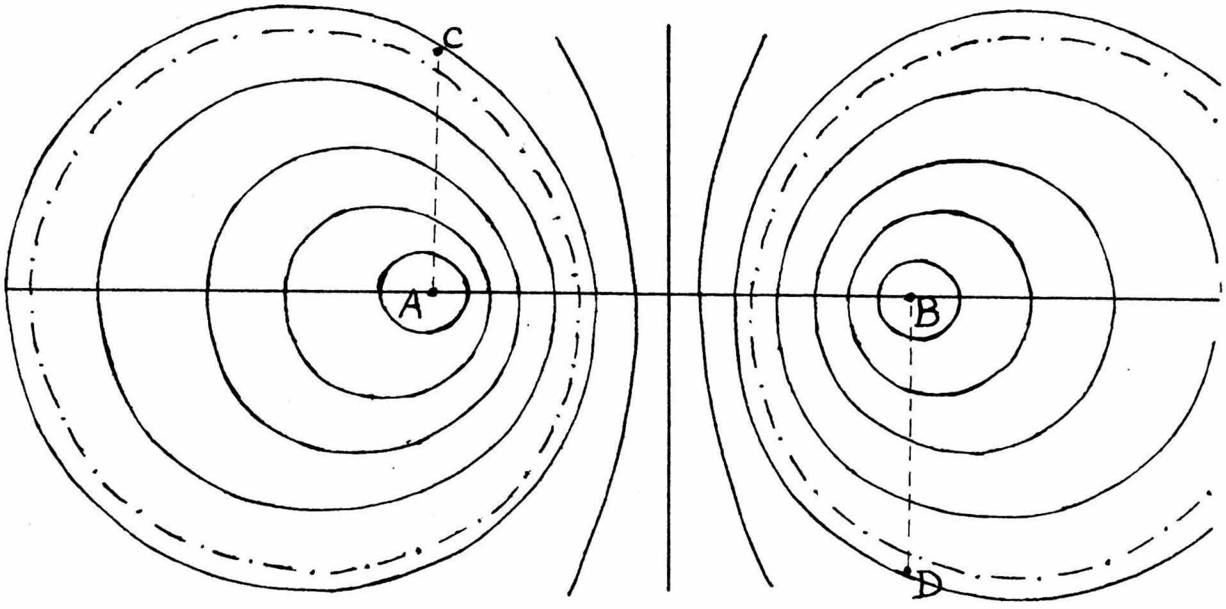

Fig. III - 7b

which the potential electrodes preferably should be located (outside the dashed and dotted lines).

The requirements for the location of the potential electrodes can now be summed up as follows:

1) More than .3" from the current electrodes, preferably $AC = CD > .4"$.

2) Outside the zones of large potential gradient, e.g. outside dashed lines, in Fig. III-7b.

3) Far enough from the circular boundary of the cores to be only moderately affected by the distortion of the lines of current due to these boundaries.

4) Meeting the above three requirements the location should be chosen so as to give the largest possible potential drop for a given current so that inherent errors are, percentage wise, as small as possible.

As can readily be seen part of these requirements tend to move the locations C and D in opposite directions to those required by the other part. Therefore a compromising position must be found.

A good compromise is obtained by placing C and D on lines perpendicular to the diameter through A and B, just outside the dashed lines. This fulfills (1), the distance AC being approximately .45". It obviously satisfies (2), and there are a maximum number of equipotential lines between them, thus satisfying (4). The effect of the boundaries was determined experimentally and found of the order of 10% of the measured voltage. This means that if we can determine the correction factor for the boundary effect with an accuracy of 10% or less, we keep the total error due to the boundaries below 1%.

The preferred positions of C and D are indicated in Fig. III-7b.

Based on the above principles two arrangements were tried out; one with AB = .905" (hereafter referred to as arrangement No. I) and one with AB = .624" (hereafter referred to as arrangement No. II).

Though No. II had slightly less influence of the walls, its sensitivity to the amount of contact area between the sample and the electrodes was considerably greater, making the accuracy with which measurements could be repeated smaller.

Therefore No. I arrangement was adopted for constant use, while No. II was kept for occasional double checks. For both arrangements empirical curves were made giving the effect of the boundary on measured resistivity as a function of the diameter and height of the sample.

The correction to be applied for the affect of the core boundaries was determined experimentally. The empirical data were separated in two groups, one representing the affect of the cylindrical boundary of the core, the other giving the affect of the bottom.

The experiments were carried out in the following manner:

A series of cylindrical glasses varying in diameter from 5.8" to 2.85" were cut down to a height of approximately 2" and then filled with water of a given resistivity to the exact height of 1.9".

Then the electrodes were put, in a symmetrical, central position above the water level and lowered to make contact with the water, care being taken that the penetration was always close to 0.5". Then the apparent resistivities were measured and plotted against the diameter

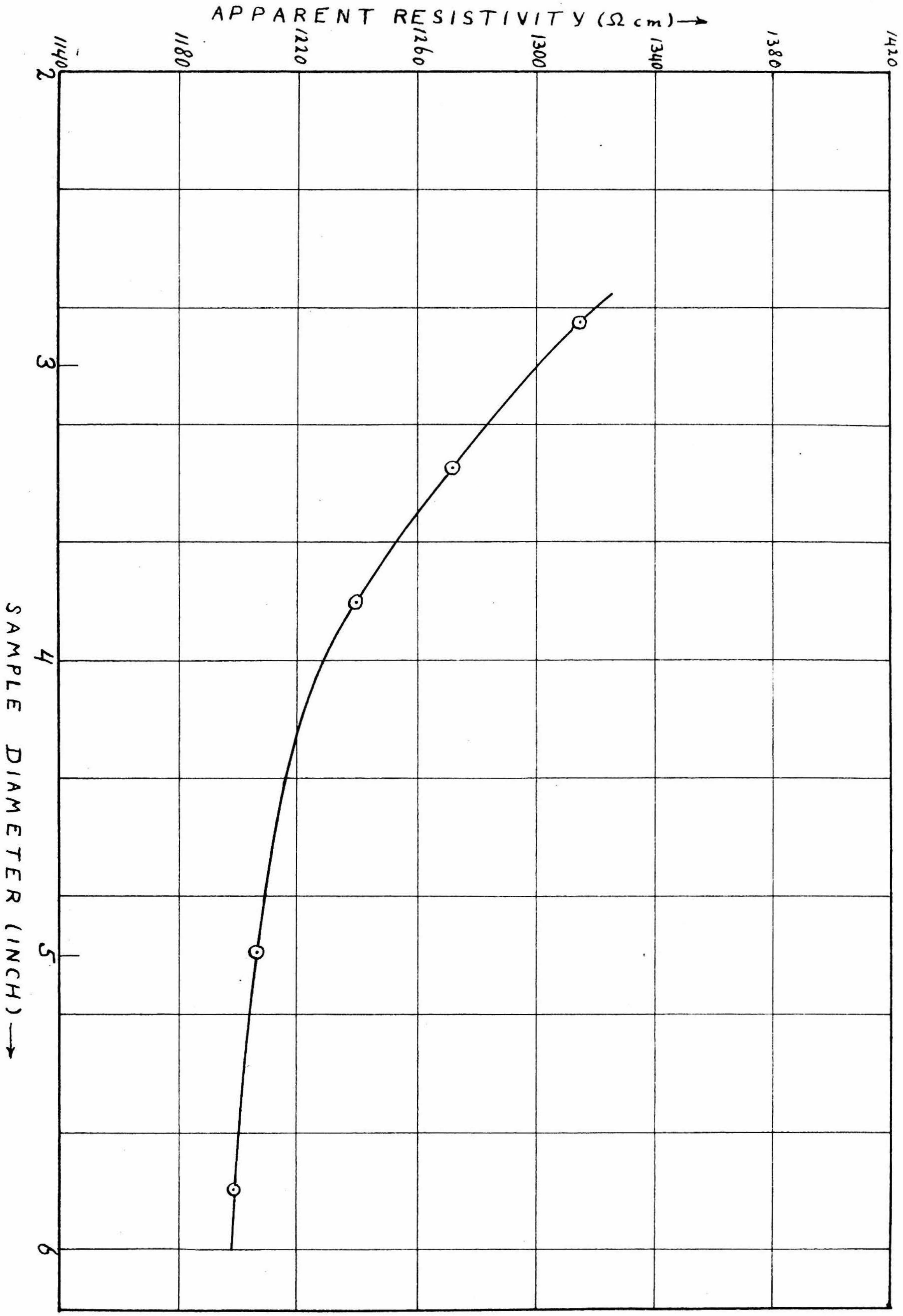
APPARENT RESISTIVITY (Ω cm)→
1140
1180
1220
1260
1300
1340
1380
1420
2
3
4
5
6
SAMPLE DIAMETER (INCH)→

Fig. III-8

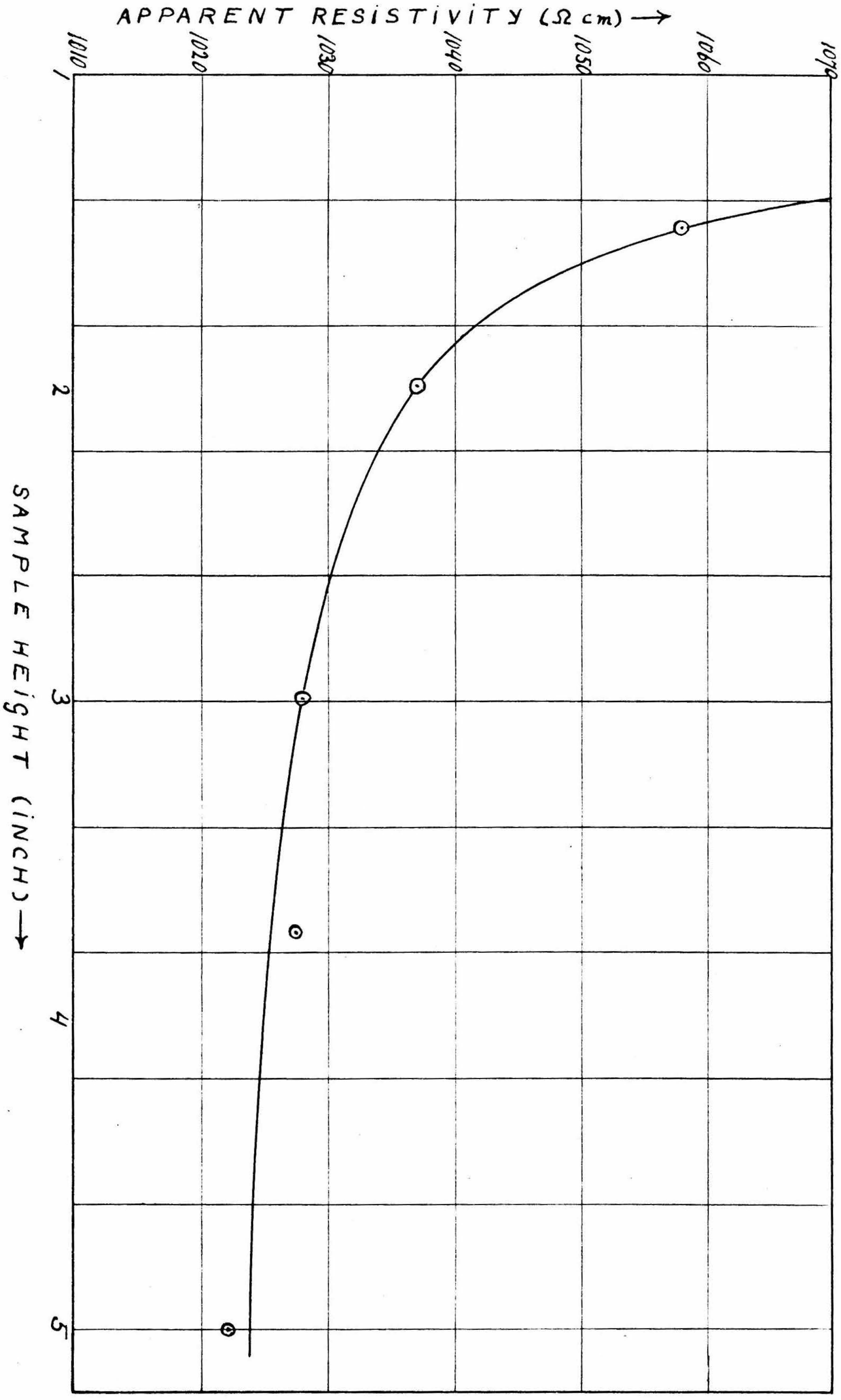
APPARENT RESISTIVITY (Ω cm) →
1010
1020
1030
1040
1050
1060
1070
SAMPLE HEIGHT (INCH) →
1
2
3
4
5

Fig. III - 9

of the glasses (I.D.). An example of the results obtained is given by Fig. III-8.

The same type of measurements were made with a series of glasses of the same diameter (2") and a height varying from 5" to 1.5" and the results were plotted giving the apparent resistivity as a function of the height of the glasses. (See Fig. III-9)

These measurements were repeated for various water resistivity over a range varying from 55 Ω cm to 15,000 Ω cm. The true resistivities were determined by measurements in a large container after preliminary measurements had shown that its walls had a negligible effect on the resistivity measured at its center.

From curves of the type of Fig. III-8 and Fig. III-9, the deviations were measured as a percentage of true resistivity. For a given height or diameter these deviations were independent of the water resistivity which also follows readily from the fact that in all cases the ratio of the resistivity outside the boundaries and the water resistivity is infinite. If beyond the boundaries is a medium of finite resistivity, ρ_2, the effect on the apparent water resistivity is a function of the factor $K = \dfrac{\rho_2 - \rho_1}{\rho_2 + \rho_1}$

However if $\rho_2 = \infty$ we have $K = \dfrac{1 - \rho_1/\rho_2}{1 + \rho_1/\rho_2} = 1 =$ constant. The deviations determined by a sufficient large number of experiments were averaged and then plotted as indicated by Fig. III-10 and Fig. III-11. The latter figures were determined for arrangement No. I and throughout the later experiments on the sandstone cores they were used to compute the correction factors to be applied to find the true resistivities of

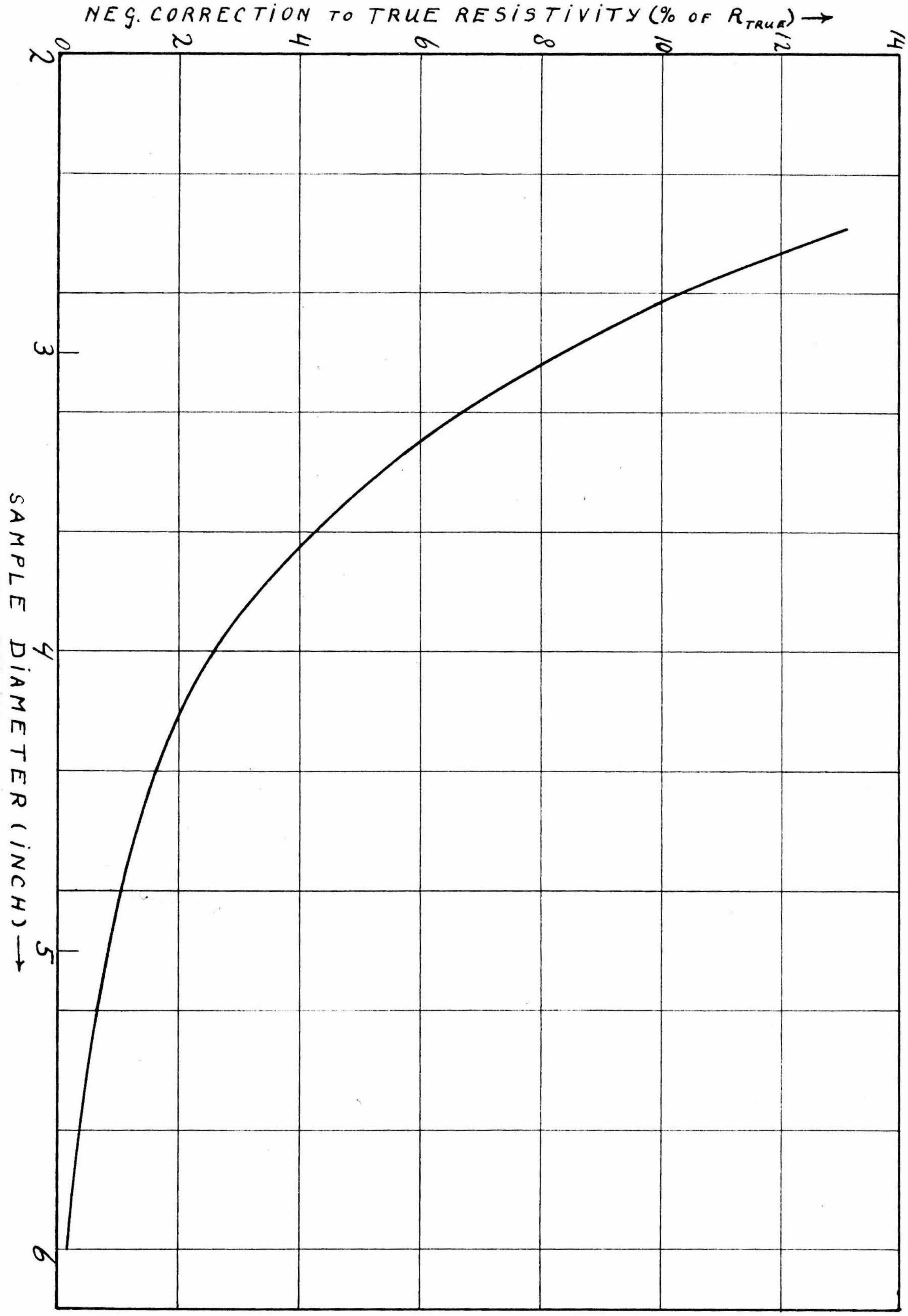
NEG. CORRECTION TO TRUE RESISTIVITY (% of R_{TRUE}) →
0
2
4
6
8
10
12
14
2
3
4
5
6
SAMPLE DIAMETER (INCH) →

Fig. III-10

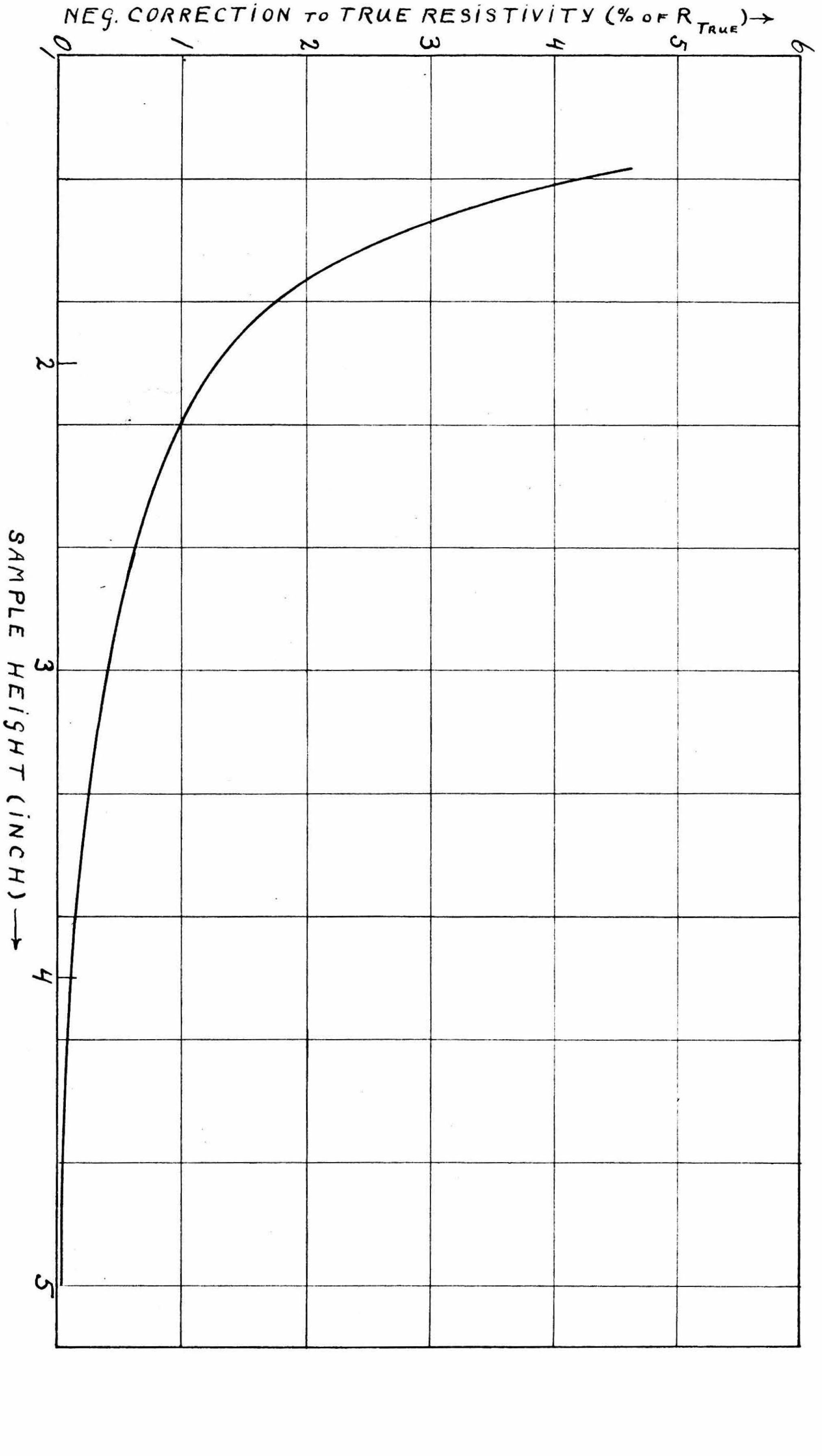
NEG. CORRECTION TO TRUE RESISTIVITY (% OF R_{TRUE}) →
0
1
2
3
4
5
6
2
3
4
5
SAMPLE HEIGHT (INCH) →

Fig. III-11

the cores.

Similar curves were made for arrangement No. II. To check whether the order of magnitude of the corrections agrees with what theoretically might be expected, we have calculated the effect of a straight boundary on a Wenner arrangement under the conditions of a similar resistivity ratio and relative distances.

The calculation was made using Tagg's formulae (11):

$$\rho_a = \rho_1 \left[1 + 4\, k\, \frac{d}{a} \left(\frac{1}{4d^2/a^2 - 4} - \frac{1}{4d^2/a^2 - 1} \right) \right] \qquad (3\text{-}4)$$

Here $_a$ is the apparent resistivity, $_1$ the water resistivity and $k = 1$. d = distance from center of electrode arrangement to the boundary = 1.5" for a sample of 3" diameter. $a = \frac{AB}{3}$ for the Wenner arrangement, so that $d/a = 4.5$. Substituting these values in (3-4) we have:

$$\rho_a = \rho_1 \left[1 + 18 \left(\frac{1}{6.8} - \frac{1}{9.8} \right) \right] = 1.09\, \rho_1$$

This means a correction of 9% has to be made to obtain ρ_1 from ρ_a. This is of the same order of magnitude as the corrections determined experimentally for our arrangement. It must be pointed out however that the conditions of our tests are much different from the ones assumed for the above calculation, the most important fact being that in our case boundaries occur at both ends. This would double the correction to be applied. Our correction, though of the same order of magnitude, is considerably lower, which indicates clearly the advantage of our arrangement over a Wenner arrangement in the case of circular boundaries.

The electrode sets were constructed in the following manner:

Steel nails of 0.5" length and .072" diameter were soldered onto the bottom end of small tie points. Then the plastic top of the tie-point was fitted into a piece of steel tubing (O.D. =.462") flush with the rim of that tubing. The lower part of the tie point was centered by a snuggly fitting lucite collar, while the space in between was filled up with a mixture of beeswax and rosin. The bottom part of the steel tubing was sealed around the nail with shellac, thus providing at all points a firm connection and good insulation between the electrode and the steel shielding. The end of the nail was filed to a blunt point, thus decreasing the diameter at the point of contact with the surface of the sample to approximately .03". The end of the electrodes protruding below the shielding was about .35" long.

The four electrodes were placed into a piece of 1/2" thick lucite (4" x 5") and cemented in place by Duco cement, the distances being approximately as indicated before.

After the electrodes were thus firmly sealed in their permanent places, the exact distances between the centers of the electrode points were measured with a micrometer. These measurements are listed below for arrangements I and II, and were used to compute the resistivity measured in terms of current and voltage drop.

Arrangement I (Fig. III-12):

AC = .446"   BD = .486"   AB = .905"   CD = 1.283"
AD = 1.040"   BC = .975"

$$\Delta V = \frac{I\rho}{2\pi}\left\{\left(\frac{1}{.446}+\frac{1}{.486}\right)-\left(\frac{1}{1.040}+\frac{1}{.975}\right)\right\}\frac{1}{2.54}$$

or $\rho = \frac{\Delta V}{I} \times 6.744\ \Omega\ \text{cm}$

Instead if I, the voltage drop $(\quad V)_I$ across a standard resistor R_I in the current circuit was measured so that we can substitute $I = \frac{(\Delta V)_I}{R_I}$ which gives:

$$\rho = \frac{\Delta V}{(\Delta V)_I} \times R_I \times 6.74 \ \Omega \text{ cm}$$

For arrangement II:

AC = .423" DB = .478" AB = .607" CD = 1.124"

AD = .759" BC = .801"

For these distances $\rho = \frac{\Delta V}{(\Delta V)_I} \times R_I \times 8.45 \ \Omega \text{ cm}$

The electric connections with the rest of the circuit were made by single pole plugs, fitting the tie points. They were soldered onto the electrode leads and fitted with shellac into steel tubing of .462" I.D.

The braid shielding of the leads was connected to the steel electrode shielding by 1/2" steel braid clamped over the upper part of the steel tubing.

The protruding edge of the plug shielding fitted tightly over the shielding of the tie points, thus making a good connection electrically.

The plug-in system was made in order to facilitate interchanging arrangements No. I and No. II.

Electrolyte Resistivity Cell

To follow the changes in resistivity of the effluent water, which was necessary in some of the experiments, the apparatus described before had to be adapted to measure the resistivity of small quantities of electrolytes.

This was done in the following manner:

A small cylindrical glass container of 1.5" diameter and 0.4" depth was placed concentrically inside a larger shallow beaker of similar shape and approximately 3 inches in diameter.

The upper edge of this beaker was cut off straight and fitted snugly in a groove cut in the lucite plate in which the electrodes are mounted. This groove was concentric with the geometric center of the electrodes. The height of the larger beaker was chosen such that upon placing the rim of the beaker in the circular groove, the points of the electrodes would just reach into the smaller container. To make a measurement the latter would be filled with a carefully measured quantity (12 cm^3) of the electrolyte of which the resistivity was to be determined, and the points of the electrodes would be dipped into the liquid by placing the lucite plate over the rim of the larger beaker, fitting the latter in the circular groove of the plate.

To insure that the position of the electrode points, with respect to the small container and the fluid level, was identical for all measurements, a mark on the large beaker was lined up with a mark on the lucite plate when placing the beaker in position and the entire system was leveled using a two dimension spirit level, placed on the lucite plate.

Because of the fixed configuration the resistivity of the electrolyte to be determined is equal to the apparent resistivity as measured in the small container times a constant correction factor, which corresponds to the cell-constant of a Kohlrausch cell.

This constant was determined by measuring the apparent resistivity of electrolytes of which the actual resistivity was found by measurements on large quantities (approx. 500 cc) using our conventional measuring system.

PART IV

Experimental Procedure

The larger part of the experiments were carried out with samples taken from outcrops of formations that are oil bearing in nearby regions.

Prominent among these are the following types:

1) A very pure quartzitic sandstone (Berea formation, lower Mississippian, Ohio)*

2) Sandstone from the Pico formation (lower Pliocene, California)

3) Sandstones from the ~~Modello~~ Modelo formation (upper Miocene, California)

Other types of sandstone used were:

1) Saugus (Pliocene - land laid)

2) A very tight Mesozoic sandstone, probably Jurassic, from outcrops near Redlands, California.

Thinsection (point-counter) analyses and sieve analyses of most of the sandstones used are given in another theses by this author (10).

To start an experiment, a cylindrical core of approximately 2.8" diameter and 2" height would be mounted in the bottom part of a cylinder of a baroid wall-building tester as described in Part III. Care had to be taken that the flat surfaces were left free and clean.

After mounting the core, the cylinder plus core would be weighed on a balance, accurate to one-tenth of a gram. The cylinder would then be placed in the baroid tester and dry CO_2 gas was forced through the core for about one-half hour. For this purpose a top lid of the baroid

---

* Obtained by the courtesy of the Union Oil Co., Production Department, Whittier, California.

tester was connected to a 40 lb. carbon dioxide bottle. The carbon dioxide would effectively replace all of the air present in the interstices of the core. After this a measured amount of water would be forced, repeatedly through the core until the resistivity of the core as measured with the four electrode system would no longer change indicating that no more gas was being removed from the core. To allow any trapped CO_2 to be completely dissolved in the water, the flushing was interrupted frequently for several hours. When resistivity became constant it was assumed that the core was 100% saturated with water. At this time the cylinder was weighed again and the difference, equalling the difference in dry and wet weight, of the core, in grams was taken to be equal to the porosity, in cubic centimeters. Using the predetermined dimensions of the core the porosity as percentage of total volume was easily computed. For several cores these porosity determinations were checked against values of porosities found from thinsections by the point counter method, and it appeared that the latter values were often a few per cent larger. This is probably due to isolated pores (non-effective porespace) which show up in the sections, but not in the measurements by imbibition. Apart from this deviation overall agreement was very satisfactory.

During flushing the water was forced through the core using nitrogen gas from a large nitrogen bottle. Rather than changing connections, two separate lines for the baroid tester were used, one permanently fitted to the connection of the carbon dioxide bottle, the other connected to the nitrogen bottle.

All core resistivities were measured by the four electrode system and amplifying circuit described in Part III. Electrolyte (water) resistivities were measured in the same way if sufficient quantities were available. For quantities smaller than 300 cc, the electrolyte resistivity cell was used.

The permeability was determined by measuring the amount of water that would flow through the core in a measured length of time under a measured pressure gradient (approximately 5 psi per inch).

The baroid tester was always used, complete with a copper screen and two rubber gaskets at the bottom and one rubber gasket at the top, to seal the lid.

After the above preliminary measurements were completed, oil, salt water or drilling mud could be placed in the upper part of the cylinder and forced to filtrate through the core.

The oil saturations, however, were mostly obtained by the capillary pressure method, using special adapters to fit the baroid cylinders. (10)

Gas-oil or gas-water mixtures could be created in the core by letting nitrogen gas escape through the core (with no liquid in the upper part of the cylinder).

As described in Part III, the drilling muds were mixed from dry powders of aquagel, zeogel, kaoline, baroid and natural clays (obtained by courtesy of the Baroid Sales Division, Los Angeles, California).

The mixing was done with a high speed soil dispersion mixer, using mixing times of approximately one hour. This gave sufficiently stable muds for our purposes. (12)

As the filtration of drilling mud is a slow process taking approximately 24 hours to obtain 100 cm of effluent filtrate from the core, the filtrate was collected in a glass bottle by a filter funnel, the bottle being closed by a rubber stopper to minimize evaporation. After given amounts of filtration the pressure was released and the resistivity of the core measured.

Additional measurements were made of the resistivity of the effluent filtrate at different times, using the electrolyte resistivity cell.

When obtaining oil saturations by the capillary pressure method, differential pressures across the oil-water interfaces up to 25 psi were used. At this pressure the "irreducible" water saturation was approached very closely for most of the samples used. The extracted water was measured in a small graduate cylinder connected by a rubber hose and glass tubing to the outlet of the baroid tester. At the end of the extraction an additional check on the amount of water extracted was made by weighing the cylinder containing the core together with the remaining oil and the adapter.

Comparison with a similar weight measurement before the extraction gave an accurate check on the amount of water removed. The volumetric and weight measurement gave very close agreement differences averaging not more than 1% of the computed saturation.

Finally upon completion of the oil saturation the resistivity of the core was measured.

After the required oil saturation was reached, the sample could be flushed with water and the resistivity change measured at regular intervals. Also the amounts of oil and water in the effluent mixture are measured volumetrically as accurate as possible.

When carrying out resistivity measurements on the cores, the pointed electrodes, were brought into good contact with the surface of the sample by pressing firmly downward on the lucite plate, supporting the electrodes. Care had to be taken that the pressure was applied evenly.

All voltages were measured on the same scale of the multimeter. Always the largest one of the voltages between the potential electrodes and across the standard resistor in the current circuit, was measured first and adjusted by the output regulator of the oscillator to read at the top part of the multimeter scale. Then, without any changes to the main circuit, the amplifier input was changed to the other voltage via the central switch board. After reading the second voltage, the amplifier would be plugged back to the first one and another reading was taken of the first voltage. The two readings for the first voltage were averaged and the obtained value used together with the second voltage reading. This procedure was used to allow for small changes in the current electrodes during the measurement.

The entire measurement was always repeated for a lower oscillator output, thus obtaining two independent readings for the voltage-current ratios, used for the resistivity computations.

PART V

Theory of the Displacement of the Non-Wetting Phase by Water During Radial Infiltration

The mechanism of fluid displacement in sands has been treated for the case of uni-directional flow by Buckley and Leverett (13).

A brief outline will be given of the part of their discussion that is of interest to our case, whereupon derivations will be made to apply to the case of radial infiltration.

For simplicity we will confine our reasoning to the case of an oil sand being flushed by water; but the same principles apply equally well to gas sands.

The net rate of accumulation of the displacing fluid which is equal to the net oil displacement will be proportional to the difference between the rate at which the displacing fluid enters any given volume of the sand and the rate at which it leaves that same volume.

Confining our attention to a unit volume of the sand and denoting the total fluid flow through this volume in cm^3/sec by p, and the fractions of the fluid flow comprising of water when entering and leaving the volume respectively by a and a' we have:

Entering the unit volume: ap cm^3 of water per second

Leaving the unit volume: $a'p$ cm^3 of water per second

Remaining in the unit volume: $p\ (a - a') = \Delta ap$ cm^3 of water per second

Δa is the rate of accumulation of the water in the unit volume.

If S_W is the water saturation and θ denotes time we may write therefore:

$$\frac{\partial S_W}{\partial \theta} = \frac{\Delta ap}{\varphi} \quad \text{where } \varphi \text{ is the fractional porosity.}$$

If u indicates length in the direction of the fluid flow we can write the following material balance:

$$\left(\frac{\partial S_W}{\partial \theta}\right)_u = \frac{-q_T}{A\varphi}\left(\frac{\partial f_W}{\partial u}\right)_\theta \tag{5-1}$$

Here we have replaced a by the infinitesimal ratio $\frac{\partial f_W}{\partial u}$, where f_W is the fraction of the flow comprising the displacing fluid ($f_W \equiv a$). And instead of p (the flow through 1 cm^3 cross-sectional area) we write the ratio of the total flow, q_T over the total cross-sectional area (A).

Equation (5-1) may be transformed in the following manner:

Let $\frac{q_T}{A\varphi} = \lambda$ We then may write:

$$\left(\frac{\partial S_W}{\partial \theta}\right)_u = -\lambda\left(\frac{\partial f_W}{\partial S_W}\right)_\theta\left(\frac{\partial S_W}{\partial u}\right)_\theta \tag{5-2}$$

As will be shown later f_W is a function of S_W only when we neglect capillary and gravitational forces. Therefore

$$S_W = S_W(u_1, \theta)$$

We now impose the additional condition S_W = constant with time, that is we concentrate our attention upon the progression of the locus of points for which S_W has a certain constant value.

This implies that:

$$\frac{dS_W}{d\theta} = \left(\frac{\partial S_W}{\partial \theta}\right)_u + \left(\frac{\partial S_W}{\partial u}\right)_\theta \left(\frac{\partial u}{\partial \theta}\right)_{S_W} = 0 \quad \text{or} \quad \left(\frac{\partial u}{\partial \theta}\right)_{S_W} = -\frac{\left(\frac{\partial S_W}{\partial \theta}\right)_u}{\left(\frac{\partial S_W}{\partial u}\right)_\theta}$$

Substituting the expression for $\left(\frac{\partial S_W}{\partial \theta}\right)_u$ from (5-2) we have:

$$\left(\frac{\partial x}{\partial \theta}\right)_{S_w} = \lambda\left(\frac{\partial f_w}{\partial S_w}\right)_\theta = \frac{q_T}{A\,\varphi}\left(\frac{\partial f_w}{\partial S_w}\right)_\theta \qquad (5\text{-}3)$$

For the case of uni-directional flow the locus of points for which S_w constant, is a plane perpendicular to the direction of flow.

Equation (5-3) states that the rate of advance of such plane where a certain fixed saturation prevails, is proportional to the change in composition of the flowing stream, caused by a small change in saturation of the displacing fluid.

Neglecting the effects of capillarity and gravity, f_w is related to the properties of the system in the following manner:

$$f_w = \frac{K_w/\mu_w}{K_w/\mu_w + K_o/\mu_o} = \frac{1}{1 + \frac{K_o\mu_w}{K_w\mu_o}} \qquad (5\text{-}4)$$

where K_w and K_o are the relative permeabilities of the sand to water and oil respectively while μ_w and μ_o are the viscosities of the water and the oil.

Relation (5-4) follows directly from the definitions of relative permeabilities.

A representative value for the absolute viscosity of a 30° A.P.I. gravity oil under reservoir conditions is 2 centipoises so that $\frac{\mu_w}{\mu_o} \approx \frac{1}{2}$ if we assume $\mu_w = 1$ centipoise. Using equation (5-4) we can determine f_w as a function of S_w from the relationships of relative permeabilities to water saturation, which have been determined experimentally both for oil and gas-water mixtures, for various unconsolidated sands and for consolidated sandstones (14, 15, 16, 17).

Referring back to equation (5-3) the basic relation between the position along the path of flow, saturation and time may be written as

$$\Delta u = \frac{Q_T}{A} \left(\frac{d\, f_W}{d\, S_W}\right) \Delta \theta$$

or in terms of total amount of displacing fluid entering the system (Q_T):

$$u = \frac{Q_T}{A} \frac{d\, f_W}{d\, S_W} + C \qquad (5\text{-}5)$$

For $Q_T = 0$ we have $u = (u_{S_W})_o$ so that $C = (u_{S_W})_o$ = distance at which a given S_W occurs initially.

Displacement in the Case of Radial Flow

Consider a sector of a cylindrical slab of permeable rock into which radial infiltration takes place with its apex at the center of the drill hole. Let the intersected surface area of the boreface be 1 cm^2. If the radial flow per 1 cm^2 of the boreface is again p cm^3/sec, we see that p cm^3 of fluid flow through any concentric section of our sector in one second. The sector as described above is shown in Fig. V-1.

We now consider a small section of the sector, of which the center is at a distance of u cm from the boreface and which width and height are both 1 cm. The curved boundaries of this section will vary from $\frac{(r_o + u - \frac{1}{2})}{r_o}$ to $\frac{(r_o + u + \frac{1}{2})}{r_o}$ where r_o is the drill hole diameter.

The volume of this section is $\frac{\pi(r_o + u + \frac{1}{2})^2 - \pi(r_o + u - \frac{1}{2})^2}{2\, r_o} = \frac{r_o + u}{r_o}$. Again if a and a' indicate the fractions of water in the influent and effluent mixtures and $\Delta a = a - a'$ we have:

In $\frac{r_o + u}{r_o}$ cm^3 remain Δa p cm^3 of water per sec. so that

$$\left(\frac{\partial S_W}{\partial \theta}\right)_u = \frac{\Delta a\, p}{\varphi\left(\frac{r_o + u}{r_o}\right)} \quad \text{or} \quad \left(\frac{\partial S_W}{\partial \theta}\right)_u = \frac{-q_T}{A\varphi}\left(\frac{\partial f_W}{\partial u}\right)_\theta \frac{r_o}{r_o + u} \qquad (5\text{-}6)$$

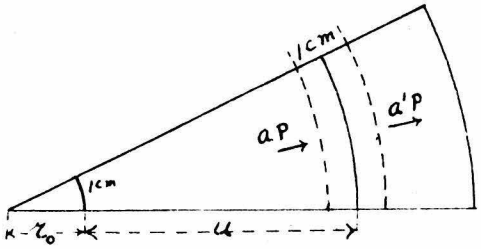

Fig. V-1

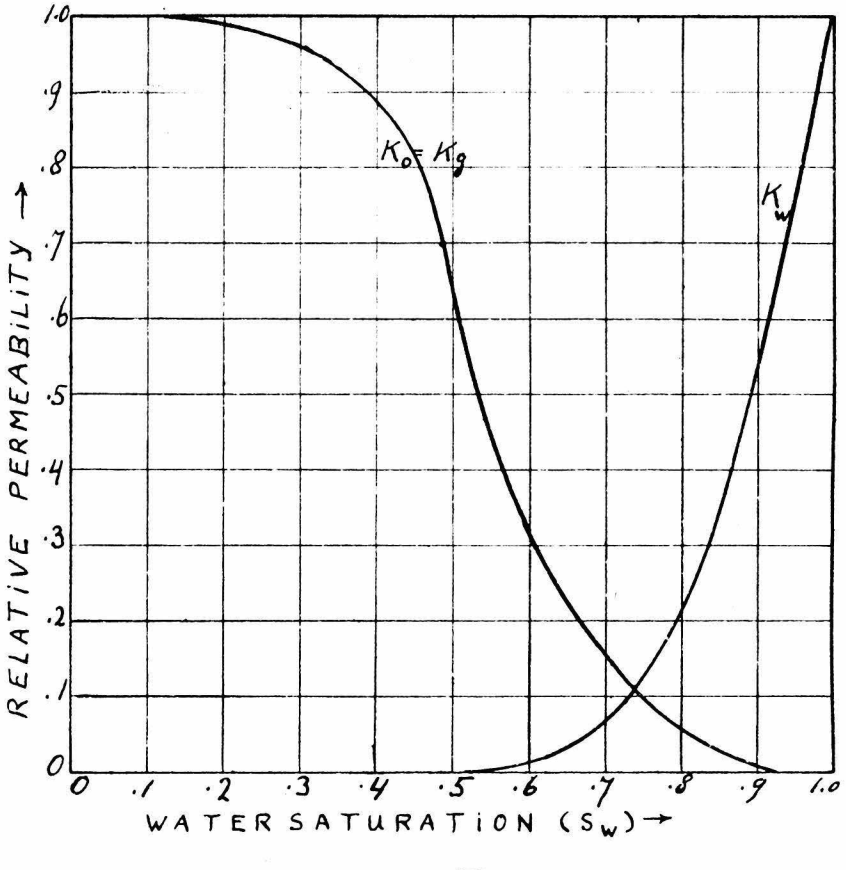

Fig. V-2
(AFTER BOTSET)

The minus sign is necessitated by the fact that f_w decreases with increasing u.

A is the surface of the boreface of the sandsection under consideration.

In a similar manner as described for the case of uni-directional flow, equation (5-6) may be transformed into:

$$\left(\frac{\partial u}{\partial \theta}\right)_{S_w} = \frac{q_T}{\varphi A}\left(\frac{\partial f_w}{\partial S_w}\right)_\theta \quad \frac{r_o}{u + r_o}$$

or in terms of the total amount of water infiltration:

$$\int_0^u (u + r_o)\, d\, u = \frac{r_o}{\varphi A}\left(\frac{\partial f_w}{\partial S_w}\right)_\theta \int_0^\theta q_T\, d\theta$$

or $$\frac{u^2}{2} + u\, r_o + C = \frac{r_o}{\varphi A}\left(\frac{\partial f_w}{\partial S_w}\right) Q_T \qquad (5\text{-}7)$$

For $Q_T = 0$, that is before infiltration has started, S_w will be equal to the connate water saturation of the undisturbed formation and will be the same for all radial distances from the boreface. The discontinuity at the boreface may be replaced by a continuous increase of S_w from its actual value in the formation to 1.0 between $u = + 0$ and $u = - 0$. All values of S_w that will be found within the infiltrated zone after infiltration has taken place for a given length of time, may therefore be assumed to exist initially in the interval between $u = + 0$ and $u = - 0$. From the initial condition $u_{S_w} = 0$ for $Q_T = 0$ we find from equation (5-7) that $C = 0$ so that we may write: $u^2 - 2\, u\, r_o - 2P = 0$

with $$P = \frac{r_o}{\varphi A}\left(\frac{d\, f_w}{d\, S_w}\right) Q_T$$

This gives $$u \quad \frac{-\, 2\, r_o \pm (4\, r_o^2 + 8P)^{\frac{1}{2}}}{2}$$

and as u is always positive this becomes:

$$u = (r_o^2 + 2\,p)^{\frac{1}{2}} - r_o \qquad (5\text{-}8)$$

For a given Q_T we can calculate therefore at which distance from the boreface an arbitrary saturation will prevail, if the initial saturation and the relative permeability versus saturation relationships are known.

Rose (18) has shown that the relative permeability characteristics for both wetting and non-wetting phase, are dependent only on the saturation values at which the respective relative permeabilities become zero. These values in turn are closely related to the bound water content of the formations. We may assume therefore that all rocks with the same bound water content, have roughly the same relative permeability saturation characteristics and it seems likely therefore that there exists a fixed relationship between the saturation distribution in the infiltrated zone and the bound water content of the formation.

The above assumptions are supported by the work of Tixier (19) who obtained a reasonable correlation between the average water saturation in the infiltrated zone and the original water content of the formations, from field studies in the Rocky Mountain oil fields.

For thick oil sands the initial connate water content is approximately equal to the irreducible or bound water saturation in the entire section, except for a transition zone near the bottom of the sand.

Unfortunately data in the literature giving relative permeabilities and bound water contents are very scarce.

Some data are given in a paper by E. R. Brownscombe et al (20) and some information could be assembled from independent papers on experiments performed on the same type of sandstone.

As a first example we will use the data published on Nichols Buff sandstone.

The relative permeability relationships were experimentally determined by Botset (16) and are reproduced in Fig. V-2.

Fig. V-3 gives f_W for $\frac{\mu_W}{\mu_o} = \frac{1}{2}$ and $\mu_W/\mu_o = .06$ while Fig. V-4 gives $\frac{d\ f_W}{d\ S_W}$ versus S_W for the same two cases. Rose estimates the bound water content for the Nichols Buff sandstone to be approximately .35 .

From Figs. V-3 and V-4 and using equation (5-8) we can compute the infiltrated zone saturation distribution assuming the initial connate water content to be equal to the irreducible water saturation $(S_W)_o = .35$. As we are considering only the effects of lateral invasion the initial saturation is constant for all values of $u > 0$.

From evaluation of experimental results to be described later, we know that an infiltration of 25 cm^3 through each cm^2 of the boreface represents an average amount of infiltration in most cases. For the sake of simplicity we will assume that

$$r_o = 10 \text{ cm } (d_o \approx 8") \qquad \text{and} \qquad \varphi = .25$$

We have then: $u = (100 + 2P)^{\frac{1}{2}} - 10$

$$\text{and} \qquad P = \frac{10}{.25} \times \frac{25\ d\ f_W}{d\ S_W} = \frac{1000\ d\ f_W}{d\ S_W}$$

$$\text{or} \qquad u = 10\left(1 + \frac{20\ d\ f_W}{d\ S_W}\right)^{1/2} - 10 \qquad (5\text{-}8a)$$

The saturation distribution for this case is now computed graphically by taking u as absissa and S_W as ordinate.

The initial distribution is thus represented by a straight horizontal

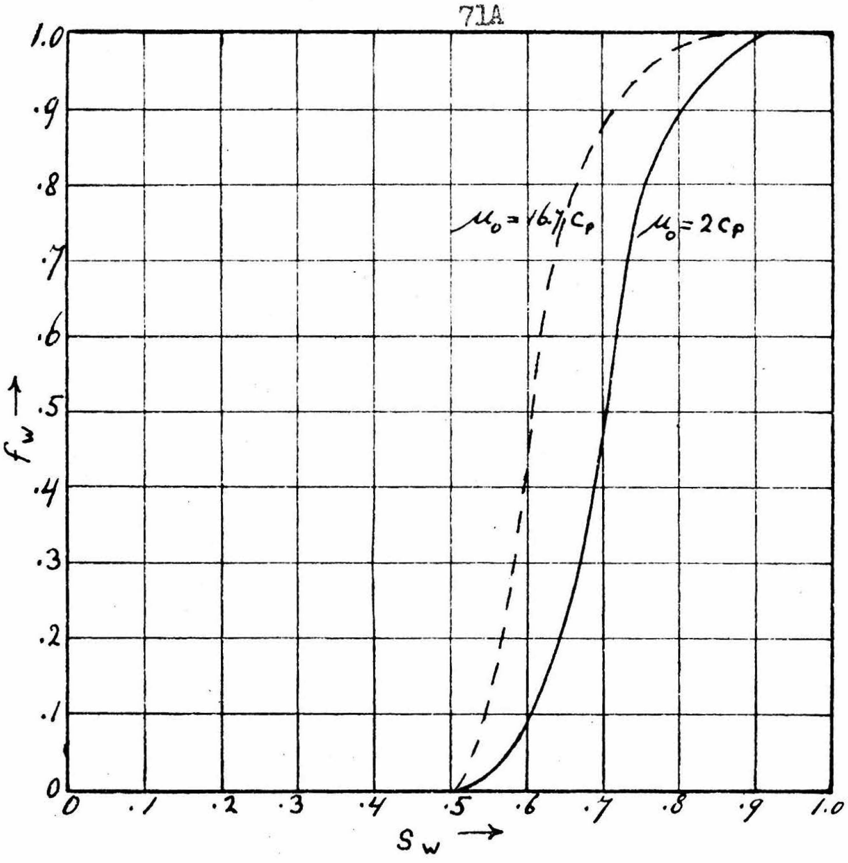
1.0
.9
.8
.7
.6
.5
.4
.3
.2
.1
0
f_w
0
.1
.2
.3
.4
.5
.6
.7
.8
.9
1.0
S_w
$\mu_o = 16.7\,c_p$
$\mu_o = 2\,c_p$

Fig. V-3

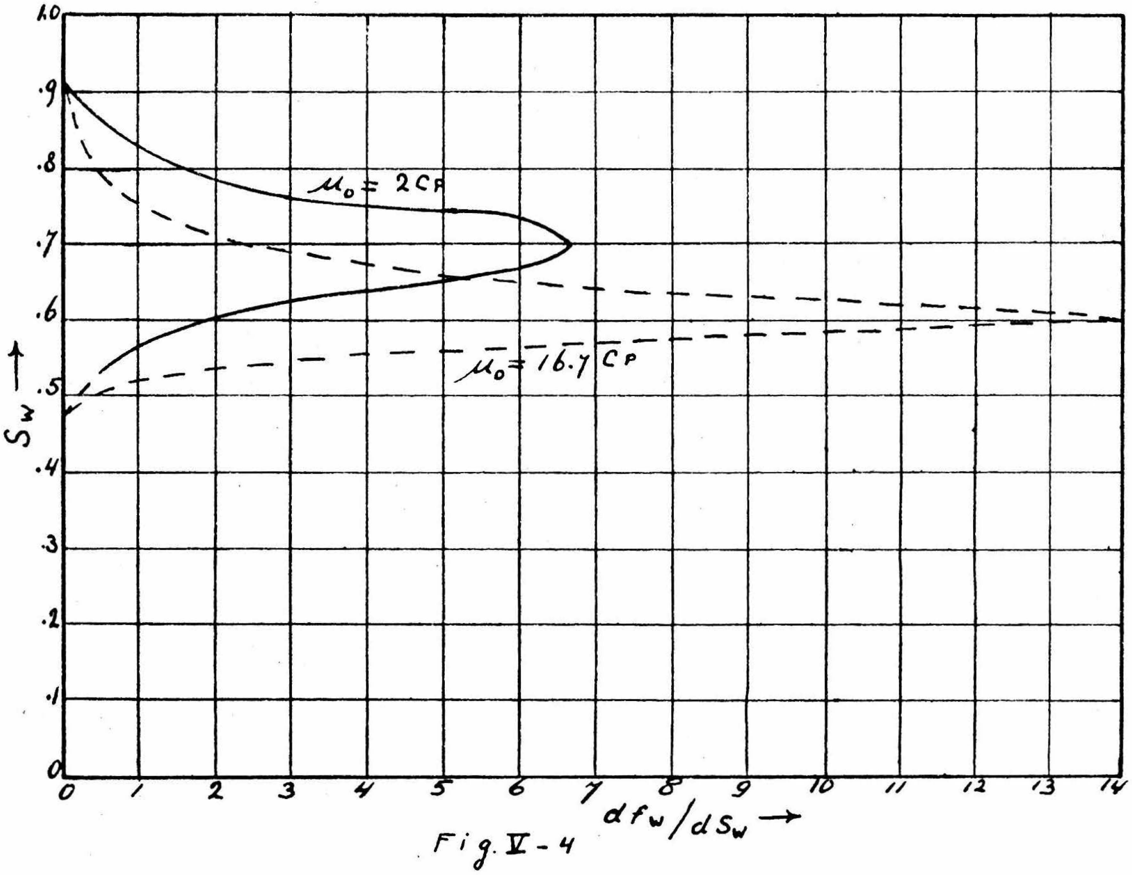
1.0
.9
.8
.7
.6
.5
.4
.3
.2
.1
0
S_w
0
1
2
3
4
5
6
7
8
9
10
11
12
13
14
df_w/dS_w
$\mu_o = 2\,c_p$
$\mu_o = 16.7\,c_p$

Fig. V - 4

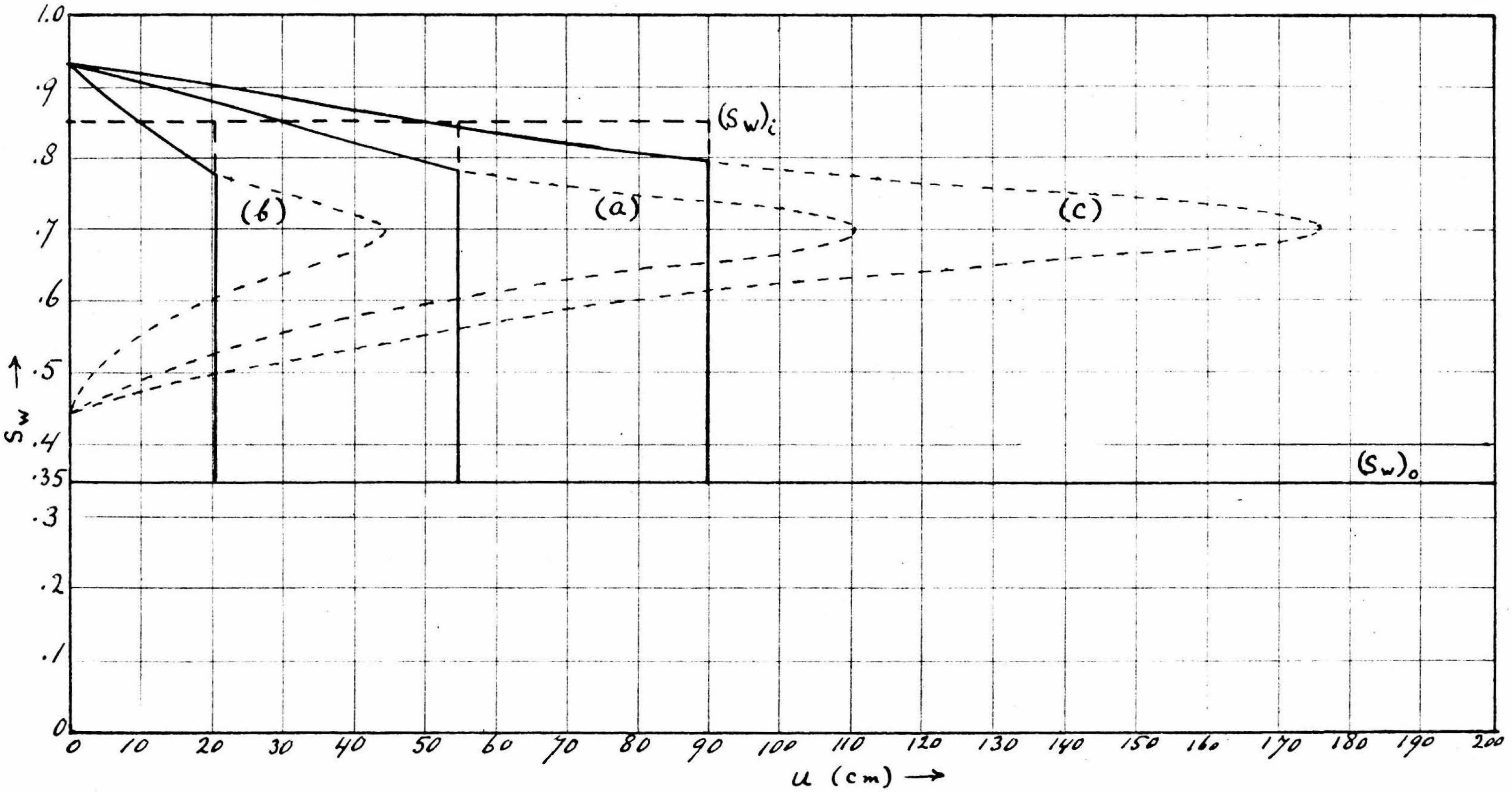
1.0
.9
.8
.7
.6
.5
.4
.35
.3
.2
.1
0
S_w →
0
10
20
30
40
50
60
70
80
90
100
110
120
130
140
150
160
170
180
190
200
u (cm) →
$(S_w)_i$
$(S_w)_o$
(a)
(b)
(c)

Fig. V-5

line ($S_w = .35$) from $u = 0$ to $u = \infty$ and a straight vertical line ($u = 0$) from $S_w = .35$ to $S_w = 1.0$. For all values of S_w we now calculate u from equation (5-8a). The resulting saturation distribution is plotted by laying off from any point S_w on the initial curve a distance equal to u on a line parallel to the absisca. The resulting curve is shown in Fig. V-5.

We see that the curve for S_w and u is multiple valued for all values of u.

Buckley and Leverett obtained a similar result for the case of uni-directional flow. Obviously this result is a physical impossibility. As pointed out by Buckley and Leverett, the correct interpretation is that a portion of the curve is imaginary and that the real saturation versus distance graph is discontinuous with a discontinuity at a certain point u_1.

To find u_1 we must make a new material balance based on the fact that in the sector under consideration the total inflow equals the fractional increase in water saturation times the pore volume in which the increase takes place.

The latter part of the equality may be represented by

$$\int_0^{u_1} A \, \frac{r_0 + u}{r_0} \cdot \varphi \cdot \Delta(S_w)_u \, d\, u$$

and we have therefore

$$\int_0^{u_1} \frac{r_0 + u}{r_0} \cdot \Delta\, (S_w)_u \, d\, u = \frac{Q_T}{A\,\varphi} = \frac{25}{.25} = 100$$

The integrand is plotted and u_1 is determined such that the area under the curve between the ordinates $u = 0$ and $u = u_1$ equals 100.

Due to effects of capillarity the actual saturation graph will have no sharp discontinuity but the corners will be somewhat rounded. The discontinuity (or the steep part) of the saturation distribution curve coincides with what is termed the outer boundary of the invaded zone and the radius of the invaded zone equals $r_o - u_1$.

We see that the saturation in the invaded zone is not constant, but varies with the radial distance from the boreface. For practical purposes however, it may be approximated by a constant saturation of intermediate magnitude. In our example this value would be at $S_w = .85$.

It might be expected that the degree of infiltration will influence the average saturation within the invaded zone. To check this possibility the saturation distribution will be computed for two other invasion diameters.

We will first compute the distribution in the case of little infiltration. Let $\frac{(Q_T)_2}{A} = 5 \text{ cm}^3$ then $\frac{(Q_T)_2}{A\,\varphi} = 20$ and $P = 200 \frac{d\,f_w}{d\,S_w}$ so that $u = 10\,(1 - 4\,\frac{d\,f_w}{d\,S_w})^{\frac{1}{2}} - 10$.

The resulting values for u are plotted in Fig. V-5 curve (b) and the relation:

$$\int_0^{u_2} \frac{r_o + u}{r_o} \cdot \Delta\,(S_w)_u\, d\,u = \frac{(Q_T)_2}{A\,\varphi} = 20$$

is solved graphically for u_2.

We obtain $u_2 = 20.4$ cm. This means $d_1 = 30.4$ cm and $d_1/d_o = 3.04$.

We see that in this case the subordinate phase of displacement is more prominent, that is the saturation within the infiltrated zone changes more rapidly with radial distance than in the case of larger infiltration. Approximating the actual distribution again by a constant, $(S_w)_1$, we find however that the average saturation has not changed appreciably and is still approximately .85 .

Finally we will compute the saturation distribution for large infiltration. Let $\frac{(Q_T)_3}{A} = 60$ so that $\frac{(Q_T)_3}{\varphi A} = 240$ and $P = 2400 \frac{d\, f_W}{d\, S_W}$.

This gives: $u = 10 \left(1 + 48 \frac{d\, f_W}{d\, S_W}\right)^{\frac{1}{2}} - 10$

The resulting values for u are plotted in Fig. V-5, curve (c).

From $\int_0^{u_3} \frac{r_o + u}{r_o} \cdot \Delta (S_W)_u \, d\, u = \frac{(Q_T)_3}{A \varphi} = 240$

we find $u_3 = 90$ cm or $d_i = 10\, d_o$.

We observe that for large infiltration radii, the subordinate phase of displacement is really unimportant and the assumption of a constant infiltrated zone saturation is very reasonable. The average saturation still equals .85 .

The above computations lead us to the following conclusions:

The approximation of the infiltrated zone saturation distribution by a constant, for oil sands, is more accurate for large radii of infiltration, than for smaller ones.

The average saturation of the infiltrated zone of an oil sand $(S_W)_i$ is independent of the amount of infiltration.

Effect of the Viscosity of the Non-Wetting Phase

In the preceding paragraphs the residual saturation in the infiltrated zone was computed for a certain type of sandstone and a viscosity ratio $\frac{\mu_W}{\mu_O} = \frac{1}{2}$.

The latter is a good value for gas saturated crudes under average reservoir conditions. However, most of our laboratory investigations

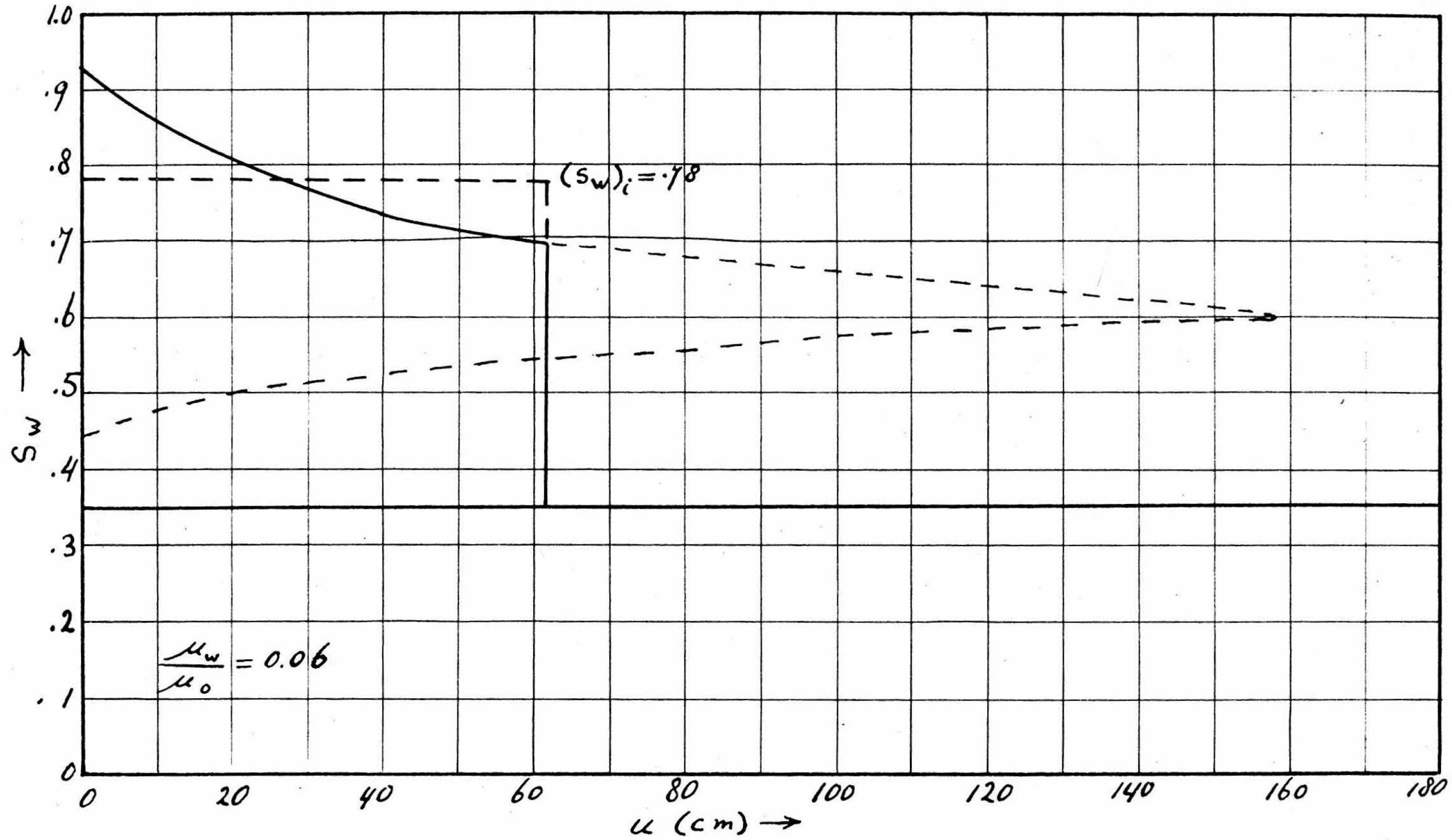
1.0
.9
.8
.7
.6
.5
.4
.3
.2
.1
0
S_w →
$(S_w)_i = .78$
$\frac{\mu_w}{\mu_o} = 0.06$
0
20
40
60
80
100
120
140
160
180
u (cm) →

Fig. V - 6

were carried out using a 30.2° A.P.I. gravity oil at approximately 70° F and atmospheric pressure.

The viscosity of the oil under these conditions is in the neighborhood of 17 centipoises. This value was taken from a graph given by Beal (21) relating absolute viscosity to degrees of gravity for gas-free crudes at various temperatures.

In order to convert the laboratory data to reservoir conditions, we will compute the residual oil saturation for the same sandstone as above and a viscosity ratio

$$\frac{\mu_W}{\mu_o} = 0.06 \quad (\text{or } \mu_o = 16.7 \text{ cp}).$$

$\frac{df_W}{dS_W}$ as a function of S_W is given in Fig. V-4.

As the influence of amount of invasion was shown to be negligible, we will only carry out the computation for average invasion $(\frac{Q_T}{A}) = 25$.

For this case we had: $u = 10\left(1 - 20\frac{d\,f_W}{d\,S_W}\right)^{\frac{1}{2}} - 10$

The corresponding saturation distribution is given in Fig. V-6. The location of the discontinuity (boundary of invaded zone) was found, by the method described before, to be 61.6 cm from the boreface.

We see that $(S_W)_1 = .78$ or almost 9% smaller than in the case of displacement of oil of 2 cp.

It must be pointed out here that the computation of saturation distributions by the above method depends strongly on the extreme values of the saturations at which the oil and water relative permeabilities become zero. These have heretofore not been determined with sufficient accuracy to make the above method of quantitative importance. However, the method is very useful in outlining qualitative relationships.

Infiltration and Displacements of Non-Wetting Phase In Gas Sands

In a gas sand the theoretical irreducible water saturation is probably smaller than for the same sand partially saturated with oil. However, in practice, capillary pressures are limited in magnitude and the actual water saturation prevailing in the larger part of a thick gas sand will be close to the irreducible or bound water saturation as defined in the case of an oil sand.

As pointed out by Rose (18), for a given reservoir rock, the gas-relative permeability, in the case of a gas-water system equals the oil-relative permeability in the case of an oil-water system. Also the water-relative permeability is independent of the nature of the non-wetting phase.

The computation of the saturation distribution upon invasion of a gas sand will furnish us therefore, additional information on the relationship between infiltrated zone saturation and non-wetting phase viscosities.

A representative value for the ratio of the gas-viscosity over the water-viscosity is: $\mu_g/\mu_w = 0.02$

This gives:

$$f_w = \frac{1}{1 + \frac{K_g \mu_w}{K_w \mu_g}} = \frac{1}{1 + 50\, K_g/K_w}$$

The computed f_w is given in terms of its natural logarithm in Fig. V-7. The required values for K_w and $K_g = K_o$ were taken again from the relative permeability data for the Nichols Buff sandstone. (See Fig. V-2)

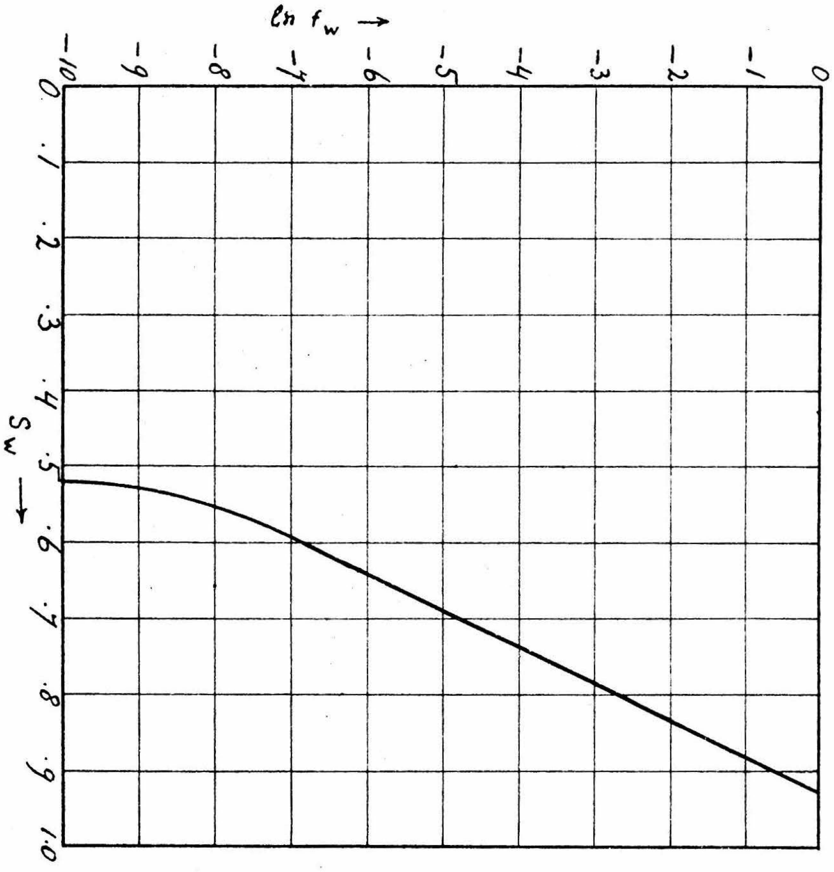

Fig. VI-7

$\frac{d\,f_w}{d\,S_w}$ was computed using:

$$\frac{d \ln f_w}{d\,S_w} = \frac{d \ln f_w}{d\,f_w}\,\frac{d\,f_w}{d\,S_w} = \frac{1}{f_w}\,\frac{d\,f_w}{d\,S_w}$$

The values of the various quantities are tabulated in Table V-A:

TABLE V-A

S_w	f_w	$\ln f_w$	$\frac{d \ln f_w}{d\,S_w}$	$\frac{d\,f_w}{d\,S_w}$
.5	0	-8.1	30	.014
.55	.00046	-8.1	30	.014
.60	.0010	-6.9	20.7	.020
.70	.0083	-4.79	20.7	.172
.80	.0725	-2.61	20.7	1.50
.85	.187	-1.71	20.7	3.98
.88	.374	-1.08	23.3	8.73
.89	.454	-0.79	23.3	10.6
.90	.520	-0.65	24.0	12.5
.91	.71	-0.342	33.0	25.0
.92	1.00	0	0	0

Using again the formula: $u = 10\,(1 + 20\,\frac{d\,f_w}{d\,S_w})^{\frac{1}{2}} - 10$

we find u as a function of S_w (See Fig. V-8).

For the distance of the discontinuity to the boreface we find

$u_1 = 50.25$ cm

As the upper branch of the graph of $u = g(S_w)$ varies only between $S_w = .92$ and $S_w = .91$ the infiltrated zone saturation lies between these limits for all interior points of that zone, regardless of the

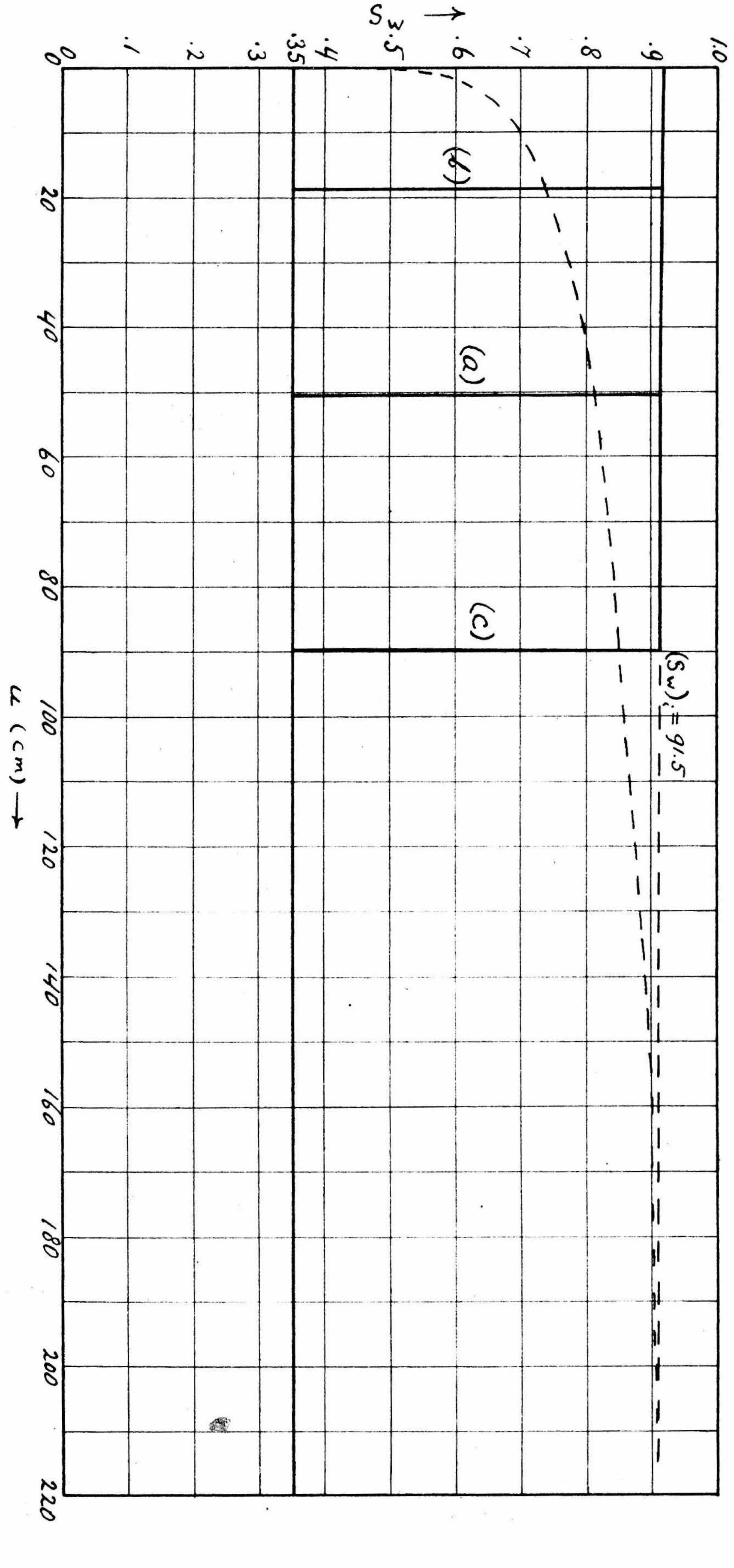
S3.5 →
0
.1
.2
.3
.35
.4
.5
.6
.7
.8
.9
1.0
(b)
(a)
(c)
(Sw)i = 91.5
u (cm) →
0
20
40
60
80
100
120
140
160
180
200
220

Fig. V-8

amount of infiltration. Fig. V-8 shows the saturation profile for two other radii of infiltration, namely:

$r_i = 28.6$ cm ($u = 18.6$) and $r_i = 100$ cm ($u = 90$ cm)

For the relation between the water saturation of the infiltrated zone and the viscosity of the non-wetting phase, for Nichols Buff sandstone, the assembled data are given in Table V-B:

TABLE V-B

μ_o	μ_w/μ_o	$(S_w)_i$
16.7	0.06	.78
2	0.5	.85
0.02	50	.91

We see from Table V-B that the dependence of $(S_w)_i$ on the non-wetting phase viscosity is larger in the region of low viscosities (crude oils) than in the region of high viscosities (natural gases).

Influence of the Rate of Infiltration on the Invaded Zone Saturation

For oil-water mixtures, Leverett (15) has demonstrated that the relative permeabilities depend to some extent on the factor $\frac{\pi N}{P D}$ where π is the displacement pressure of the sand to the non-wetting phase, N the length of the sample, $\frac{P}{N}$ the pressure gradient and D the average pore diameter.

This complex parameter can be reduced to a simpler form in the following manner.

As shown by Rose and Bruce (22) we may write for the displacement pressure:

$$\pi = \gamma \left(\frac{1}{k}\right)^{\frac{1}{2}} \quad (K/f)^{-\frac{1}{2}}$$

where γ is the interfacial tension for the fluid system in question, k is the Kozeny constant of the rock,   its specific permeability and f its fractional porosity.

For simplicity we write $\pi = C_1 \left(\frac{K}{f}\right)^{\frac{1}{2}}$ with C_1 depending only on the Kozeny constant and being therefore nearly constant for most clean sands.

The average pore diameter as used by Leverett was defined by

$D = 5.63 \times 10^{-4} (K/f)^{\frac{1}{2}}$ or $D = C_2 (K/f)^{\frac{1}{2}}$

We have therefore:

$$\frac{\pi N}{P\ D} = \frac{C_1}{P/N\ C_2\ (\ K/f)} = C_3 \frac{f}{P/N \cdot K}$$

Finally the quantity K x P/N is proportional to the rate of flow, F, so that $\frac{\pi N}{P\ D} \approx C \frac{f}{F}$.

The fractional porosity (f) of reservoir rocks will differ for various formations at most by a factor of two or three and plays therefore a minor role in the determination of the infiltration characteristics.

A quantitative analysis of the factors controlling the role of mud invasion, around bore holes was given by Williams (23).

The computations carried out by Williams showed that an average value for the rate of mud infiltration (ν) into a permeable formation is 0.10 bbls/hr/ft (expressed as bbls of filtrate lost from the hole per hr., per foot of hole). Extreme values for this quantity are 1.00 and 0.01 bbls/hr/ft representing an extremely rapid and an extremely slow rate of infiltration.

The experiments and calculations by Williams also show that for a given speed of circulation of the drilling mud, the rate of radial invasion of the mud filtrate is independent of time. As the mudcake is very impervious, in comparison to the reservoir rocks, the rate of invasion is essentially only dependent upon the mudcake characteristics and the total differential pressure between the mud and the formation.

For radial flow, the cross-section perpendicular to the flow is proportional to the distance from the center of the hole. The rate of flow through a unit cross-section therefore is inversely proportional to the radial distance from the axis of the hole. Thus between the outer points of an infiltrated zone with a diameter 10 times the hole diameter and the points near the boreface, in the same zone, there exists a difference of a factor 10, in the rate of flow.

To obtain an estimate of the importance of the difference and variations in the rate of flow with regard to the saturation distribution in the infiltrated zone, we will use the experimental data given by Leverett (24).

These data represent the relations between f_w and S_w for pressure gradients ranging from 9 cm H_g/cm^2 to 0.06 cm H_g/cm^2 obtained on a sand of 1.04 darcies permeability. These values are equivalent to a water flow of .012 cm^3 and $.82 \times 10^{-4}$ cm^3 per cm^2 cross-section per second.

The infiltration rates as given by Williams, compare to this as follows for an 8" hole:

1 bbl/hr/ft of hole = .166 $cm^3/sec/cm^2$ of boreface

0.1 bbl/hr/ft of hole = .0166 $cm^3/sec/cm^2$ of boreface

0.01 bbl/hr/ft of hole = .00166 $cm^3/sec/cm^2$ of boreface

At a distance of 9 times the radius of the hole from the boreface, these values become respectively:

.0166, .00166 and 1.66×10^{-4} $cm^3/sec/cm^2$

We see that Leverett's data cover most of the range of actually occurring rates of infiltration.

Fig. V-9 gives f_w as a function of S_w for F = .012 $cm^3/sec/cm^2$ and Fig. V-10 gives the same relationship for F = $.82 \times 10^{-4}$ $cm^3/sec/cm^2$ as presented by Leverett.

Figs. V-9 and V-10 also show $\frac{d\ f_w}{d\ S_w}$ as a function of S_w for both cases.

The water saturation distribution is again computed in the manner previously described, for average invasion diameter.

The results are shown in Fig. V-11. Curve (a) gives the saturation distribution for F = .012 and curve (b) shows the distribution for F = $.82 \times 10^{-4} cm^3/sec/cm^2$.

The distribution graph for average infiltration rate for this particular sand, will be between the two curves just below curve (a).

We see that there is a marked difference between the average infiltrated zone saturations, for the two extreme cases (81.5% water saturation in case a) as compared to 72% for case (b).

Here again it must be stressed that these values only give an

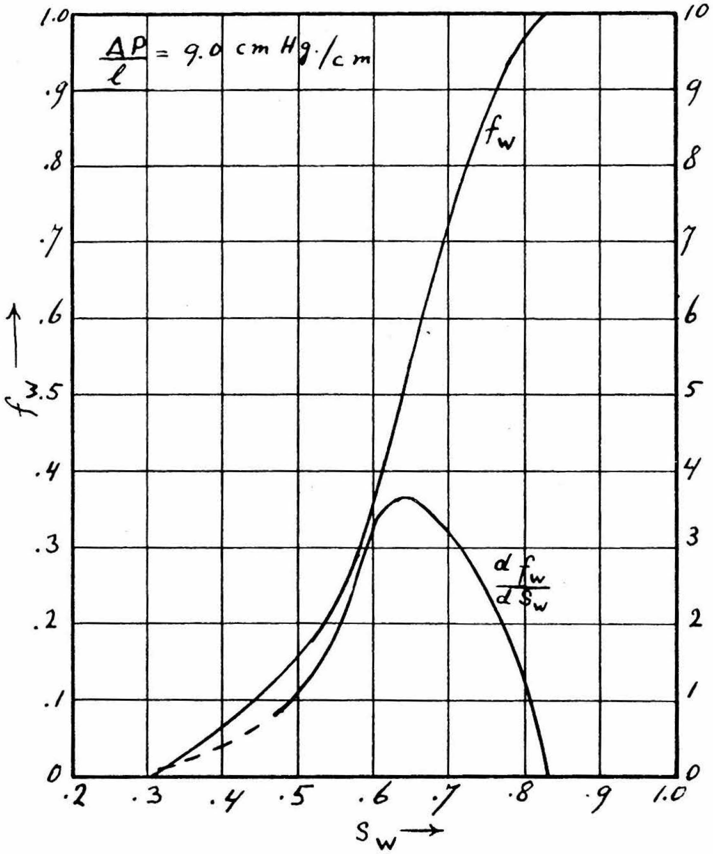

Fig. V - 9

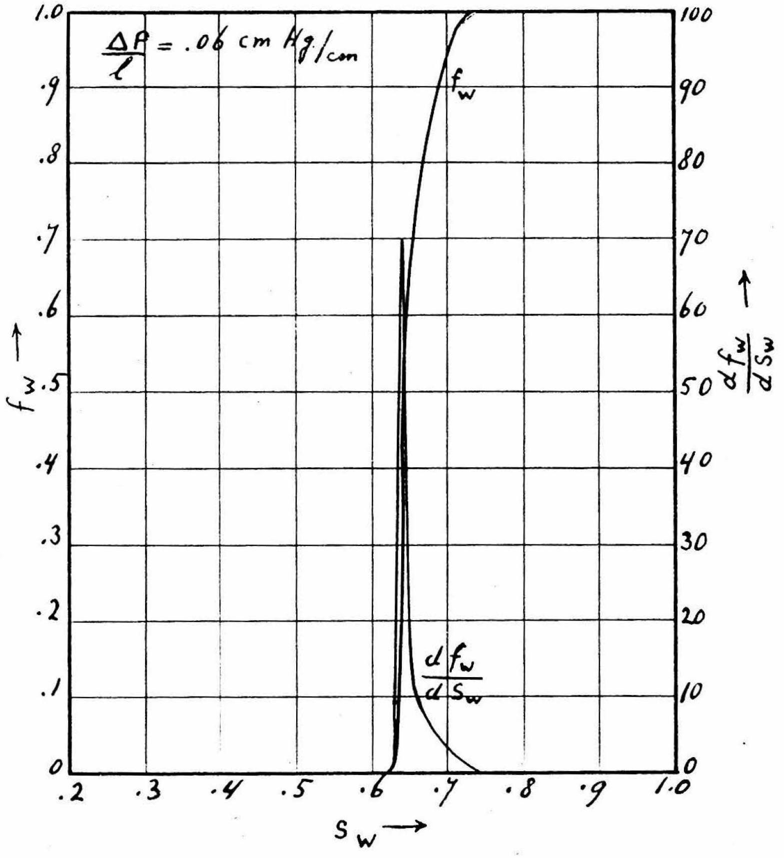

Fig. V - 10.

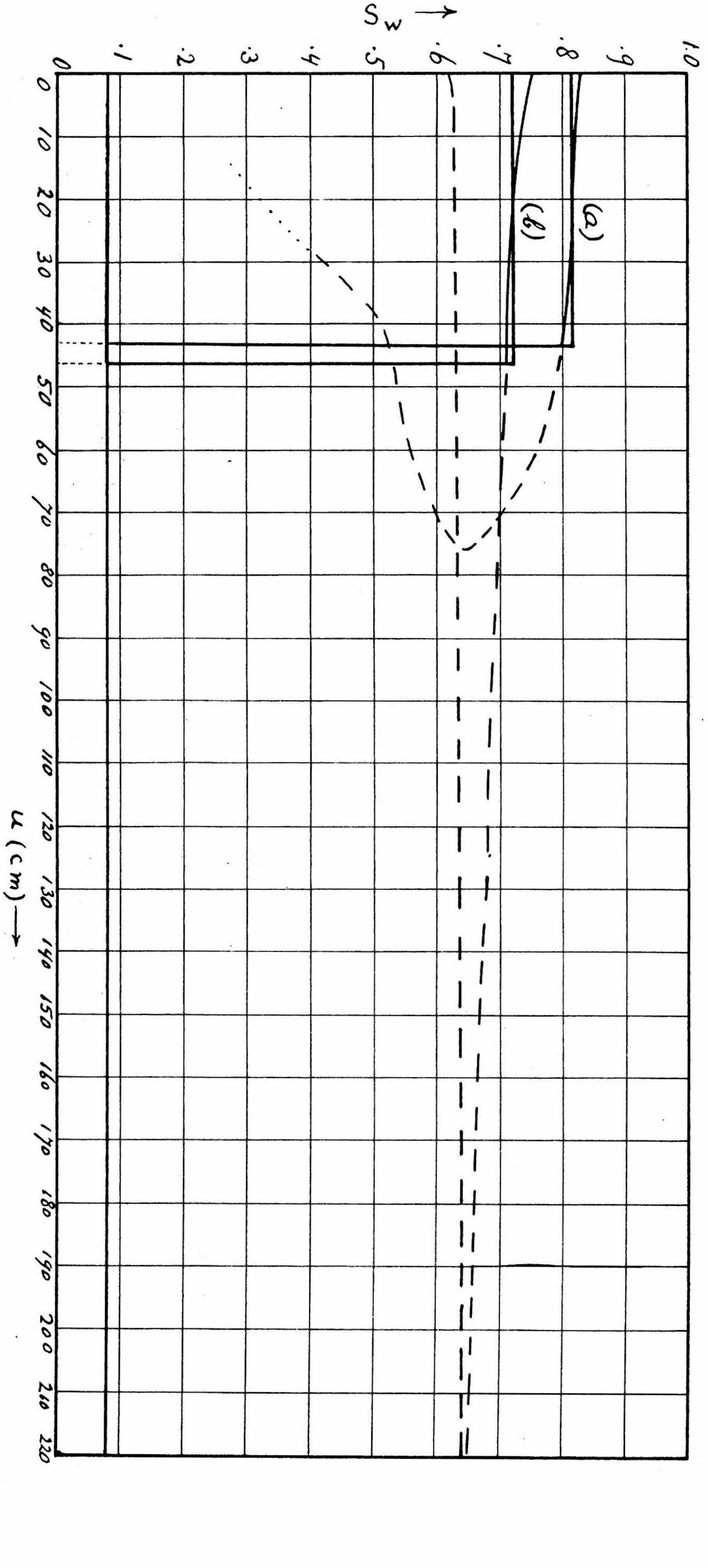

Sw →
0
.1
.2
.3
.4
.5
.6
.7
.8
.9
1.0
0
10
20
30
40
50
60
70
80
90
100
110
120
130
140
150
160
170
180
190
200
210
220
u (cm) →
(a)
(b)

Fig. V-11

indication of the order of magnitude of the variations involved, but cannot be used for any further quantitative computations for consolidated sandstones.

In practice it is quite possible to estimate the rate of infiltration roughly as follows:

The radius of the infiltrated zone is found from the electrolog by the procedure outlined in Part II of this thesis.

In addition the time in hours is estimated between the moment that the formation in question was first traversed by the drill, and the time that the electrolog is run.

This gives a relation between the distance penetrated by the filtrate and the time interval over which infiltration has been taking place.

Williams calculated such relations for various rates of infiltration, and presented the results as a family of curves, giving the distance penetrated, in feet as a function of the time during which invasion takes place in hours (25).

A copy of these curves is shown in Fig. V-12, with the infiltration rate given both in bbls/hr/ft of hole and in $cm^3/sec/cm^2$ of boreface.

The curves were made up for a hole diameter of 8-3/4", which represents an average size hole. The variations in computed infiltration rates due to different hole diameters are not large enough to be included in our calculations.

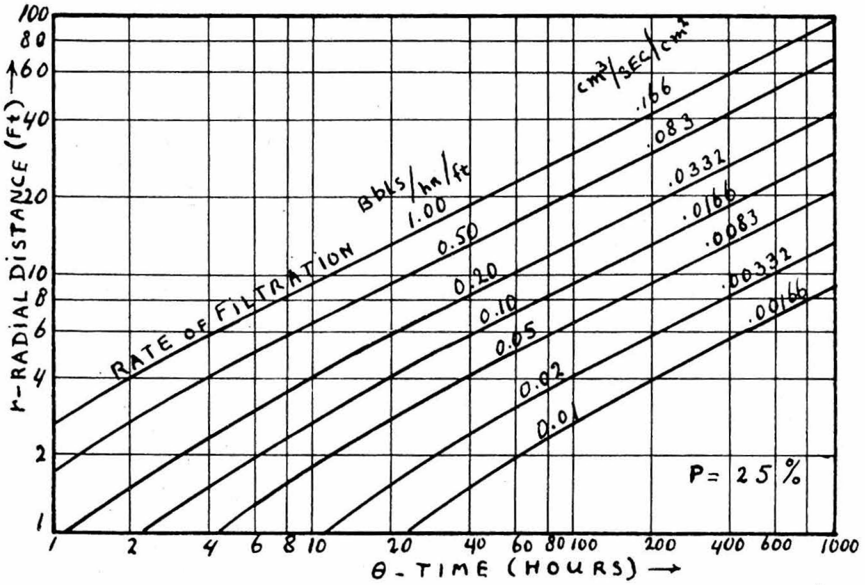

DISTANCE OF PENETRATION OF PERMEABLE STRATA
ASSUMING 80% FLUID DISPLACEMENT
AFTER M. WILLIAMS (23)
Fig. V-12

Basic Relations Between Resistivities and Fluid Contents of Porous Rocks,

and their Application to Electrolog Interpretation

Resistivities of Watersands

Until recently it was generally accepted that when a porous rock was saturated 100% with an electrolyte, the over-all resistivity of the rock was proportional to the resistivity of the electrolyte.

Analytically this could be expressed as:

$$R_o = F\ R_w \qquad (6\text{-}1)$$

where R_o is the resistivity of the rock, 100% saturated with the electrolyte of resistivity R_w. F was assumed to be a constant, independent of R_w and physically had the same meaning as the cell-constant in electrolyte conductivity measuring cells.

In the early part of the experiments connected with this work, it was noticed that when a sample was first saturated with an electrolyte of low resistivity and then flushed with large quantities of a more diluted electrolyte, the resulting resistivity invariably was lower than the value computed from (6-1). It was definitely established that during the flushing process the resistivity gradually increased due to replacement of the saline interstitial water by the fresher water. After a quantity of water equal to three to four times the total pore volume has passed through the sample, the sample resistivity starts approaching an asymptotic value. After twenty times the pore volume has passed through no further changes in the resistivity are noticed. It is the resistivity prevailing at this final stage to which we referred above as the resistivity after flushing.

To explain the fact that the resistivity obtained after flushing was smaller than the one computed from (6-1) we assumed that a part of the initial connate water was not removed from the sample, but stayed adsorbed on the surface of the solid framework of the rock. The fact that the process was not reversible, was explained by assuming a certain portion of salt ions being adsorbed at the rock surfaces, without the necessity of a "fixed" water layer. Thus the water could be replaced but a portion of the salt ions remained in the sample. Different rocks exhibited such phenomena to different extents: "clean" sandstones showed a very small retention; while shaley sands, or sandstones with a large portion of "fines" gave a much larger effect.

Tixier (19), comparing resistivities of infiltrated zones, with those of the undisturbed formations in the field, came to a similar conclusion, namely that part of the initial connate water was not removed upon invasion of the formation by mud-filtrate.

The above conclusions did not seem to be in agreement with the findings of Morgan, Muskat and Russell (26) who experimented on the mobility of interstitial water in sandstones, using both radioactive tracers and NaCl as indicators. They found that for the particular sandstone they were using, all of the connate water was replaced after approximately ten times the pore volume of the sample had been flushed through. The possibility existed, however, that the sandstone they used (Nichols Buff ss.) happened to be a particularly "clean sandstone" where the retention effect would be negligible.

This was shown not to be the case by Patnode and Wyllie (27) in a recent publication. These authors made a large series of flushing experiments using NaCl as a tracer and amongst the samples studied were sandstones of the same formation (Nichols Buff) as those used by Morgan, Muskat and Russell. Patnode and Wyllie attributed the apparent decrease in the formation factor with increasing interstitial water resistivity to the influence of conductive solids, which are present in most sandstones.

To prove that complete replacement of interstitial water takes place upon flushing with sufficient quantities of other aqueous solutions, they measured resistivities of an artificial core made up from alundum which contained no conductive solids. They found that for this case no lowering of the formation factor took place with increase in water resistivity and accepted this as proof of the complete replacement of interstitial waters in porous media, upon flushing.

It must be pointed out here that the alundum core can be compared to a completely clean sand, which would have no retention of connate water in any case and the experiment therefore proves nothing about the mobility of the connate water in sands in general.

In order to decide definitely whether or not connate water and the salt ions originally present are completely displaced upon flushing in average sandstones the following experiments were made:

Two samples of sandstones for which the apparent variations in formation factor had been found to be especially large were first saturated with a concentrated NaCl solution, of approximately 1N. After they had been completely saturated, fresh or less saline water was forced through and the resistivity of the effluent mixture was measured, with the electrolyte resistivity cell described in Part III.

The effluent water obviously is a mixture of the replaced original interstitial water and the water used for the flushing. By measuring its resistivity at intervals and knowing the resistivity of the two components we can calculate the fractions of each component in the following manner:

The concentration of a mixture of two electrolytes of given concentrations is given by:

$$\bar{C} = X_1 C_1 + X_2 C_2$$

Where $\bar{C}$, C_1, and C_2 are the concentrations of the mixture and the two components respectively; X_1 and X_2 are the amounts of the components (1) and (2), expressed as fractions of the total volume. Obviously $X_1 = 1 - X_2$, so that we have:

$$\bar{C} = X_1 C_1 + (1 - X_1) C_2$$

We now assume that the resistivity of an electrolyte is inversely proportional to its concentration. This holds true for dilute solutions, and is a fair approximation for concentrated solutions. We may then write:

$$\frac{1}{R_e} = \frac{X_1}{R_1} + \frac{1 - X_1}{R_2}$$

or $$R_e = \frac{R_1 R_2}{R_1 - X_1 (R_1 - R_2)} \tag{6-2}$$

Here R_e is the resistivity of the electrolyte mixture.

The volume fraction of the mixture represented by solution (1) is:

$$X_1 = \frac{R_2/R_e - 1}{R_2/R_1 - 1} \tag{6-3}$$

Using formula (6-3), the amount of displaced connate water was computed in each case.

The results are summarized in Table VI-A.

TABLE VI-A

Symbols used:

v_i = successive quantities of effluent mixture in cm^3.

R_e = resistivity of effluent mixture in Ω cm.

X_1 = fraction of original interstitial water in the effluent mixture.

$\sum (X_1)_i\ v_i$ = total amount of original interstitial water displaced (in cm^3)

S_i = amount of original interstitial water still retained in sample, as a percentage of the total porespace.

V_t = total accumulative amount of effluent mixture (cm^3).

I. Saugus ss. P = 21.5 cm^3 = 11.15% K = 5.32 milli darcys

$(R_w)_1$ = 12.3 Ω cm $(R_w)_2$ = 1950 Ω cm

v_i	R_e	X_i	$(X_1)\ v_i$	V_t	$\sum(X_1)_i\ v_i$	S_i
25	20.8	.603	15.08	25	15.08	29.9
25	69.4	.172	4.29	50	19.37	9.9
25	303.4	.0346	0.86	75	20.25	5.8
54	488	.0190	1.03	129	21.28	1.02
78	1160	.0041	.32	207	21.60	--

II. Modelo shaley sandstone:

P = 32.5 cm^3 = 15.04% K = 1.47 milli darcys

$(R_w)_1$ = 11.9 Ω cm $(R_w)_2$ = 106.6 Ω cm

v_i	R_e	X_i	$(X_1)\ v_i$	V_t	$\sum(X_1)_i\ v_i$	S_i
47.5	21.26	.47	22.5	47.5	22.5	30.8
50	50.55	.119	5.95	97.5	28.45	12.5
105	84.4	.029	3.26	202.5	31.71	2.4
140	102.5	.005	0.70	342.5	32.41	0.28
79	103.7	.0037	0.29	421.5	32.70	--
14.5	106.6	0.00	0.00	436	32.70	--

The examples show clearly that the interstitial water is completely replaced after ten times the pore volume has passed through the sample.

In the first examples, apparently some polution took place and R_e probably is too low in the last two stages.

In the second example, both solutions were rather concentrated to reduce effects of possible pollution of the effluent mixture. In order to avoid errors by using formula (6-3) an experimental graph of X_1 versus R_e was made up, and used to find X_1 for the effluent mixtures. This graph is shown in Fig. VI-1. Also shown is the curve corresponding to computed values of X_1 using formula (6-3).

We see that even for concentrated solutions formula (6-3) gives fairly accurate results.

The results shown in Table VI-A definitely make the salt water retention hypothesis untenable. The explanation of the apparent decrease of the formation factor with increasing water resistivity offered by Patnode and Wyllie is a very logical one. In addition, these authors demonstrated that the conduction by part of the solids in reservoir rocks could be treated quantitatively for the case of water sands. The overall

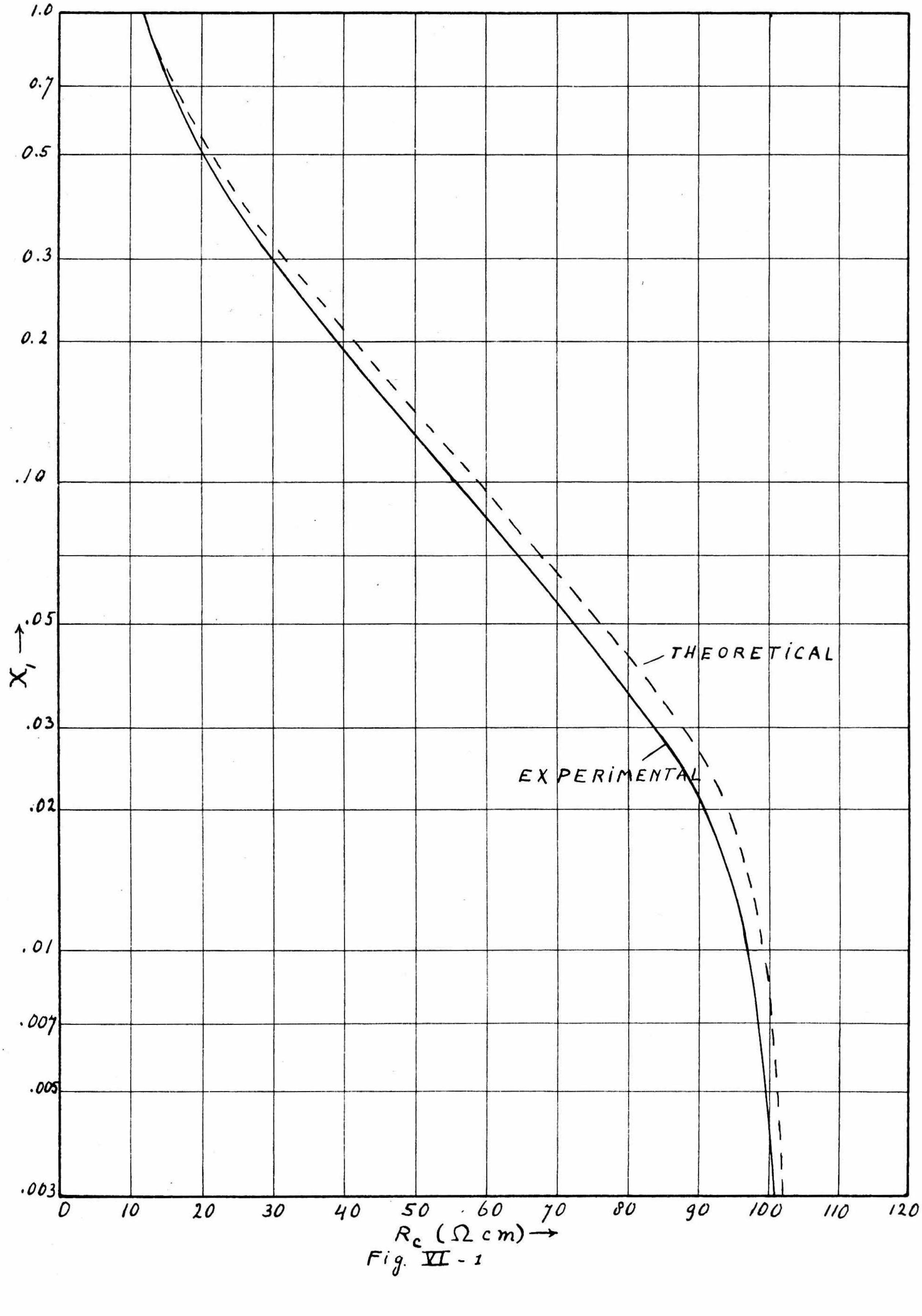
1.0
0.7
0.5
0.3
0.2
.10
.05
.03
.02
.01
.007
.005
.003
$X_1 \rightarrow$
0
10
20
30
40
50
60
70
80
90
100
110
120
R_c (Ω cm) →
THEORETICAL
EXPERIMENTAL

Fig. VI - 1

resistivity of a water saturated sandstone was expressed in the form:

$$\frac{1}{R} = \frac{1}{\rho_f} + \frac{1}{\rho_w} = \frac{1}{\rho_f} + \frac{1}{F\,R_w} \qquad (6\text{-}4)$$

Here ρ_f equals the resistivity of the conductive solids, as distributed, and ρ_w the resistivity of the water as distributed. $\rho_w = F\,R_w$ where R_w is the "bulk" water resistivity and F the formation factor, which would be found if none of the solids were conductive.

Formula (6-4) implies that the water saturated rock has an equivalent circuit consisting of two parallel resistances, one representing the resistance of the water phase and the other equal to the total resistance of the conductive solids, as distributed.

Physically this would be true, if the water and conductive solids were electrically insulated one from the other and both offered a continuous path for the current. This is not the case in a water saturated sandstone. On the contrary, the conductive solids and the water are everywhere in contact with each other and petrographic studies of thinsections of sandstones strongly suggest that in general the conductive solids do not form continuous layers or films over the sandgrains, but occur mostly in isolated small quantities randomly distributed throughout the rock.

Patnode and Wyllie proved that if the unknowns of equation (6-4), F and ρ_f, were solved from two measurements of R for corresponding values of R_w, one could calculate R for any other arbitrary value of R_w. The calculated R's were compared with measured values and a very good agreement was obtained. This was taken by Patnode and Wyllie as a proof that formula (6-4) correctly represents the current conduction through water saturated sandstones. Actually the above results only show that the conductivity of a watersand may be represented by an equation of the type $\frac{1}{R} = s - \frac{Y}{R_w}$. The experiments of Patnode and Wyllie give us no conclusive information regarding the quantities s and y.

The same authors studied the behavior of mud slurries with regard to current conduction and found the empirical formula:

$$\frac{1}{R} = \frac{N^X}{R_f} \left(1 - \frac{1}{F}\right) + \frac{1}{F R_w} \qquad (6\text{-}5)$$

where R_f is the bulk resistivity of the conductive solids, N is the fraction of conductive solids by volume and $X \approx 1$.

This again is of the type $\frac{1}{R} = s + \frac{Y}{R_w}$, and we can assume that for rocks the quantity $\frac{1}{\rho_f}$ is the equivalent of the combination $\frac{N^X}{R_f} \left(1 - \frac{1}{F}\right)$.

It was also found that for slurries containing only conductive solids, there is a linear relationship between the percentage of solids (1-P) and the conductivity of the solid phase $(1/\rho_f)$. Here P denotes the volume fraction of water, which is equivalent to the porosity in the case of a water sand.

This suggests that a homogeneous mixture of conductive solids and an electrolyte behaves exactly as a mixture of two electrolytes. For the latter we had derived the expression:

$$\frac{1}{R_o} = \frac{X_1}{R_1} + \frac{X_2}{R_2}$$

Applying this formula to a mixture of conductive solids and water we obtain:

$$\frac{1}{R_c} = \frac{X_f}{R_f} + \frac{X_w}{R_w} = \frac{1 - X_w}{R_f} + \frac{X_w}{R_w}$$

where X_f and X_w are the volume fractions of the conductive solids and the water respectively.

Rearranging gives:

$$R_c = \frac{R_w\ R_f}{R_w - X_w\ (R_w - R_f)} \qquad (6\text{-}6)$$

It seems reasonable to assume that the combination of randomly distributed conductive particles and water in a sandstone, behaves the same with respect to current conduction, as a slurry made up of the same amount of similar conductive solids and water.

The resistivity in the rock is then equal to F times the resistivity of the slurry (or the equivalent combination of conductive solids and water). Here F must be defined as the formation factor which we would find, if the conductive solids were replaced by water of the same type as that occupying the porespace.

The overall resistivity of the rock now becomes:

$$R = F\ R_c = \frac{F\ R_w\ R_f}{R_w - X_w\ (R_w - R_f)} = \frac{F\ R_w\ R_f}{(1 - X_w)\ R_w + X_w\ R_f} \qquad (6\text{-}7)$$

Letting $F\ R_f = \ell$, $X_w R_f = m$ and $1 - X_w = X_f = n$ we have:

$$R = \frac{R_w}{nR_w + m}$$

or $$\frac{1}{R} = \frac{n}{\ell} + \frac{m}{R_w} = \frac{1 - X_w}{F\ R_f} + \frac{X_w}{F\ R_w} \qquad (6\text{-}8)$$

We see that (6-8) again is of the form $\frac{1}{R} = s + \frac{y}{R_w}$ and therefore agrees with the experimental results of Patnode and Wyllie. Moreover formula (6-8) is also applicable to slurries containing both conductive and non-conductive solids. F then represents the effect of the non-conductive solids on the resistivity of the system.

Patnode (28) found that for slurries which contain only solids of high resistivity (essentially non-conductive solids) the empirical relation $F = P^{-1.6}$ exists, where P is the volume fraction of water.

Assuming that the combination of conductive solids and water is equivalent to that of an electrolyte mixture this same relation should hold also for slurries and rocks containing conductive solids, if F is defined as in equation (6-7).

If we have two values of R for two corresponding values of R_w, we may solve equation (6-8) for the two unknown quantities $\frac{1 - X_w}{F\,R_f}$ and $\frac{X_w}{F}$. The resulting expressions for these quantities will be the same as those found by Patnode and Wyllie for $\frac{1}{\rho_f}$ and $\frac{1}{F}$.

We find:

$$\frac{X_w}{F} = \frac{(R_w)_1\,(R_w)_2\,\left[(R_o)_1 - (R_o)_2\right]}{(R_o)_1\,(R_o)_2\,\left[(R_w)_1 - (R_w)_2\right]} \qquad (6\text{-}9)$$

and $$\frac{1 - X_w}{F\,R_f} = \frac{(R_w)_1\,(R_o)_2 - (R_w)_2\,(R_o)_1}{(R_o)_1\,(R_o)_2\,\left[(R_w)_1 - (R_w)_2\right]} \qquad (6\text{-}10)$$

where $(R_o)_1$ and $(R_o)_2$ are the resistivities of the sandstone completely saturated with water respectively of a resistivity $(R_w)_1$ and $(R_w)_2$.

Once $\frac{X_w}{F}$ and $\frac{1 - X_w}{F\,R_f}$ are determined we can calculate any value of R_o resulting from any water resistivity, R_w or vice Versa. In all the above expressions X_w is the volume fraction of water in the combination of conductive solids and water. Similarly $1 - X_w = X_f$ is the volume fraction of conductive solids in the same combination. If P_f denotes the amount of conductive solids as a fraction of the total rock volume we then may write:

$$X_w = \frac{P}{P + P_f} = \frac{1}{1 + p_f} \quad \text{where} \quad p_f = \frac{P_f}{P}$$

$$\text{and} \quad X_f = 1 - X_w = \frac{P_f}{P + P_f} = \frac{p_f}{1 + p_f}$$

Two experimental checks were made of the above formulae for overall resistivity using the same sandstones for which the mobility of the interstitial water was determined.

I. Saugus ss. K = 5.31 m. darcys P = 11.15%

(Sample S-3)

$(R_w)_1 = 12.3\ \Omega$ cm. $(R_o)_1 = 549\ \Omega$ cm.

$(R_w)_2 = 156{,}300\ \Omega$ cm. $(R_o)_2 = 4025\ \Omega$ cm.

$$\frac{1 - X_w}{F\,R_f} = \frac{12.3 \times 4025 - 156{,}300 \times 549}{549 \times 4025\ (12.3 - 156{,}300)} = .248 \times 10^{-3}$$

Similarly $\frac{X_w}{F} = .0193$ $\frac{F}{X_w} = 51.8$

This gives: $\frac{1}{R} = .248 \times 10^{-3} + \frac{.0193}{R_w}$

For $(R_w)_3 = 342.7$ we obtain: $(R_o)_3 = 3282\ \Omega$ cm.

The measured value was $(R_o)_3 = 3230\ \Omega$ cm.

II. Modelo shaley sand (Sample M-4)

K = 1.47 m. darcys P = 15.04%

$(R_w)_1 = 11.9\ \Omega$ cm. $(R_o)_1 = 367.7\ \Omega$ cm.

$(R_w)_2 = 1024\ \Omega$ cm. $(R_o)_2 = 2876\ \Omega$ cm.

$\frac{1 - X_w}{F\,R_f} = .32 \times 10^{-3}$ $\frac{X_w}{F} = .0286$

so that $\frac{1}{R} = .32 \times 10^{-3} + \frac{.0286}{R_w}$

For $(R_w)_3 = 106.6\ \Omega$ cm, we find $(R_o)_3 = 1700\ \Omega$ cm.

The measured value was $(R_o)_3 = 1646\ \Omega$ cm.

As stated before, the experiments of Patnode and Wyllie carried out on a much larger scale, all verify the validity of a relation of the type $\frac{1}{R} = z + \frac{Y}{R_w}$ for the case of watersands.

Resistivity of Oil and Gas Sands

Before the idea of current conduction by part of the solids in porous rocks was introduced, the relation between rock resistivity and hydrocarbon content was generally given by an empirical formula of the type:

$$S_w = \left(\frac{R_o}{R}\right)^{1/n} \qquad (6\text{-}11)$$

$$\text{or} \quad R = R_o\,(S_w)^{-n} \qquad \text{and} \qquad \frac{1}{R} = \frac{(S_w)^n}{R_o}$$

This relation was first given general significance by the work of Archie (29), who found experimentally $n \approx 2$.

Since Archie's work, several other investigators carried out extensive experiments using many types of rocks and found that the value of n will vary considerably for different types of sandstones.

n was believed to have a specific value for any given rock.

Dakhnov (5, 30) obtained from experimental data $1.7 < n < 4.3$.

Bailey and others (31) found $1 < n < 2.5$.

All these experiments were made on sandstones of which the content of conductive solids was unknown and completely neglected. It is obvious that, if the effect of conductive solids is neglected and Archie's formula applied as such, the apparent values of n will not only vary from rock to rock, but also will depend upon the water salinity.

Computations from our experimental data indicate, however, that Archie's formula does apply, with n equal to or nearly equal to 2 in cases where the influence of conductive solids is negligible or small, because of the high salinity of the interstitial water.

Table VI-B shows examples of these data.

TABLE VI-B

Sample	No.	P(%)	K m. darcys	S_w	R_w Ω cm	R_o Ω cm	R Ω cm	n
Berea ss	(0-7)	27.3	22.0	.19	40.7	568	14860	1.96
" "	(0-8)	28.9	40.2	.188	30.3	404	11470	2.0
Pico ss	P-4a	33.3	318	.295	36.1	386	4550	2.02
" "	P-4b	28.4	390	.21	35.9	271	7610	2.14
Saugus ss	S-3h	10.6	2.67	.675	38.2	1548	3478	2.06

The deviations from the value of n = 2.0 may be partly due to combined experimental errors and the influence of conductive solids. Even if these would be eliminated it would not be likely that n would have a completely constant value, but the variations in n will in general be small. Considering the enormous differences between the types of sandstones used in obtaining the data of Table VI-B, and the relatively small variations in n, it is believed that most of the anomalous values of n found by the aforementioned authors, are due to neglecting the influence of the conductive solids.

To take the effect of conductive solids into account, we must go back to the expressions for R in terms of F, R_w and the amount and (or) resistivity of the conductive solids.

It is in trying to expand these formulae to include the presence of hydrocarbons that the differences between the equations of Patnode and Wyllie and those resulting from the assumption of a homogeneous mixture of the conductive media become evident.

If one assumes an independent conduction through the conductive solids as suggested by the formula:

$$\frac{1}{R_o} = \frac{1}{\rho_f} + \frac{1}{F\ R_w}$$

the presence of oil would not have any effect on that part of the total conductivity represented by $1/\rho_f$.

It is obvious that the conduction through the water is influenced by the presence of oil in the same way as in the case where none of the solids are conductive. This means the term $\frac{1}{F\ R_w}$ is replaced by $\frac{(S_w)^n}{F\ R_w}$.

Again combining the two conductivities for the parallel paths we obtain:

$$\frac{1}{R} = 1/\rho_f + \frac{(S_w)^n}{F\ R_w} \qquad (6\text{-}12)$$

The outcome of experiments to test formula (6-12) proved the assumption of an independent conductive path through the solids untenable.

The evidence to that effect will be illustrated by an example:

A sample of Berea sandstone was saturated with water of two different salinities successively and F and ρ_f were computed, using equation (6-4), after the resistivities were measured in both cases.

The following data were obtained:

$(R_w)_1 = 13.6 \ \Omega$ cm. $(R_o)_1 = 190 \ \Omega$ cm.

$(R_w)_2 = 1009 \ \Omega$ cm. $(R_o)_2 = 8500 \ \Omega$ cm.

This leads to $F = 14.1$ and $1/\rho_f = .0000476$ or $\rho_f = 21{,}000 \ \Omega$ cm. The sample was then saturated with crude oil by the capillary pressure method until an oil saturation of 0.70 was obtained. This means $S_w = .22$.

The resistivity of the sample was now found to be $82{,}800 \ \Omega$ cm.

Applying formula (6-12) gives:

$$\frac{1}{82{,}800} = \frac{1}{21{,}000} + \frac{(.22)^n}{14.1 \times 1009} \qquad \text{which makes n imaginary.}$$

Physically, the above result means that, assuming an independent continuous path through the conductive solids, the conductivity of the conductive solids as distributed would be larger than the combined conductivity of the entire system, which of course is not possible.

This forces us to abandon the concept of a network of conductive solids with an independent resistivity of the conductive solids as distributed.

The alternative hypothesis of homogeneous mixture of the conductive media leads to the following relations:

For a water sand we have, as described before:

$R_o = F \, R_c$

Assuming now that the influence of the non-conductive solids and hydrocarbons on the conductive mixture is the same as the influence on the water conductivity (as distributed) in the absence of conductive solids we obtain:

$$S_w = \left(\frac{R_o'}{R}\right)^{\frac{1}{2}} = \left(\frac{F\ R_o'}{R}\right)^{\frac{1}{2}}$$

Here $R_o' \neq R_o$, as in the case of oil saturation the amount of interstitial water in the rock is diminished, while the content of conductive solids stays the same. Therefore the proportions of the two components in the "slurry" are different in the two cases.

We can write the above expressions as follows:

$$R_o' = \frac{F\ R_f\ R_w}{R_w - X_w'\ (R_w - R_f)} \tag{6-13}$$

$$\text{or} \quad F\ R_o' = R\ S_w^2 = \frac{F\ R_f\ R_w}{R_w - X_w'\ (R_w - R_f)} \tag{6-14}$$

Here $X_w' = \frac{P\ S_w}{P\ S_w + P_f}$

In the case of a water sand we had $X_w = \frac{P}{P + P_f}$ which gives $\frac{P_f}{P} = \frac{1}{X_w} - 1$.

$$\text{Substituting gives} \quad X_w' = \frac{S_w}{S_w + 1/X_w - 1} \tag{6-15}$$

Referring back to the parameters $\ell = F\ R_f$, $m = X_w R_f$ and $n = 1 - X_w$ we have

$$\left(\frac{P}{P_f} =\right)\frac{X_w}{1 - X_w} = \frac{\ell/n}{\ell/m\ R_f} = \frac{m}{n\ R_f} \quad \text{or} \quad X_w = \frac{m/n}{R_f + m/n}$$

Similarly $X_w' = \frac{m/n}{m/n + R_f/S_w}$

If we have two equations of the type

$$(R_o)_1 = \frac{F\ R_f\ (R_w)_1}{(R_w)_1 - X_w\left[(R_w)_1 - R_f\right]} \tag{6-16}$$

where the respective values of $(R_o)_i$ and $(R_w)_i$ are known we can solve for the ratios /n and /m from which we obtain m/n.

Combining one of the equations (6-16) with equation (6-14) we have for the case that R_w is the same in both expressions:

$$R_o \left[R_w - X_w (R_w - R_f)\right] = R S_w^2 \left[R_w - X_w' (R_w - R_f)\right]$$

Substituting the expressions for X_w and X_w' and rearranging, we obtain:

$$\frac{m/n}{R_f + m/n} R_o - \frac{m/n\ R\ S_w^2}{m/n + R_f/S_w} = \frac{R_o R_w - R\ S_w^2\ R_w}{R_w - R_f} \tag{6-17}$$

This is a cubic equation for S_w and S_w could be found if R_f is known.

R_f is the bulk resistivity of the conductive solids occurring in reservoir rocks. In general, these consist mostly of argillaceous materials, combined with substances like limonite, etc. The bulk resistivity of such material must have a value within a definite rather limited range, comparable with the bulk resistivities of shales. As pointed out by Patnode and Wyllie, the actual resistivity of neighboring shales might be a good approximation except for cases where the content of limonite and similar substances is large. We might therefore assume a value of R_f within its probable range and solve for S_w.

As the error in R_f may be appreciable, it is of importance to know how sensitive equation (6-17) is to variations in R_f.

To demonstrate the effect of such variations, equation (6-17) was applied to the case of the Berea sandstone (sample 0-10), and solved for S_w, assuming values of R_f respectively of 10, 50, and 100 Ω cm. These values are representative for the range of values of the resistivities of shales.

For our example we had:

$$m/n = \frac{21,000}{14.1} = 1490 \qquad R_w = 1009 \ \Omega \text{ cm.}$$

$$R_o = 8500 \ \Omega \text{ cm.} \qquad R = 82,800 \ \Omega \text{ cm.}$$

Substituting these values in equation (6-17) gives us three values for S_w, of which two are negative and therefore of no physical meaning. The third value is the actually prevailing water saturation.

The following values were obtained:

R_f (Ω cm)	S_w
100	0.245
50	0.227
10	0.210

The experimentally determined value of S_w (obtained both volumetrically and by weighing) was .220 .

This demonstrates that even with a large uncertainty in R_f, the "homogeneous mixture" hypothesis leads to formulae that approximate actual conditions well enough for all practical purposes. The results obtained also prove that a rough estimate of R_f gives a fairly accurate value for S_w.

Knowing the actual value of S_w we are in a position to compute the true value of R_f. This is most easily done graphically. Using this procedure we find $R_f = 33 \ \Omega$ cm.

The discussed experiments and derivations serve to outline the general relations between the resistivity and the fluid content of porous rocks.

Application of the Derived Formulae to Electrolog Interpretation

In practice, the electrolog gives us for each formation two quantities; namely, the true resistivity of the undisturbed formation, and the resistivity of the infiltrated zone.

In some cases, however, the upper part of a formation may be saturated with oil or gas and the lower part with water. This is often the case in wells at the periphery of a field or structure where the oil-water interface cuts the tilted beds. Where we have such a combination of an oil zone and a water zone in the same reservoir rock, the electrolog furnishes us four quantities; namely, the true resistivities of the oil sand and of the watersand, and the invaded zone resistivities for both zones.

The fact that both zones are in the same reservoir rock is concluded from the self potential curve of the log, which shows the combination as one unit.

Fig. VI-2 gives a somewhat idealised example of the electrolog curves for such combination.

From the values of R_t and R_i of the water zone and the R_t of the oil zone, S_w may be calculated following the procedure outlined for the example of the Berea sandstone, after having assumed a value for R_f.

Using the additional equation furnished by the measurement of R_i of the oil zone it is possible, however, to compute the actual value of R_f, if we know the relation between S_w and $(S_w)_i$, the water saturation of the infiltrated zone. It was shown by Tixier (19) that the latter relation is of the form $(S_w)_i^{n} = S_w^{\cancel{n}}$, where $n \approx 2$. The details of this relation will be discussed in the next part of this thesis.

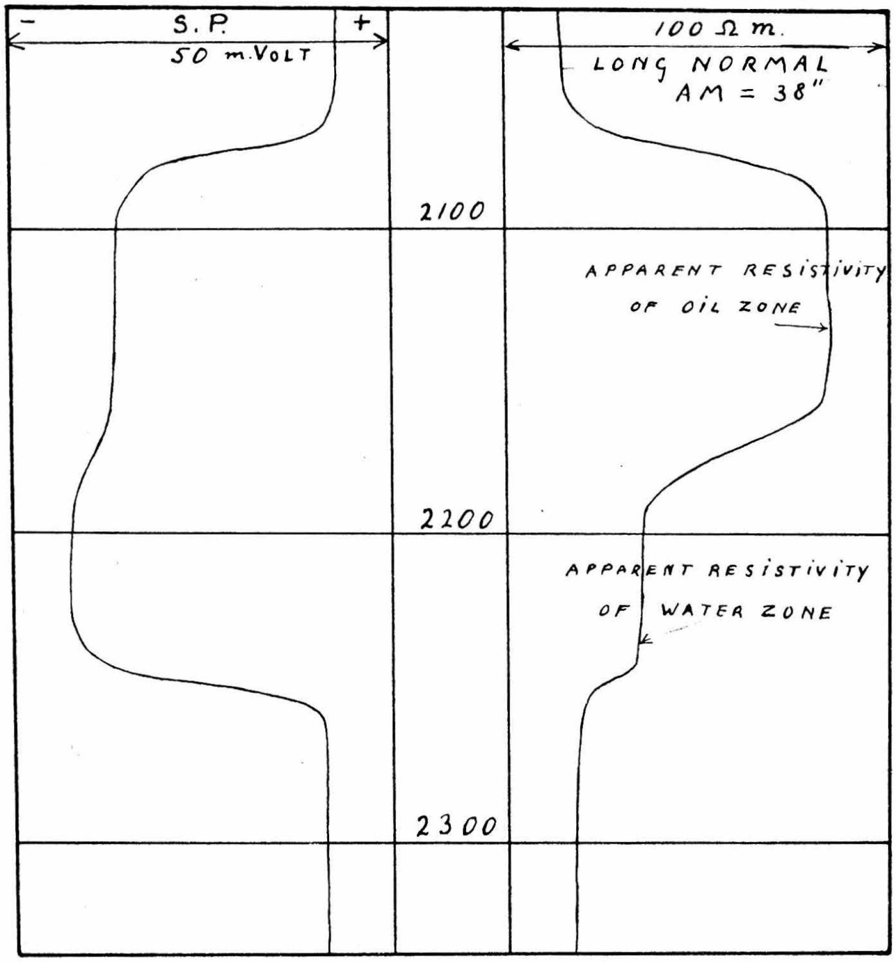
–
S.P.
+
50 m.VOLT
100 Ω m.
LONG NORMAL
AM = 38"
2100
APPARENT RESISTIVITY
OF OIL ZONE
2200
APPARENT RESISTIVITY
OF WATER ZONE
2300

Fig. VI - 2

Summarizing the relationships for the case where we have a distinct oil zone and water zone in the same rock unit we have:

From the R_i and the R_t of the water sand, denoted respectively by $(R_i)_1$ and $(R_t)_1$ we find from equations (6-9), (6-10) and the definitions of m and n:

$$N = m/n = \frac{R_w\, R_{mf} \left[(R_t)_1 - (R_i)_1 \right]}{R_w\, (R_i)_1 - R_{mf}\, (R_t)_1} \quad \text{or} \quad 1/N = \frac{(R_{mf}/R_w)\, R_t - R_i}{R_{mf}\, (R_i - R_t)} \tag{6-18}$$

where R_{mf} is the mud filtrate resistivity.

Denoting the R_i and R_t of the oil zone by $(R_i)_2$ and $(R_t)_2$ we may write the equation (6-17) as:

$$\frac{m/n}{R_f + m/n}\,(R_t)_1 - \frac{m/n}{m/n + R_f/S_w}\,(R_t)_2\, S_w^{\,2} = \frac{(R_t)_1\, R_w - (R_t)_2\, S_w^{\,2}\, R_w}{R_w - R_f} \tag{6-19}$$

$$\frac{m/n}{R_f + m/n}\,(R_t)_1 - \frac{m/n}{m/n + R_f/(S_w)^{\frac{1}{2}}}\,(R_i)_2\, S_w = \frac{(R_t)_1\, R_w - (R_i)_2\, S_w\, R_w}{R_w - R_f} \tag{6-20}$$

Assuming values of R_f we can plot S_w as a function of R_f for relations (6-19) and (6-20). The actual R_f and S_w are found as the respective values at the intersection of the two graphs.

In most cases, however, there is no distinct separation between a water and an oil horizon in the same rock unit and we do not know whether the rock contains any hydrocarbons or not. In these cases we must try to solve for S_w. If $S_w = 1$ we have a water sand, if $S_w < 1$ we have an oil or gas sand. As we cannot solve for m/n directly we must go back to the original relations for X_w' of the undisturbed formation and X_w'' of the infiltrated zone.

On page 98 we showed that

$$X_w' = \frac{N}{N + R_f/S_w} \qquad \text{with} \qquad N \equiv m/n$$

If we use again $(S_w)_i^2 = S_w$ we have for the invaded zone

$$X_w'' = \frac{N}{N + R_f/(S_w)_i} = \frac{N}{N + R_f/(S_w)^{\frac{1}{2}}}$$

Using a probable value for R_f, for instance $R_f = 30\ \Omega$ cm and substituting the above expressions in equation (6-14) we obtain:

$$R_t\,(S_w^2) = \frac{30\,F\,R_w}{R_w - \dfrac{N}{N + 30/S_w}\,(R_w - 30)} \tag{6-21}$$

$$\text{and } R_i\,S_w = \frac{30\,F\,R_{mf}}{R_{mf} - \dfrac{N}{N + 30/(S_w)^{\frac{1}{2}}}\,(R_{mf} - 30)} \tag{6-22}$$

As was shown on page 98

$$\frac{P}{P_f} = \frac{N}{R_f} \quad \text{or} \quad 1/N = \frac{P_f}{P}\,\frac{1}{R_f} = \frac{p_f}{R_f} \tag{6-23}$$

with $p_f = P_f/P$.

In equation (6-23) p_f denotes the amount of conductive solids per unit porespace, while R_f is nearly a constant. This suggests that N is related to the electrochemical formation coefficient, C. The latter quantity was introduced and discussed in detail in a thesis by this author (32) on the characteristics of electrochemical potentials encountered in drillholes.

Fig. VI-3 shows the relation between values of N and C determined for various sandstones. Although the number of points given in VI-3 is small, the great differences in the types of sandstones tested make it quite evident that the correlation represents a general relationship.

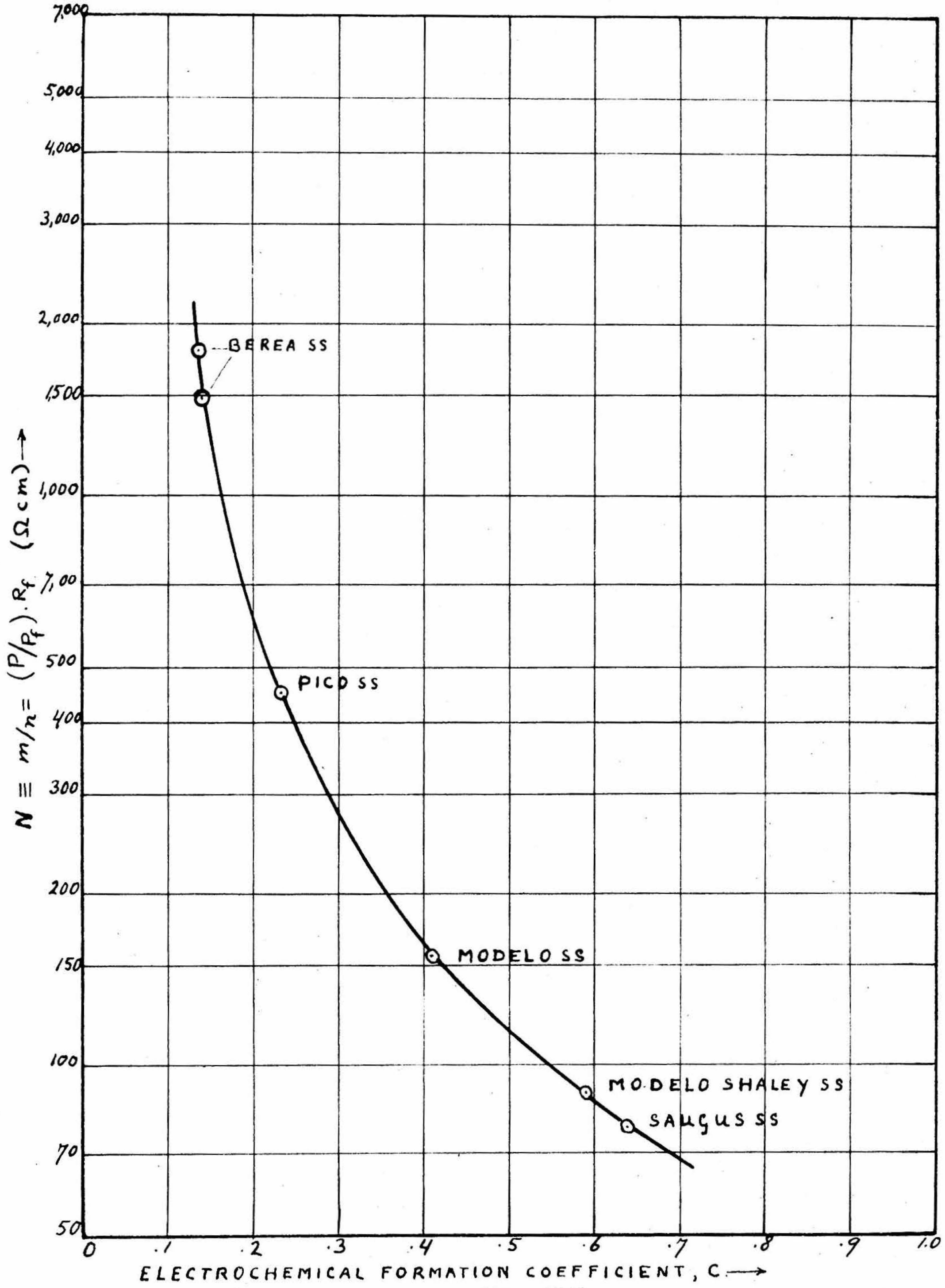
7,000
5,000
4,000
3,000
2,000
1,500
1,000
7,00
500
400
300
200
150
100
70
50
0
.1
.2
.3
.4
.5
.6
.7
.8
.9
1.0
N ≡ m/n = (P/P_f) · R_f (Ω cm) →
ELECTROCHEMICAL FORMATION COEFFICIENT, C →
BEREA SS
PICO SS
MODELO SS
MODELO SHALEY SS
SAUGUS SS

Fig. VI - 3

In the above mentioned thesis it was also shown, how using the relation between N and C, and data obtained from the self potential curves registered on the electrologs, we can determine both N and R_W for water sands.

For all the horizons in a particular well that are typically water-bearing R_W may be computed. For all horizons that might be suspected to contain hydrocarbons the value for R_W is interpolated between those for the nearest water sands and N is determined using the self potential kick for the formation in question.

Equation (6-21) and (6-22) then permit us to compute S_W and F, which is most easily done graphically.

F is of importance for the determination of porosity using the empirical formula

$$F = P^{-1.6}$$

Knowing the porosity and the oil saturation ($S_O = 1 - S_W$) we can calculate the total amount of oil present per acre foot of the oil horizon.

PART VII

Experimentally Determined Characteristics of the Infiltrated Zones of Permeable Formations

1) Resistivity profiles

a) Water sands

In the preceding parts of this thesis, some of the factors governing the characteristics of the infiltrated zones of permeable formations have been discussed. The primary purpose of this section is to determine the actually existing resistivity distributions in the invaded zones, as functions of the radial distance from the boreface.

As outlined in Part IV all experiments were performed on relatively small cylindrical samples, with a controlled initial fluid content which were submitted to uni-directional invasion by the infiltrating water. In most of the experiments, water of a given salinity was used to invade the samples, instead of actual drilling muds. This was done to avoid the retarding action of the mudcakes formed on the face of the samples.

At the beginning of the experimental work drilling muds of various compositions were forced through samples of Berea and Pico sandstones.

These experiments showed that all colloidal material from the muds were sieved out, at the face of the sandstones or in the first few centimeters of the rock. The filtrates obtained through cores of 2" length were in all respects (resistivity and absence of colloidal material) identical to filtrates obtained through Whatman #52 filter paper. This means that for all practical purposes no errors are introduced by using simple aqueous solutions instead of drilling muds, in experiments on the changes in resistivities and fluid contents of rocks upon invasion.

After any arbitrary amount of fluid had passed through the sample the resistivity of the sample could be measured, and in this way graphs were made up, showing the sample resistivity as a function of the amount of fluid passed through the sample.

In the case of radial infiltration around a drill hole, the amount of fluid passed through a unit cross-sectional area perpendicular to the direction of flow will be a function of the radial distance from the boreface. Therefore the resistivities of our samples after various amounts of flushing by the infiltrating water, correspond to the resistivities of points at various distances from the boreface, in the actual invaded zones of permeable formations. Unfortunately the relations are complicated by the influence of the longitudinal dimensions of the cores.

The resistivity measurements do not represent the conditions at a single point, but give a weighted average for the entire core. The weighting is a function of the electrode spacing and the distance from the face of the core, at which the measurements are made.

Measurements of the content of the flushed out connate water in the effluent mixture, however, provide us a means of approximating the average amount of connate water left in the core. We also know the amount of filtrate passing through the upper face of the core and the amount of filtrate in the effluent which equals the amount that passed through the lower (out-flow) face. These values may be combined to give an average amount of filtrate passed through the core. We can plot therefore the average amount of connate water retained in the core, as a function of the average amount of filtrate passed through.

Fig. VII-1 shows this relation for the Saugus ss. From the data the corresponding sample resistivities may be calculated, using the methods outlined in Part VI of this thesis:

$(R_w)_1 = 39.8 \ \Omega$ cm. $\qquad (R_o)_1 = 1362 \ \Omega$ cm.

$(R_w)_2 = 993 \ \Omega$ cm. $\qquad (R_o)_2 = 4700 \ \Omega$ cm.

From these values we obtain:

$$\frac{X_w}{F} = .02163 \qquad \frac{1 - X_w}{F R_f} = .191 \times 10^{-3}$$

so that $1/R = .191 \times 10^{-3} + \frac{.02163}{R_w}$

For the mixture of initial connate water and invading water in the core R_w is found as:

$$R_w = \frac{(R_w)_1 \ (R_w)_2}{X_1 \ (R_w)_2 + (1 - X_1) \ (R_w)_1} = \frac{39.500}{993 \ X_1 + 39.8 \ (1 - X_1)}$$

where X_1 is obtained from Fig. VII-1.

The resulting values of R for various amounts of filtrate passed through the sample are plotted in Fig. VII-2.

Also shown in Fig. VII-2 are three points representing direct measurements of the sample resistivity for given amounts of influent filtrate. We see that taking the measured resistivity of the sample as average sample resistivity and the influent filtrate as average amount of flushing, does not introduce any serious errors.

Once the variation of the resistivity with amount of filtrate passed through the sample has been determined, the changes in resistivity as a function of the radial distance r from the boreface, in

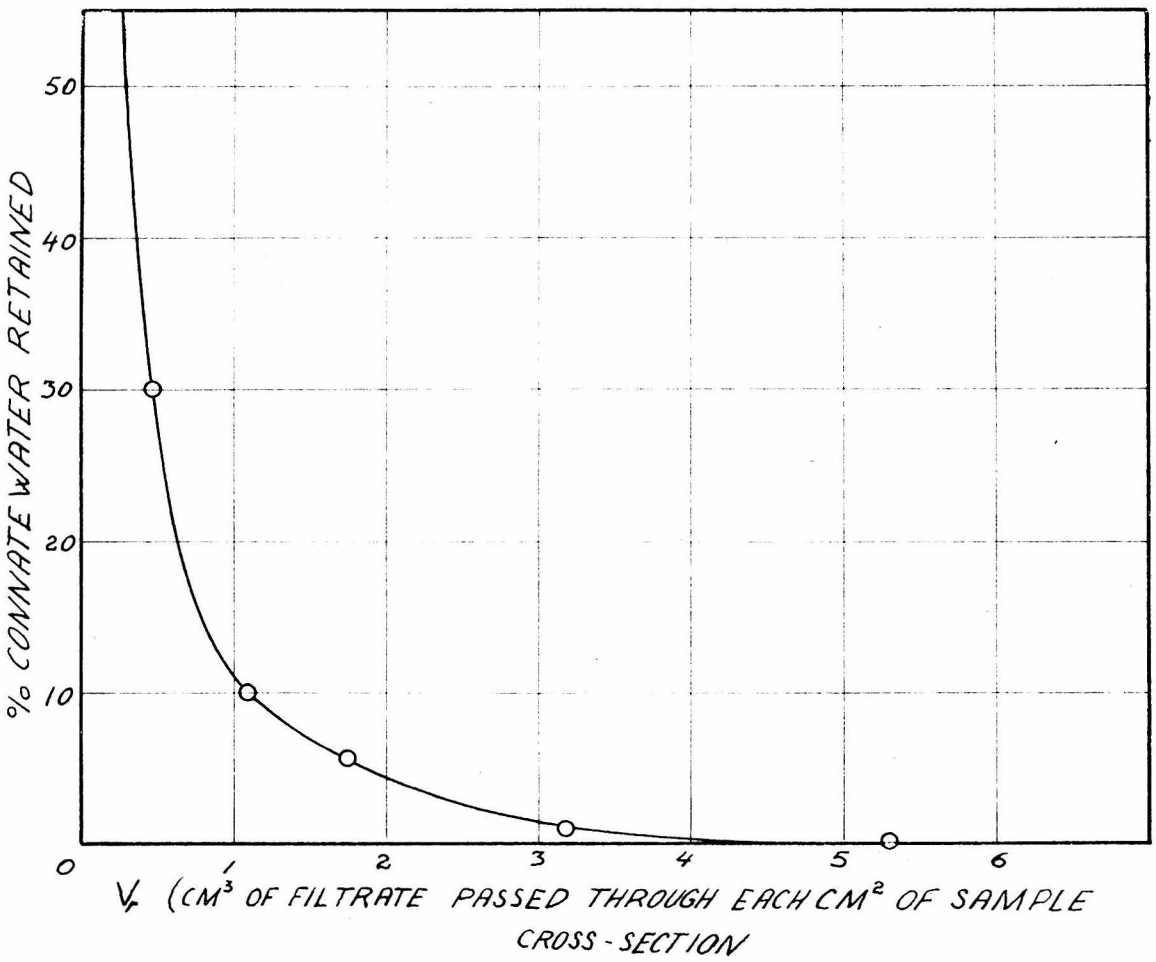
50
40
30
20
10
0
1
2
3
4
5
6
% CONNATE WATER RETAINED
V_r (CM^3 OF FILTRATE PASSED THROUGH EACH CM^2 OF SAMPLE CROSS-SECTION

FIG VIII-1

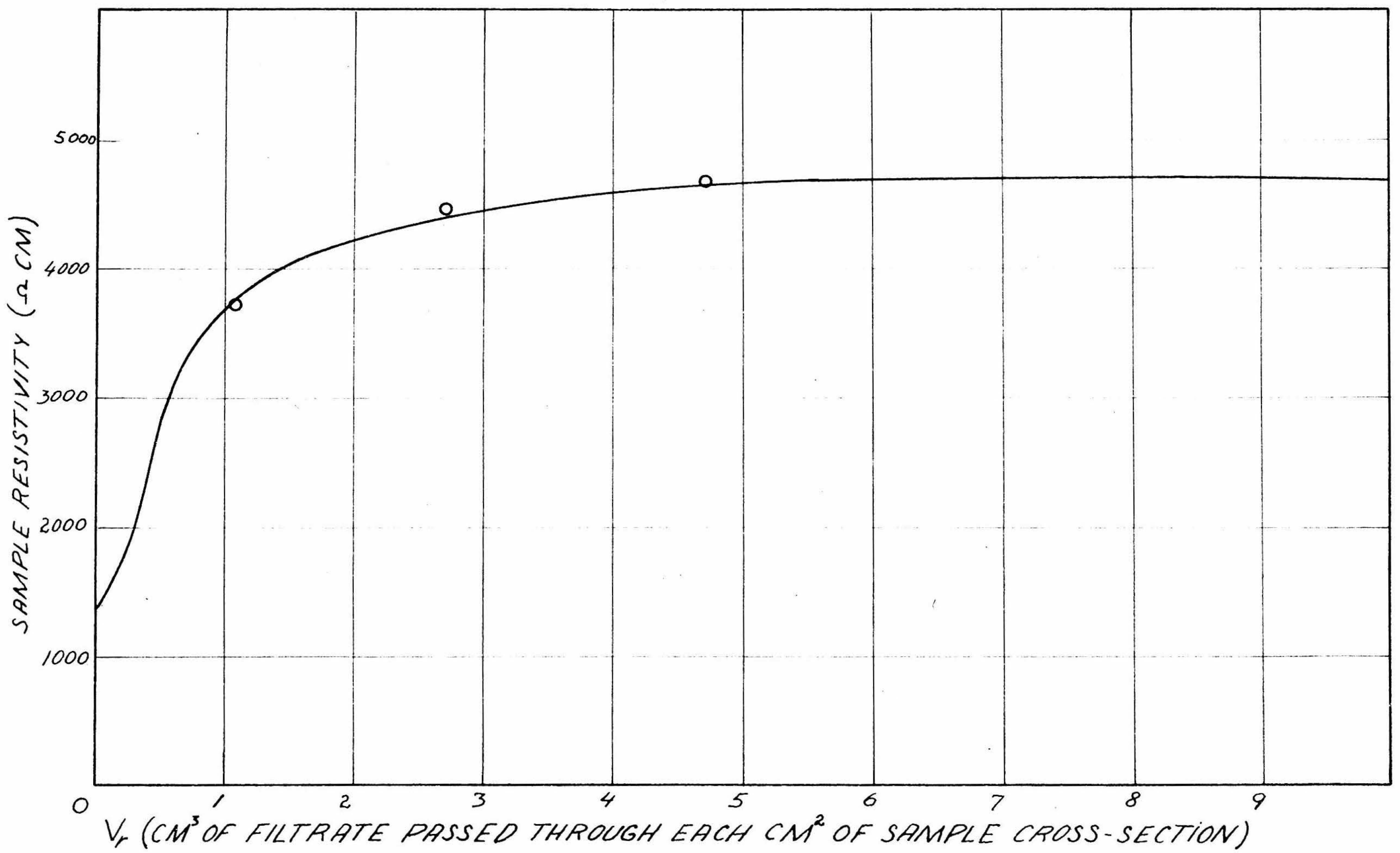
SAMPLE RESISTIVITY (Ω CM)
5000
4000
3000
2000
1000
0
1
2
3
4
5
6
7
8
9
V_r (CM^3 OF FILTRATE PASSED THROUGH EACH CM^2 OF SAMPLE CROSS-SECTION)

FIG VII-2

the case of radial infiltration, may be computed in the following manner:

Consider a slice of 1 cm. thickness of the borehole and infiltrated zone. In this slice we will limit our attention to a sector, corresponding to 1 cm. circumference of the drill hole cross-section. (See Fig. VII-3). The intersection of this sector with the boreface has a surface area of 1 cm^2. We now divide this sector into volumes V_1, V_2, etc., by arches concentric with the borehole, corresponding to equal increments in r. In each of these volumes we assume the amount of invading liquid retained to be constant. If the amount of invading liquid retained in volume V_1 is denoted by X_1, in volume V_2 by X_2, etc., we first assume that $X_1 = (X)_{r_0}$, $X_2 = (X)_{r_1}$, etc. This means that in each volume we make X equal to its actual value at the inner boundary of the volume.

Using this assumption we have:

Amount of invading liquid remaining in $V_1 = \frac{r_1^2 - r_0^2}{2\,r_0} \cdot \varphi \cdot (X)_{r_0}$

Where φ is the fractional porosity and $\frac{r_1^2 - r_0^2}{2\,r_0} =$

$$\frac{1}{2\pi r_0} \times \pi (r_1^2 - r_0^2) = V_1$$

If $(v)_{r_0}$ is the total quantity entering the sector through its 1 cm^2 cross-section at the boreface we have:

Flowing into V_2: $\quad (v)_{r_0} = \frac{r_1^2 - r_0^2}{2\,r_0} \cdot \varphi \cdot (X)_{r_0}$

and the amount of invading liquid per cm^2 of the inner boundary of V_2 is:

$$(v)_{r_1} = r_0/r_1 \left[(v)_{r_0} - \frac{r_1^2 - r_0^2}{2\,r_0} \cdot \varphi\,(X)_{r_0} \right]$$

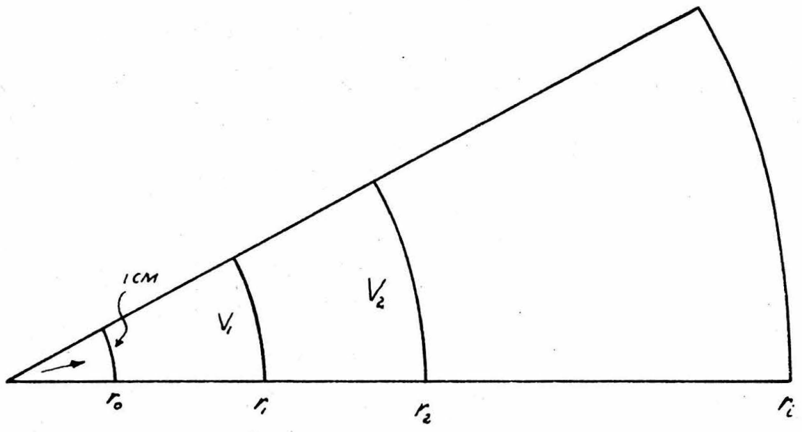

FIG VIII-3

$(v)_{r_3}$, etc.

The general formula for v_r becomes:

$$\frac{r_{n+1}}{r_o}(v)_{r_{n+1}} = \frac{r_n (v)_{r_n}}{r_o} - \frac{(r_{n+1})^2 - (r_n)^2}{2\, r_o} \cdot \varphi \cdot (X)_{r_n} \qquad (7\text{-}1)$$

$(X)_{r_n}$ is found from Fig. VII-1 corresponding to an amount $(v)_{r_n}$ of invading liquid, which was determined from the preceding equation.

In this manner we find v_r as a function of r. Another approximation of this relation can be made by assuming $X_1 = (X)_{r_1}$; $X_2 = (X)_{r_2}$ etc., that is by making X in each volume equal to its actual value at the outer boundary of the volume.

The actual conditions will result in a relation which falls in between the two approximations determined above.

Fig. VII-4 gives v_r as a function of r, calculated in the above manner, showing both the bracketing values and the averaged relationship. The latter is used for further computations.

We now have v_r as a function of r and the resistivity R as a function of v_r. Combining the two relations gives R as a function of r, which means the actual resistivity in the infiltrated zone as a function of the radial distance from the center of the hole.

Fig. VII-5 shows this actual resistivity distribution. We see that the resistivity in the infiltrated zone is not constant throughout the entire zone, and that the outer boundary is not a sharp discontinuity in the resistivity distribution. For all practical purposes we may however replace the transition zone by two parts of constant resistivity separated by a discontinuity as indicated by the dashed line in Fig. VII-5.

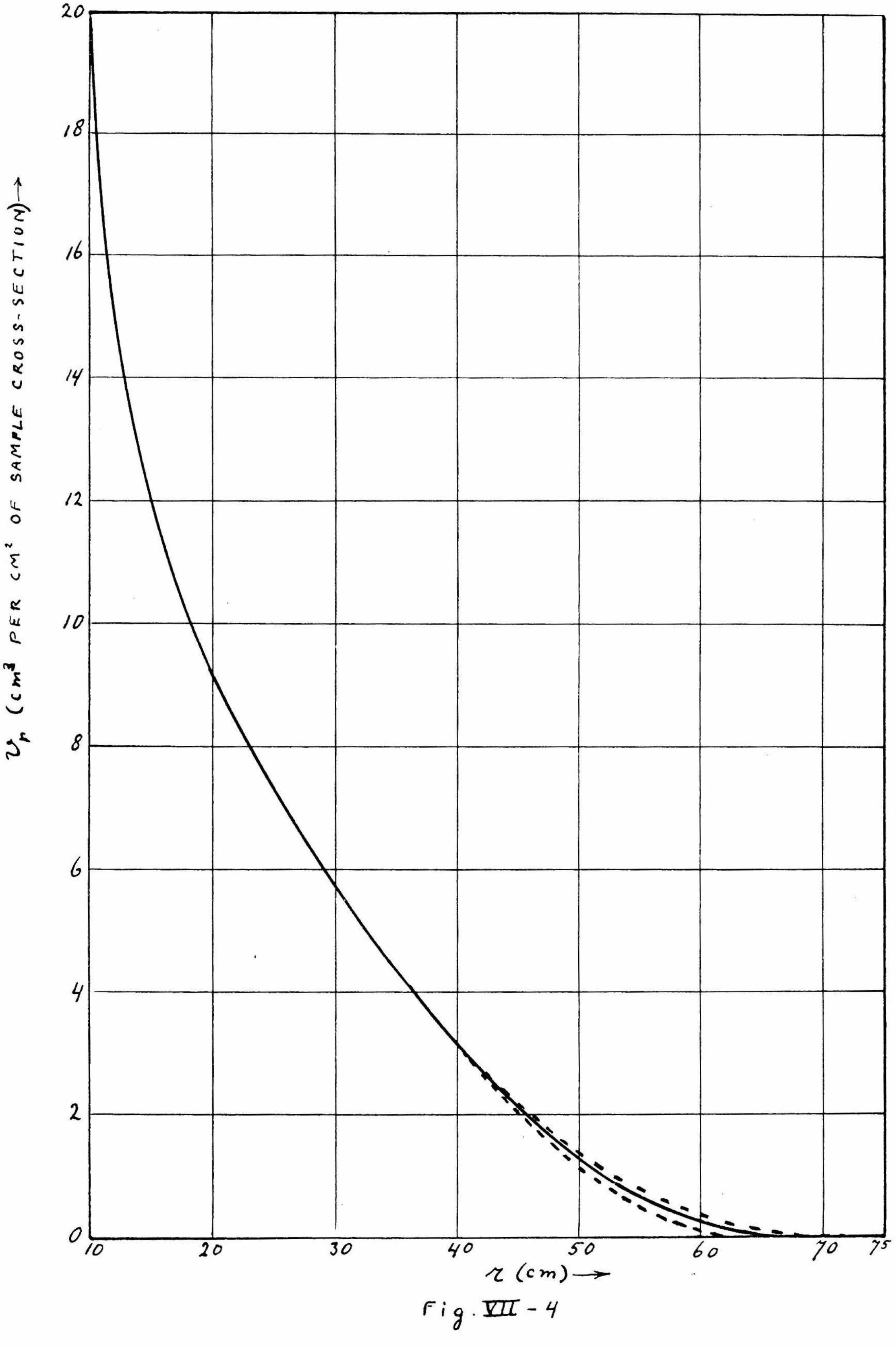
20
18
16
14
12
10
8
6
4
2
0
10
20
30
40
50
60
70
75
v_r (cm^3 PER CM^2 OF SAMPLE CROSS-SECTION)→
r (cm)→

Fig. VII - 4

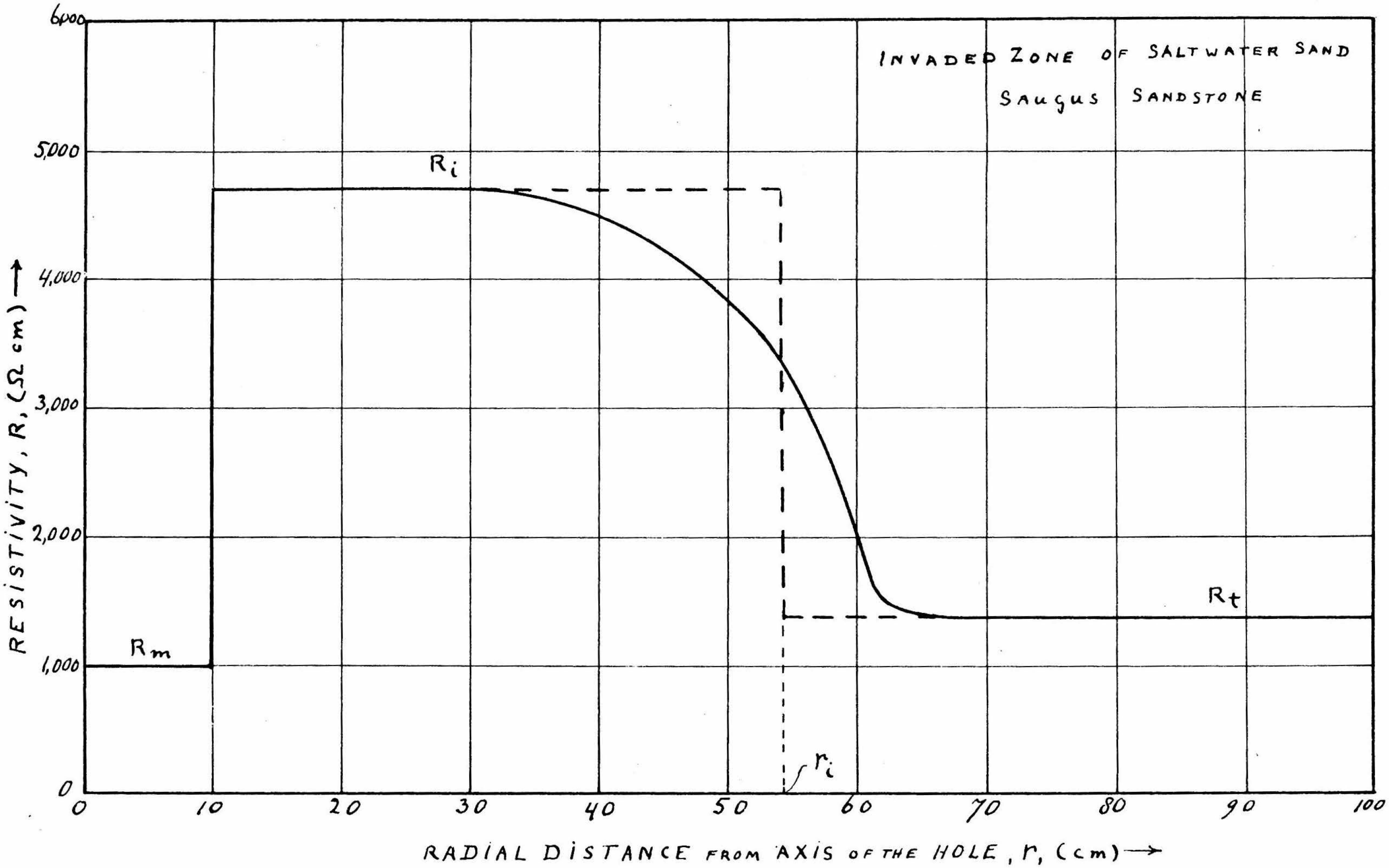
INVADED ZONE OF SALTWATER SAND
SAUGUS SANDSTONE
R_i
R_m
R_t
r_i
6,000
5,000
4,000
3,000
2,000
1,000
0
0
10
20
30
40
50
60
70
80
90
100
RESISTIVITY, R, (Ω cm) →
RADIAL DISTANCE FROM AXIS OF THE HOLE, r, (cm) →

Fig. VII - 5

The radius of the infiltrated zone, as determined with the aid of apparent resistivity curves, by the method described in Part II of this thesis, represents the distance from the axis of the hole to this hypothetical discontinuity. In Fig. VII-5 the radius of infiltration, r_i, equals 54.5 cm. As we had assumed $r_o = 10$ cm. we have in this case $r_i = 5.45\ r_o$. This represents an average amount of infiltration.

For larger amounts of infiltration the transition zone remains practically unchanged, while the zone of constant resistivity becomes larger. In such cases, the approximation made by representing the actual resistivity distribution by a constant R_i, becomes better.

For smaller radii of infiltration the zone of constant resistivity becomes smaller and the approximation used for purposes of interpretation becomes less accurate.

In the case of invasion of a fresh water sand by a more saline mudfiltrate, the resistivity distribution exhibits the same characteristics as those shown in Fig. VII-5, except that the true resistivity is larger than the infiltrated zone resistivity. The transition zone is therefore represented by an upward curve. All remarks made regarding the approximation of the actual resistivity by a constant resistivity, R_i, apply also in this case.

The displacement of the connate water by the mudfiltrate can be regarded in part as a piston mechanism, where the filtrate pushes a fraction of the connate water ahead of itself. However, an important part of the removal of the connate water is due to diffusion of the salt ions into the mudfiltrate. It would be logical to assume that the non-bound connate water is removed by the piston mechanism of the invading fluid, especially in the larger pores. The bound water gives off its salt ions by diffusion into the less saline filtrate.

To check these assumptions, the influence of the rate of invasion on the character of the transition zone was determined experimentally. The results are shown in Fig. VII-6, which gives the amounts of connate water, replaced by the filtrate, as a function of the amount of filtrate passed through the sample, for the Saugus sandstone.

We see that the smaller the pressure gradient for a given sample, or the smaller the rate of flow during infiltration, the more rapid the replacement of the connate water takes place.

This means that for slow rates of infiltration the transition zones of the resistivity profiles of the invaded zones, will be relatively less important.

In practice the pressure gradients encountered during the infiltration of permeable formations are mostly smaller than the gradient under which invasion took place in the experimental case, worked out and shown in Figs. VII-1 through VII-5. In this case the pressure gradient was 43 psi/inch.

The transition zones of the resistivity profiles will therefore in general be smaller than the one shown in Fig. VII-5 and the approximation made by assuming R_i = constant, will be better than in our example.

The removal of salt ions by diffusion into the mudfiltrate for a given amount of filtrate passed through a unit volume of rock depends more directly on the rate of flow of the filtrate than on the pressure gradient.

This means that in very permeable sands the rate of removal of the

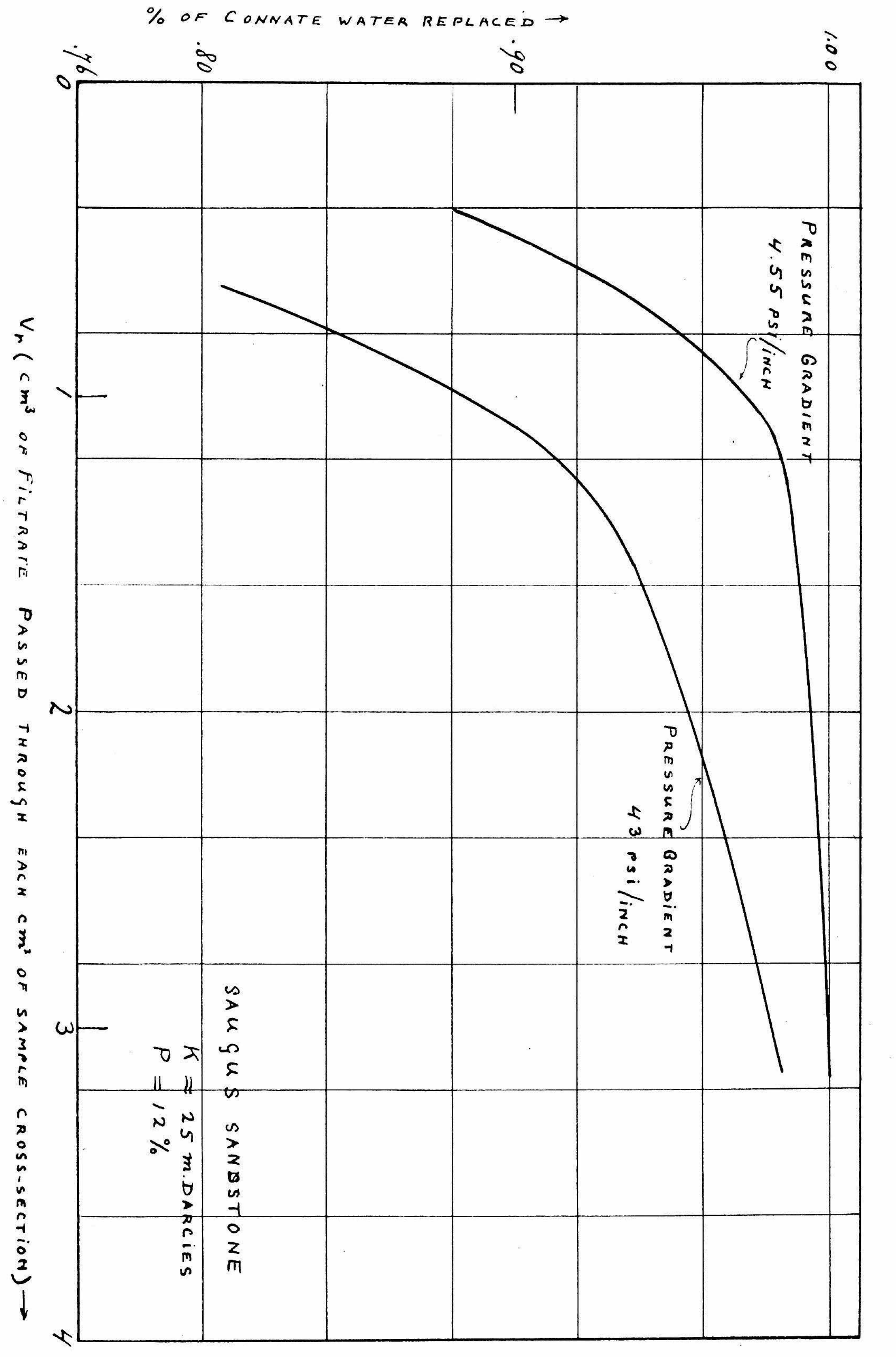
% OF CONNATE WATER REPLACED →
.76
.80
.90
1.00
0
1
2
3
4
V_r (cm^3 OF FILTRATE PASSED THROUGH EACH cm^2 OF SAMPLE CROSS-SECTION) →
PRESSURE GRADIENT 4.55 PSI/INCH
PRESSURE GRADIENT 43 PSI/INCH
SAUGUS SANDSTONE
K ≅ 25 m.DARCIES
P = 12%

Fig. VII-6

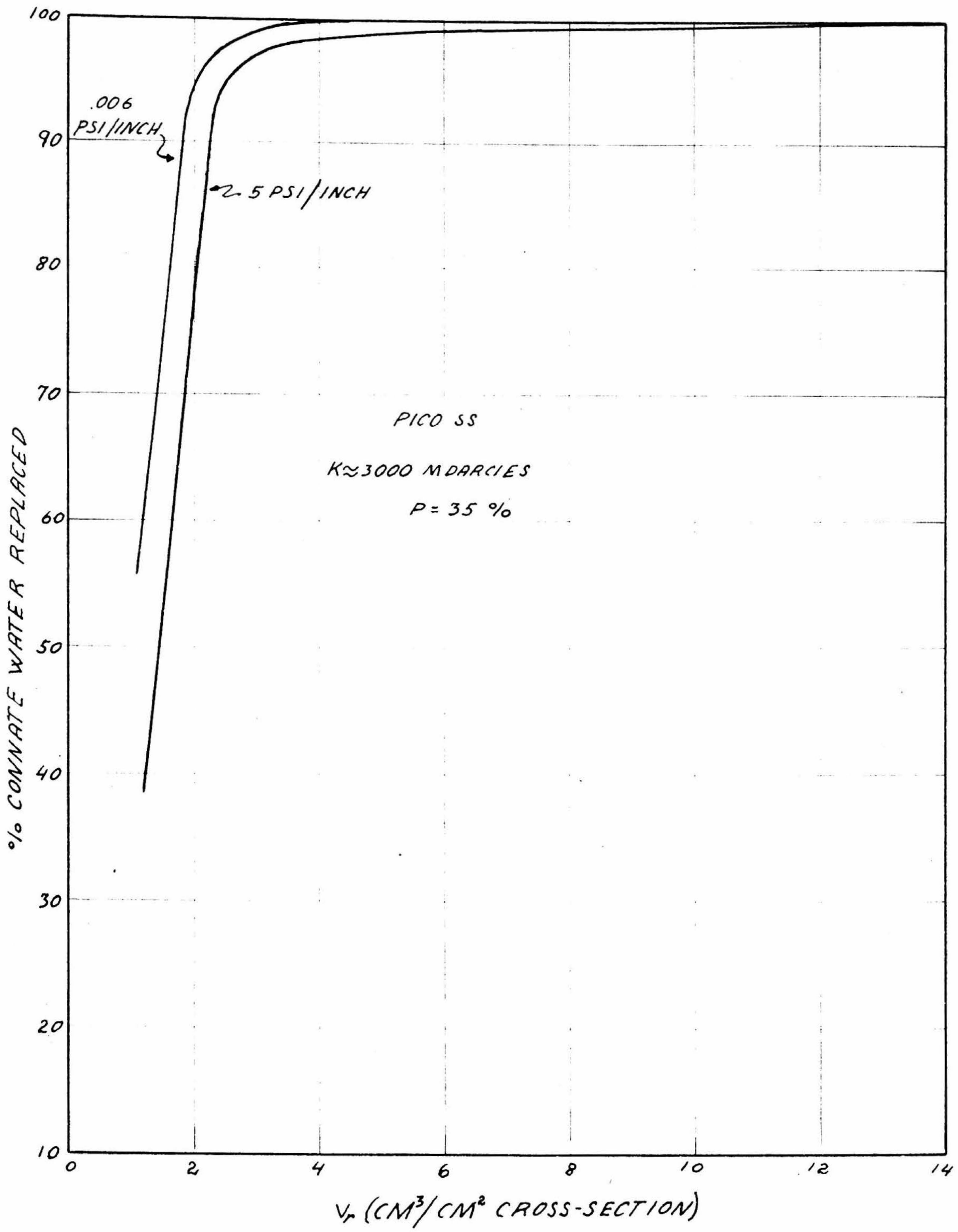

100
90
80
70
60
50
40
30
20
10
0
2
4
6
8
10
12
14
% CONNATE WATER REPLACED
Vr (CM³/CM² CROSS-SECTION)
.006 PSI/INCH
2.5 PSI/INCH
PICO SS
K≈3000 MDARCIES
P = 35 %

FIG VII-7

salt ions from the bound water will be slower than in a relatively tight sand. However this effect is partly offset by the fact that there exists a rough correlation between percentage of bound water and permeability of sediments.

The more permeable formations will have less bound water and larger pores and therefore the amount of salt ions to be removed strictly by diffusion will be percentagewise smaller.

In order to obtain a clear indication of the overall effect of permeability on the replacement rate of the connate water, experiments were made on a very permeable Pico sandstone ($K \approx 300$ m. darcys) and the results were compared with those obtained for the Saugus ss ($K \approx 2.5$ m. darcys).

Fig. VII-7 gives the % connate water replaced as a function of v_r for two different pressure gradients for the Pico sandstone.

Comparison with Fig. VII-6 shows that for the same pressure gradient the connate water replacement is more rapid in the less permeable sand.

b) Oil sands

The resistivity distribution in the invaded zones of oil sands depends upon two factors. The first is the displacement of part of the oil by the invading fluid; the second factor is the replacement of the connate water by the mudfiltrate.

As the displacement of the oil does not depend upon the resistivity of the invading mudfiltrate, its effect on the resistivity can be found by using a mudfiltrate of the same salinity as the connate water.

We can further simplify the procedure of obtaining the relation between amount of oil displaced, and radial distance from the boreface, by using very saline connate water and mud filtrate, so that we may use Archie's formula to relate the oil saturation and the resistivity at any point.

In Part V it was shown on theoretical grounds that the oil saturation in the infiltrated zone is related to the bound water content of the rock and also that the oil displacement depends upon the oil viscosity and the rate of infiltration. These relations will be checked quantitatively in the following sections. At this stage however we want to obtain primarily a qualitative picture of the resistivity distribution in the invaded zone as a function of radial distance from the boreface.

Fig. VII-8 and Fig. VII-9 represent the resistivity variation with amount of filtrate passed through each cm^2 of cross-sectional area perpendicular to the flow, respectively for a sample of Saugus ss (S-4a) and a Berea ss (0-9).

In Part VI of this thesis it was shown that for sufficiently small values of the water resistivity we may apply Archie's formula directly to calculate the water saturation. The samples used to demonstrate this fact were all saturated under high capillary pressures and contained practically only their bound water. During the process of invasion the water content is increased and the effect of conductive solids on the resistivity should therefore become even smaller. For these reasons it is quite safe to find the water saturation at the respective stages of invasion using Archie's formula, with the resistivity index $n = 2$. The water resistivities were 28.2 Ω cm. in the case of the Saugus ss and 27.2 Ω cm for the Berea ss. The connate water in both cases was

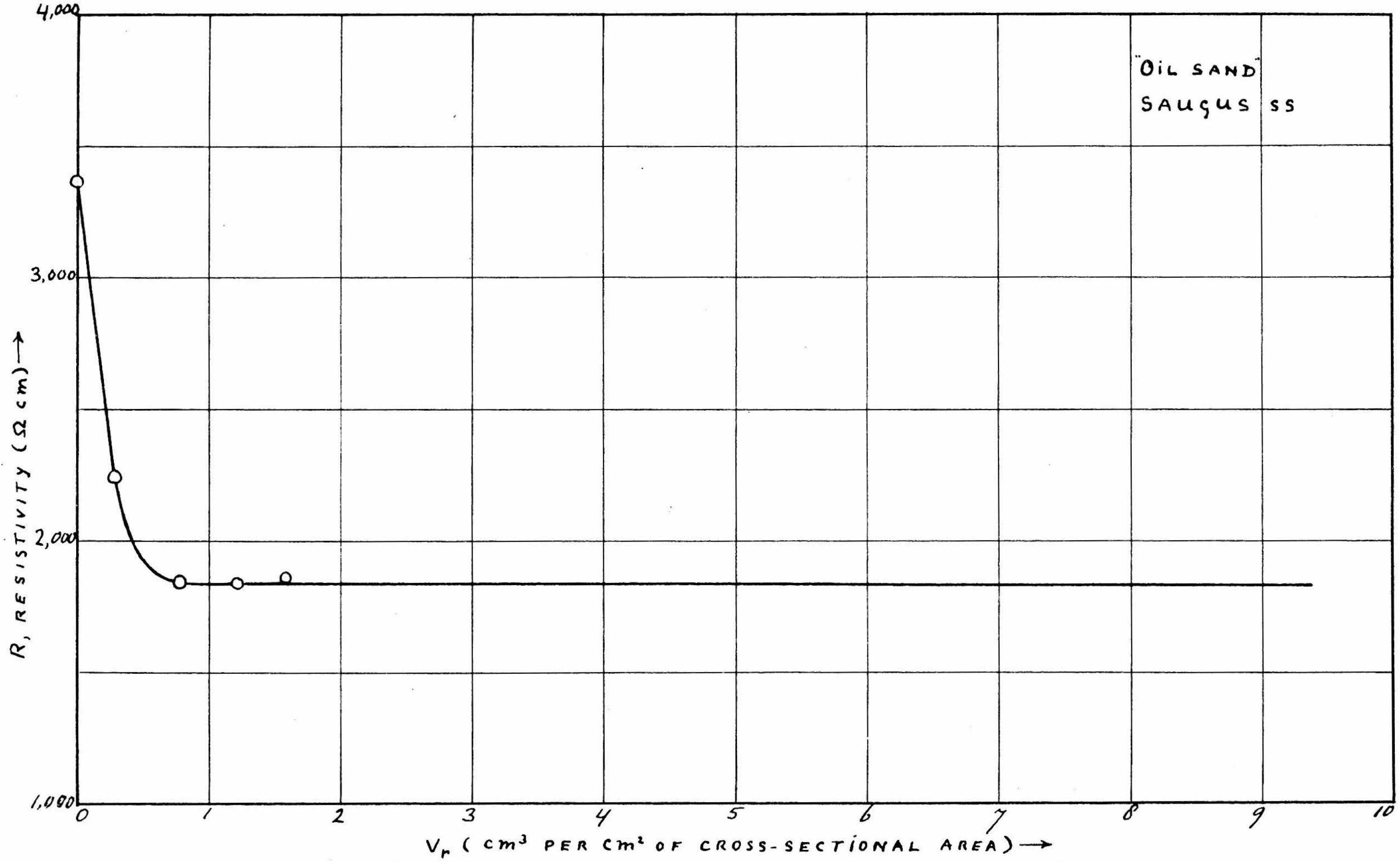
"Oil sand"
Saugus ss
R, resistivity (Ω cm) →
4,000
3,000
2,000
1,000
0
1
2
3
4
5
6
7
8
9
10
V_r (cm³ per cm² of cross-sectional area) →

Fig. VII - 8

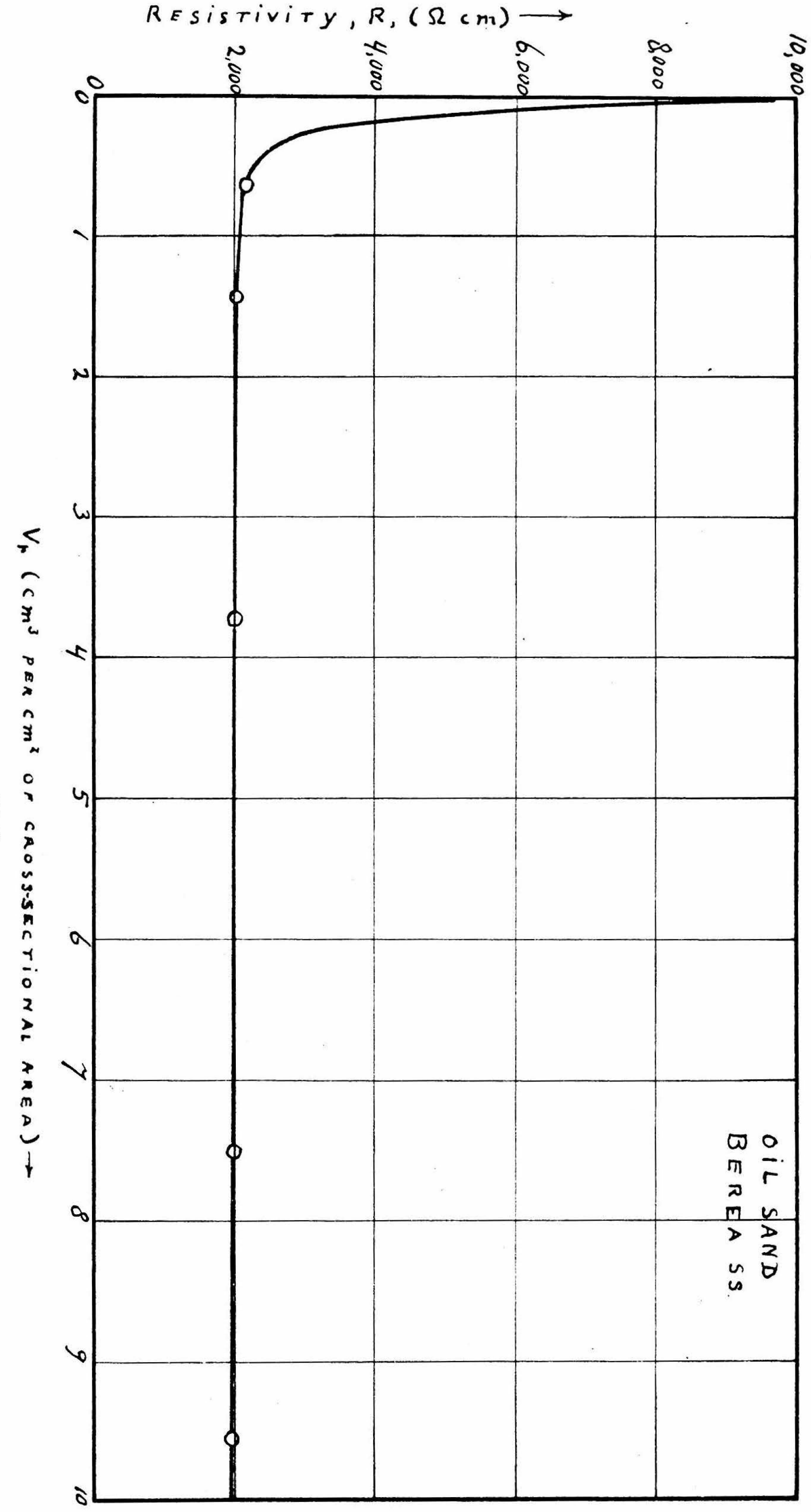
Resistivity, R, (Ω cm) →
0
2,000
4,000
6,000
8,000
10,000
0
1
2
3
4
5
6
7
8
9
10
V_p (cm³ per cm² of cross-sectional area) →
OIL SAND
BEREA SS

Fig. VII-9

identical with the invading water.

From the computed water saturations, we easily find the amounts of oil removed, which equal the amounts of filtrate retained as fractions of the total porespace, for each amount of infiltration at which a resistivity measurement of the sample was made. These fractions are shown as a function of v_r in Fig. VII-10, curves (a) and (b).

Using the data of Fig. VII-10 and formula (7-1) we can again plot v_r versus r. These plots are shown in Fig. VII-11.

Finally combining the data of Fig. VII-11 and Fig. VII-8 we can plot the resistivity as a function of the radial distance from the boreface, for the invaded zone of the Saugus ss. Combining the data of Fig. VII-9 and Fig. VII-11 we obtain a similar plot for the Berea sandstone. The computed resistivity distributions are shown for the Saugus ss and the Berea sandstone, respectively in Fig. VII-12 and Fig. VII-13.

We see that for sandstones of high bound water content C_W, and low porosity, as in the case of the Saugus ss, the transition zone of the resistivity profile is quite important.

On the other hand, for sands of low bound water content and high porosity, the transition zone becomes completely negligible.

Again for larger infiltration radii for a given sandstone the constant part of the resistivity profile becomes relatively more important, while for smaller radii of invasion the approximation of the resistivity distribution by a constant R_i becomes poorer.

As stated before, the above two cases only represent the effect of oil displacement in the infiltrated zones on the resistivity, as the

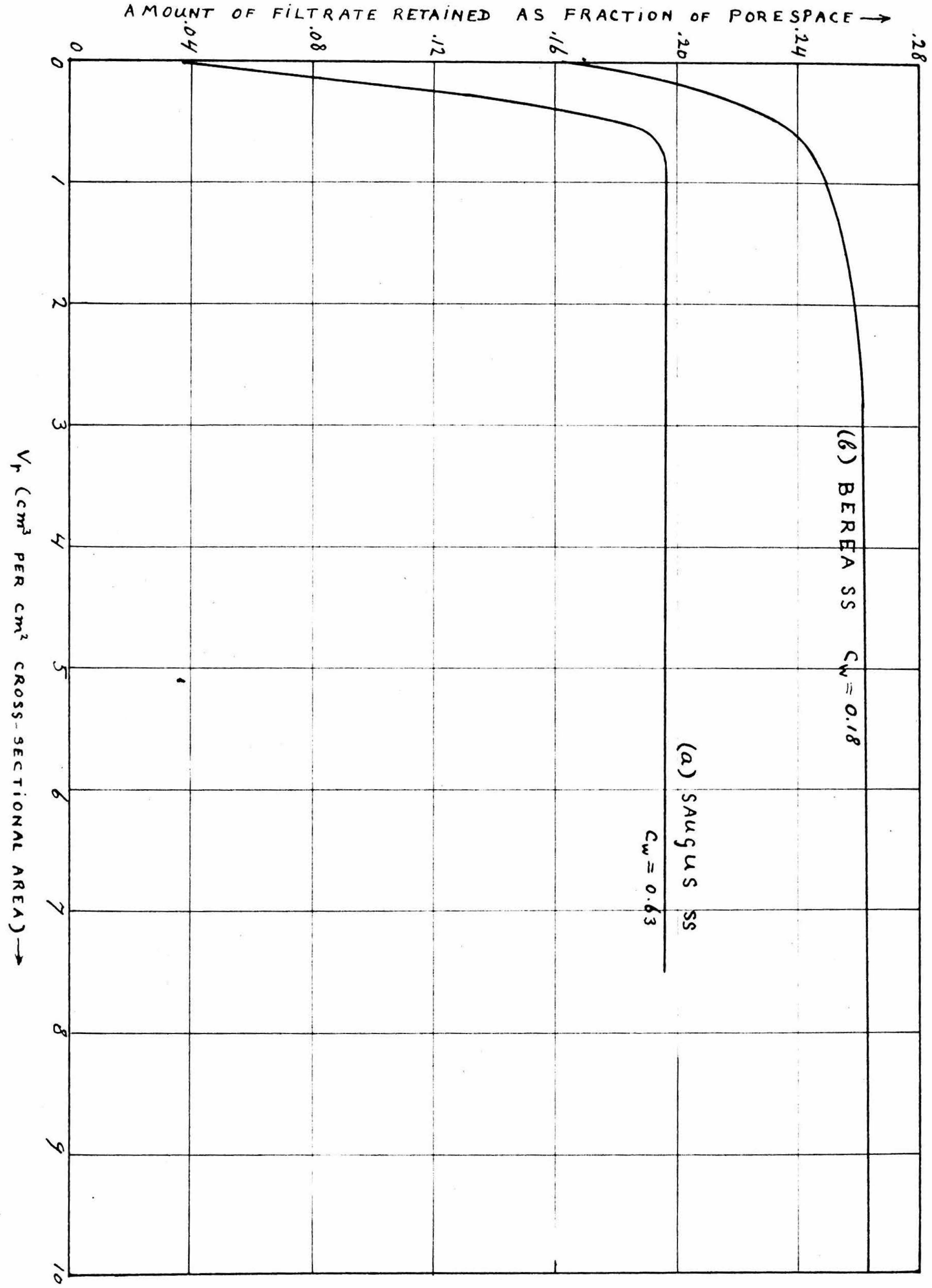
AMOUNT OF FILTRATE RETAINED AS FRACTION OF PORESPACE →
0
.04
.08
.12
.16
.20
.24
.28
0
1
2
3
4
5
6
7
8
9
10
V_r (cm³ PER cm² CROSS-SECTIONAL AREA) →
(b) BEREA SS $C_w = 0.18$
(a) SAUGUS SS
$C_w = 0.63$

Fig VII -10

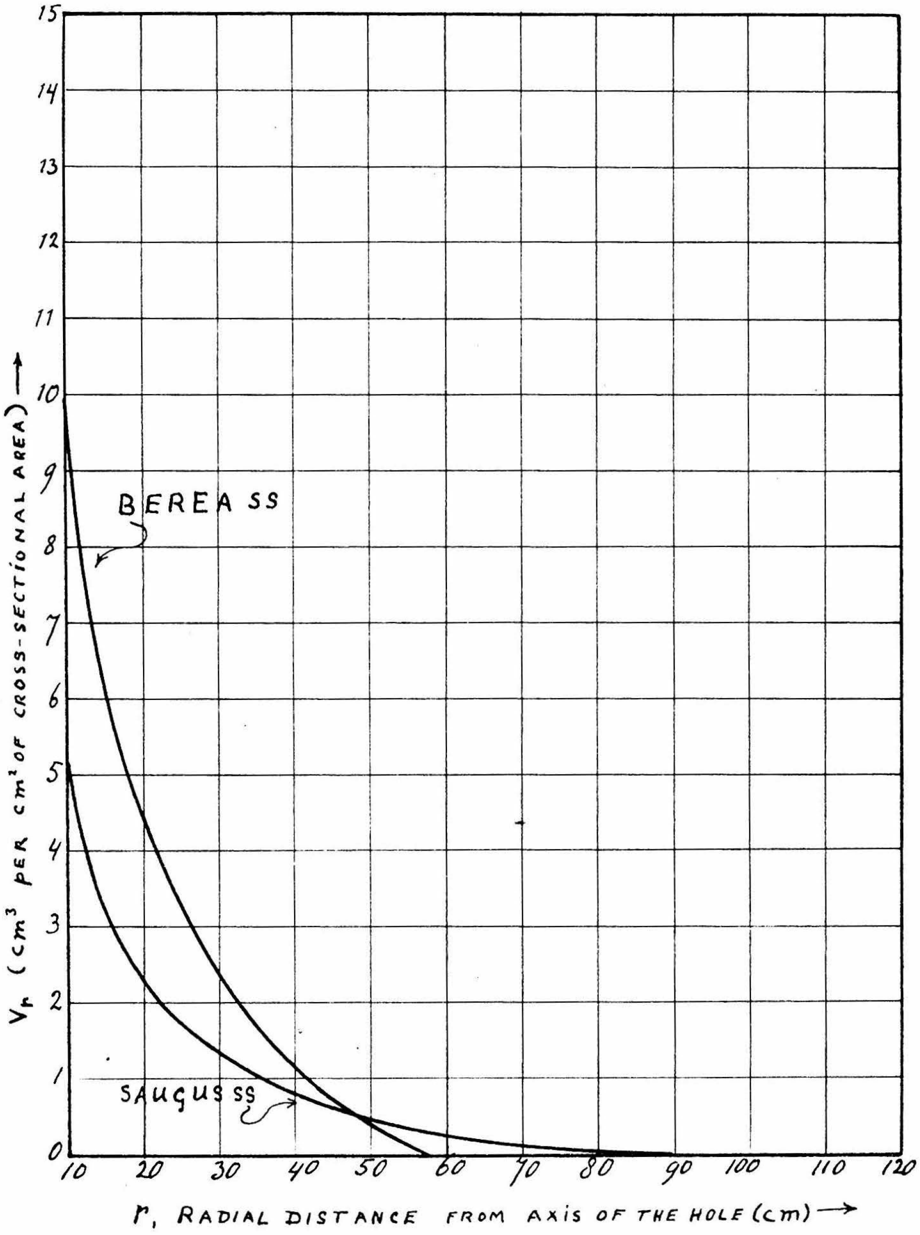

15
14
13
12
11
10
9
8
7
6
5
4
3
2
1
0
V_r (cm^3 PER cm^2 OF CROSS-SECTIONAL AREA) →
BEREA SS
SAUGUS SS
10
20
30
40
50
60
70
80
90
100
110
120
r, RADIAL DISTANCE FROM AXIS OF THE HOLE (cm) →

Fig. VII -11

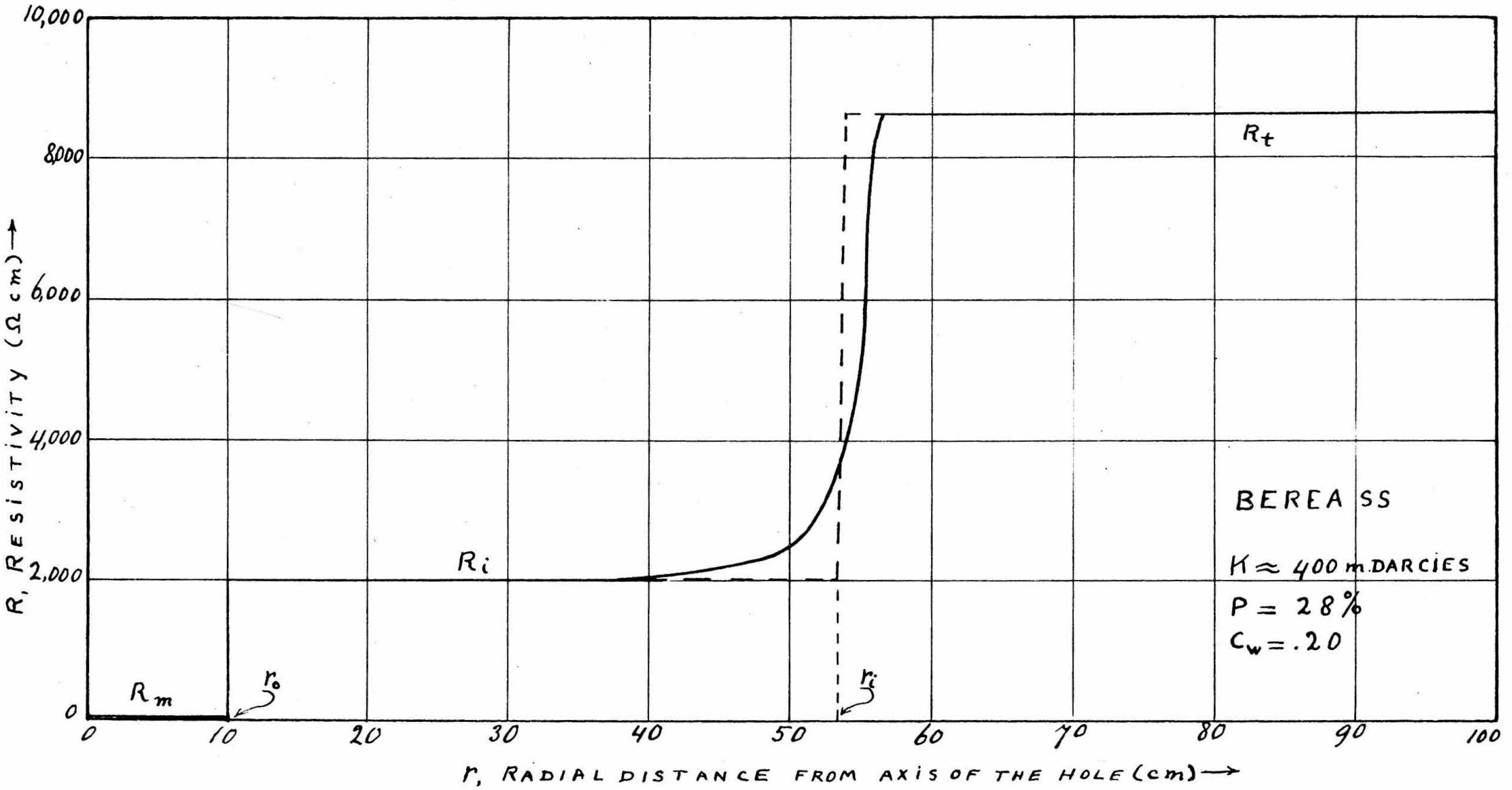
10,000
8,000
6,000
4,000
2,000
0
R, Resistivity (Ω cm) →
R_t
R_i
R_m
r_o
r_i
BEREA SS
K ≈ 400 m.DARCIES
P = 28%
C_w = .20
0
10
20
30
40
50
60
70
80
90
100
r, RADIAL DISTANCE FROM AXIS OF THE HOLE (cm) →

Fig. VII - 13

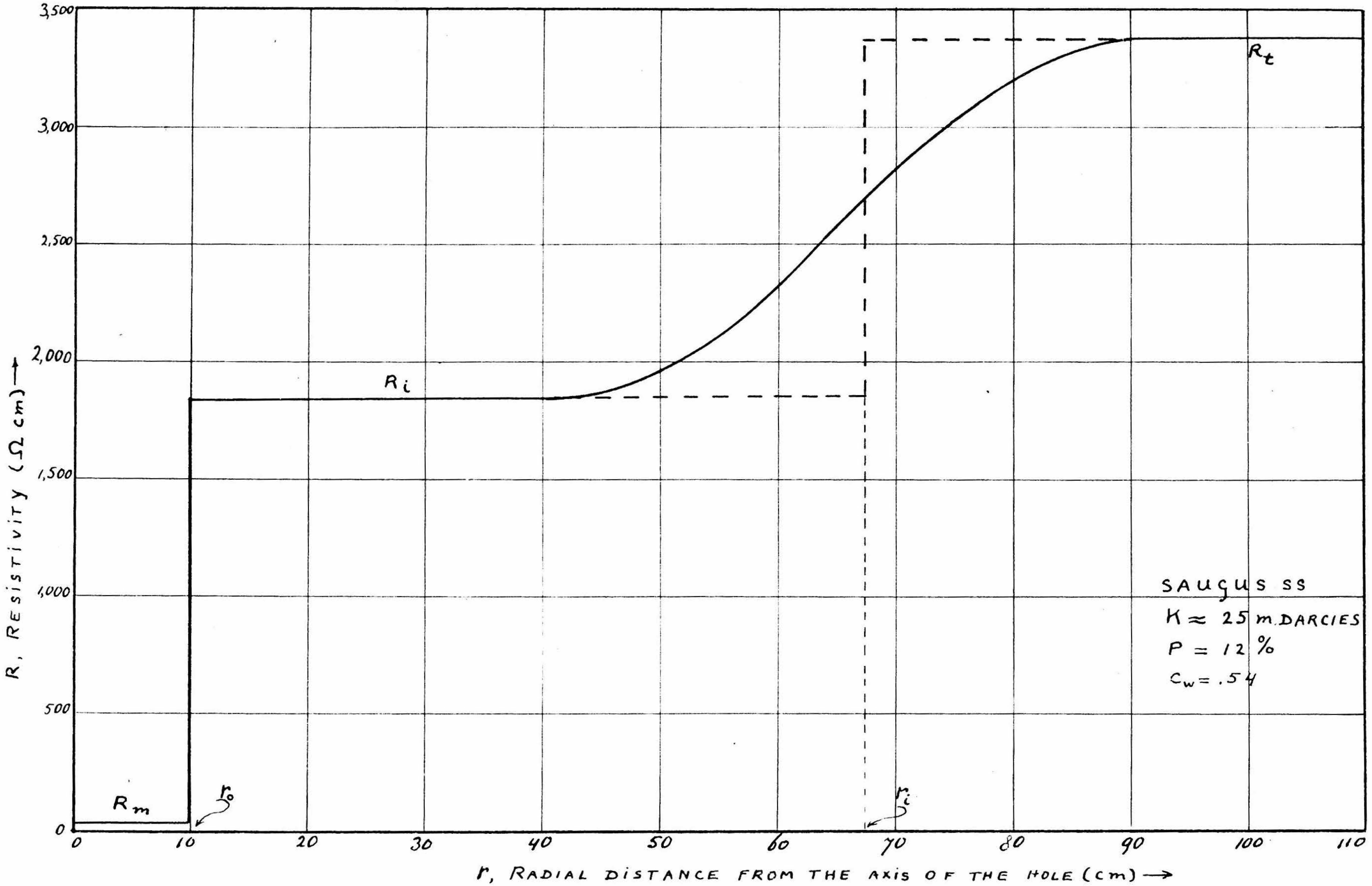
3,500
3,000
2,500
2,000
1,500
1,000
500
0
R, Resistivity (Ω cm) →
0
10
20
30
40
50
60
70
80
90
100
110
r, Radial distance from the axis of the hole (cm) →
R_m
R_i
R_t
r_o
r_i
SAUGUS SS
K ≈ 25 m.DARCIES
P = 12 %
C_w = .54

Fig. VII - 12

invading fluid was made identical to the connate water.

If, as is usually the case, the mud filtrate is less saline than the connate water, we have superimposed on the effects of oil displacement the resistivity changes due to replacement of the connate water by the mud filtrate.

The two effects are of opposite sign, and often are of almost equal magnitude, so that for many oil sands the resistivity of the infiltrated zone does not differ much from the true resistivity of the formation.

The computing of the resistivity distribution in the invaded zone in this case is quite complicated. The simultaneous change in oil content and interstitial water composition makes it impossible to compute the amount of filtrate retained in the core from single resistivity measurements.

For these reasons an experiment was performed using a Berea sandstone sample identical to those used in the preceding experiments. This sample was saturated with oil to an oil saturation of approximately 79%, which is the same saturation as prevailed initially in the preceding experiment where the invading water was identical to the connate water.

As the oil displacement does not depend upon the salt content of the invading water, we may use the graph for the Berea sandstone in Fig. VII-10 to determine the amount of oil displaced or the corresponding water-saturation for any amount of infiltration. The amounts of oil displaced for various amounts of infiltration (v_r) are denoted by $(x_r)_{oil}$ and listed in Table VII-A, together with the corresponding water saturations (S_w) and the measured resistivities of the sample (R).

To find the total amount of infiltrating fluid retained in the sample, we have to add onto the amount retained by displacement of oil the quantity retained by replacement of the original connate water. To find this latter quantity we must calculate the interstitial water resistivity after various amounts of infiltration. The water resistivity then serves as an indication of the fraction of the interstitial water consisting of the invading fluid and the fraction consisting of the original connate water.

To calculate the water resistivity Archie's formula may only be applied where the interstitial water resistivity is sufficiently low, as was pointed out before. As soon as part of the original saline connate water is replaced by mud filtrate this holds no longer true and we have to use formula (6-14) to calculate the interstitial water resistivity.

Equation (6-14) relates the water resistivity to the other parameters involved in the following manner:

$$R\ S_w{}^2 = \frac{F\ R_f\ R_w}{R_w - X_w'\ (R_w - R_f)}$$

where

$$X_w' = \frac{m/n}{m/n + R_f/S_w}$$

We found previously that for the Berea sandstones $R_f \approx 33\ \Omega$ cm. It remains therefore to determine the values of F and m/n for the sample in question. This is done by measuring the resistivity of the sample when 100% water saturated for two different water resistivities.

m/n is found from equations (6-9) and (6-10) as:

$$m/n = \frac{(R_w)_1 \, (R_w)_2 \left[(R_o)_1 - (R_o)_2 \right]}{(R_w)_1 \, (R_o)_2 - (R_w)_2 \, (R_o)_1}$$

Also we have from equation (6-9):

$$\frac{X_w}{F} = \frac{(R_w)_1 \, (R_w)_2 \left[(R_o)_1 - (R_o)_2 \right]}{(R_o)_1 \, (R_o)_2 \left[(R_w)_1 - (R_w)_2 \right]} \qquad \text{with} \qquad X_w = \frac{m/n}{m/n + R_f}$$

which gives us the value of F.

Using the relations the following results were obtained:

$(R_w)_1 = 10.6 \ \Omega$ cm $\qquad (R_o)_1 = 182 \ \Omega$ cm

$(R_w)_2 = 1131 \ \Omega$ cm $\qquad (R_o)_2 = 11{,}310 \ \Omega$ cm

$X_w/F = 0.0577 \qquad m/n = 1554$

$F = 16.98 \qquad X_w = .98$

Using these data we obtain the values of R_w from equation (6-14).

Finally the fraction of invading fluid in the interstitial water is found using equation (6-2) and the computed values of R_w.

Equation (6-2) may be written as:

$$1 - X_1 = X_2 = \frac{1 - R_1/R_c}{1 - R_1/R_2}$$

where R_1, R_2 and R_c are respectively the resistivities of the original connate water, of the invading fluid, and of the interstitial water mixture upon invasion. X_1 and X_2 are respectively the fraction of connate water and of invading fluid in the interstitial water.

$R_1 = 12.2 \ \Omega$ cm; $R_2 = 955 \ \Omega$ cm.

Table VII-A lists the computed values of X_2. Multiplying these with the corresponding values of the water saturation, S_w, we obtain the amount of invading fluid retained, as a function of the porespace. This quantity is denoted by $(X_r)_t$ and is also tabulated in Table VII-A.

TABLE VII-A

v_r	R Ω cm	$(x_r)_{oil}$	S_w	X_w'	R_w	X_2	$(X_r)_t$
0	5010	0	.202	.907	12.2	0	0
0.223	2750	.205	.407	.95	26	.537	.219
0.473	2690	.232	.434	.953	29.6	.590	.240
0.696	5510	.242	.444	.955	66.9	.820	.368
1.002	14,910	.249	.451	.955	213	.966	.436
1.560	20,940	.255	.457	.956	380	.981	.448
2.090	21,300	.258	.460	.957	393	.983	.452
2.480	21,640	.268	.462	.957	413	.985	.455
8.000	24,000	extrapolated					.462

The initial water saturation, before flushing was started, was calculated to be .202 using equation (6-17). Using Archie's formula gave $S_w = .206$, which is a very good approximation as would be expected for the very low resistivity of the connate water.

Having determined the amounts of infiltrating fluid, $(X_r)_t$, as a function of the amount of infiltration, v_r, we can again compute the resistivity distribution for the infiltrated zones of any arbitrarily chosen invasion diameter, in exactly the same manner as described for the case of invasion of a salt sand.

Fig. VII-14 shows the measured values of R, as a function of v_r, while Fig. VII-15 gives the actual resistivity profile for the invaded zone of an oil sand with saline connate water.

We see from Fig. VII-14 that upon invasion the resistivity first

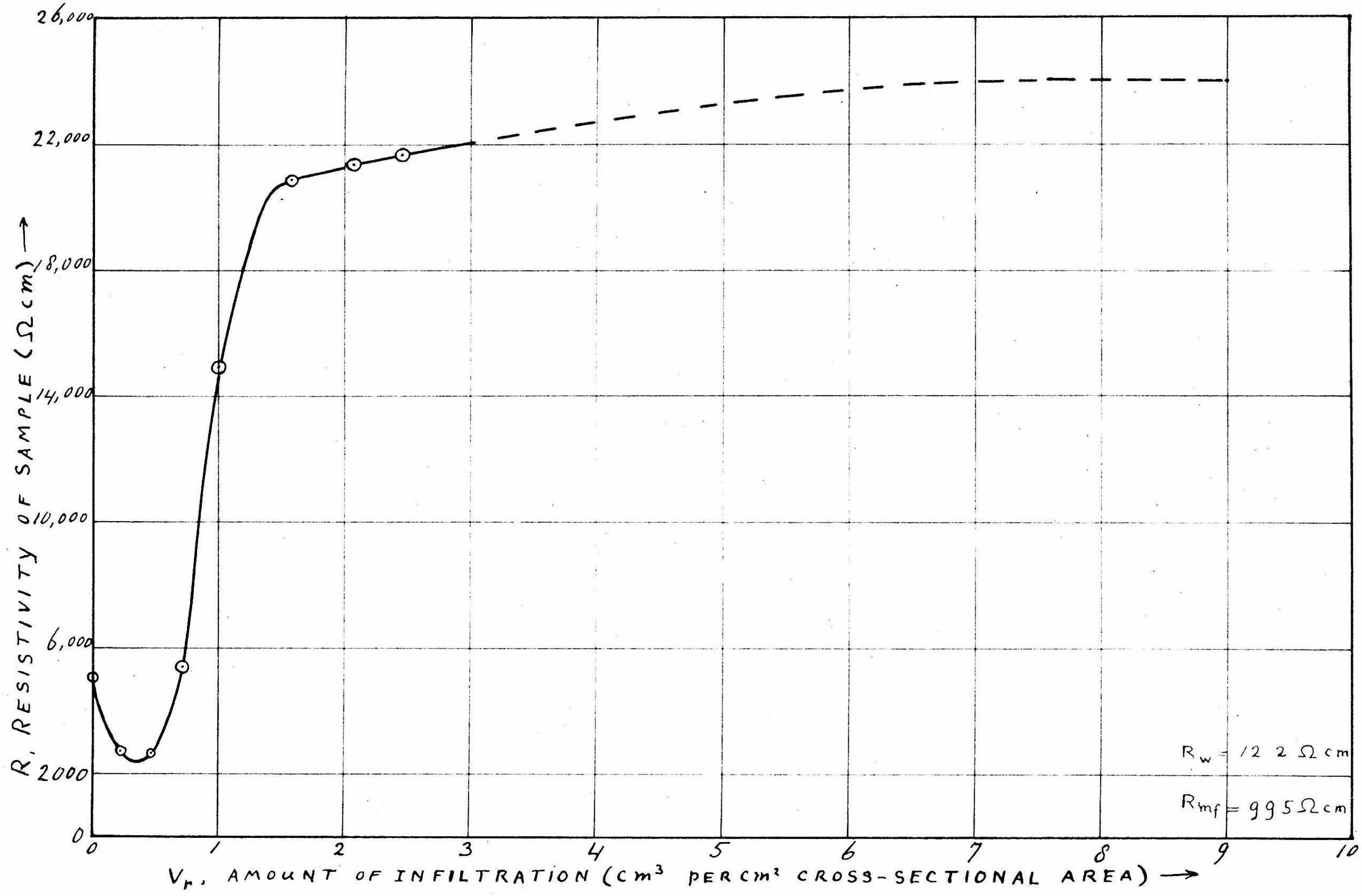
R, RESISTIVITY OF SAMPLE (Ω cm) →
26,000
22,000
18,000
14,000
10,000
6,000
2000
0
0
1
2
3
4
5
6
7
8
9
10
V_r, AMOUNT OF INFILTRATION (cm³ PER cm² CROSS-SECTIONAL AREA) →
R_w = 12 2 Ω cm
R_mf = 995 Ω cm

Fig. VII-14

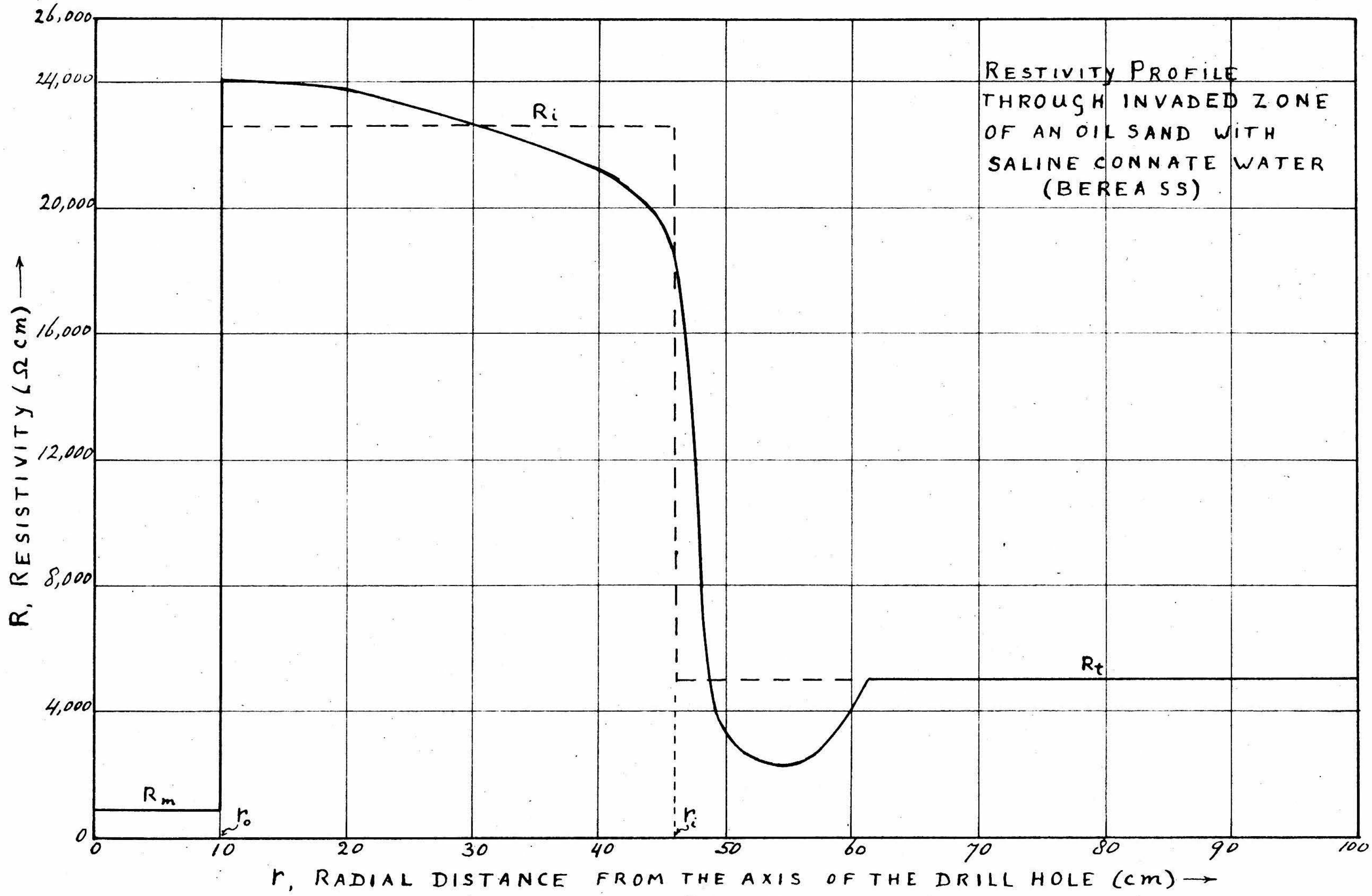
RESTIVITY PROFILE
THROUGH INVADED ZONE
OF AN OIL SAND WITH
SALINE CONNATE WATER
(BEREA SS)
R, RESISTIVITY (Ω cm) →
26,000
24,000
20,000
16,000
12,000
8,000
4,000
0
Ri
Rm
Rt
r₀
rᵢ
0
10
20
30
40
50
60
70
80
90
100
r, RADIAL DISTANCE FROM THE AXIS OF THE DRILL HOLE (cm) →

Fig. VII - 15

decreases, goes through a minimum and then sharply increases. This is caused by the fact that the oil is removed more rapidly than the connate water. The replacement of oil by the invading water decreases the resistivity. However as soon as the larger part of the saline connate water starts being replaced by the less saline mudfiltrate, the resistivity rises sharply.

As shown in Fig. VII-15 the infiltrated zone resistivity may be much higher than the true formation resistivity, if the salinity contrast between the connate water and the mudfiltrate is large enough. In our example, $\frac{R_{mf}}{R_w} = 78.5$. In many practical cases the contrast will be much smaller and R_i and R_t may be very nearly equal. If the mudfiltrate is as saline as the connate water or more saline, the infiltrated zone resistivity will naturally be smaller than the true resistivity. However these cases will be exceptions rather than the rule.

e) Gas sands

In Part V of this thesis some computations on the saturation distribution in the invaded zones of gas sands, based on published relative permeability data, were carried out. The results showed an almost constant saturation throughout the entire infiltrated zone. It was pointed out however that the relative permeability data are not reliable close to the points where the permeability of one of the phases approaches zero. In the case of gas sands, because of the low viscosity of the gas compared to the water, very small values of the relative permeability to gas are still of noticeable importance in determining the amount of gas that will be displaced upon invasion by water.

Experimentally determined saturation distribution data for a gas sand showed that indeed the relative permeability relations are not reliable for gas displacement computations. The experiment on the character of the infiltrated zone of gas sands was carried out in exactly the same manner as that described for the case of an oil sand. The sample used was Berea sandstone which contained a very small fraction of bentonite. The gas used was nitrogen gas. By the capillary pressure method water from the core was displaced by gas until a gas saturation of .506 was reached.

The resistivity of the connate water was made low so that Archie's formula could be applied with fair accuracy and the invading water was made identical to the connate water. Resistivity measurements gave for the 100% water saturation sand $(R_o)_1 = 182\ \Omega$ cm and at $S_g = .506$ we found $R = 752\ \Omega$ cm.

Applying Archie's formula gives $S_g = 1 - S_w = .48$. Or using $(S_w)^n = \frac{(R_o)_1}{R}$ we find $n = 1.95$. We see that Archie's formula with $n = 2$ gives us a reasonable approximation of S_w for gas sands as well as for oil sands, if the effect of conductive solids may be neglected.

Resistivity measurements for a different value of the connate water resistivity and application of equations (6-9) and (6-10) gave

$$\frac{1}{R_o} = 0.372 \times 10^{-4} + \frac{0.0577}{R_w}$$

For the gas displacement experiment we had $R_w = 10.6\ \Omega$ cm, and we see that in this case the factor representing the influence of the conductive solids is indeed negligible.

The sample resistivity is given as a function of the amount of invading water passed through the sample in Fig. VII-16.

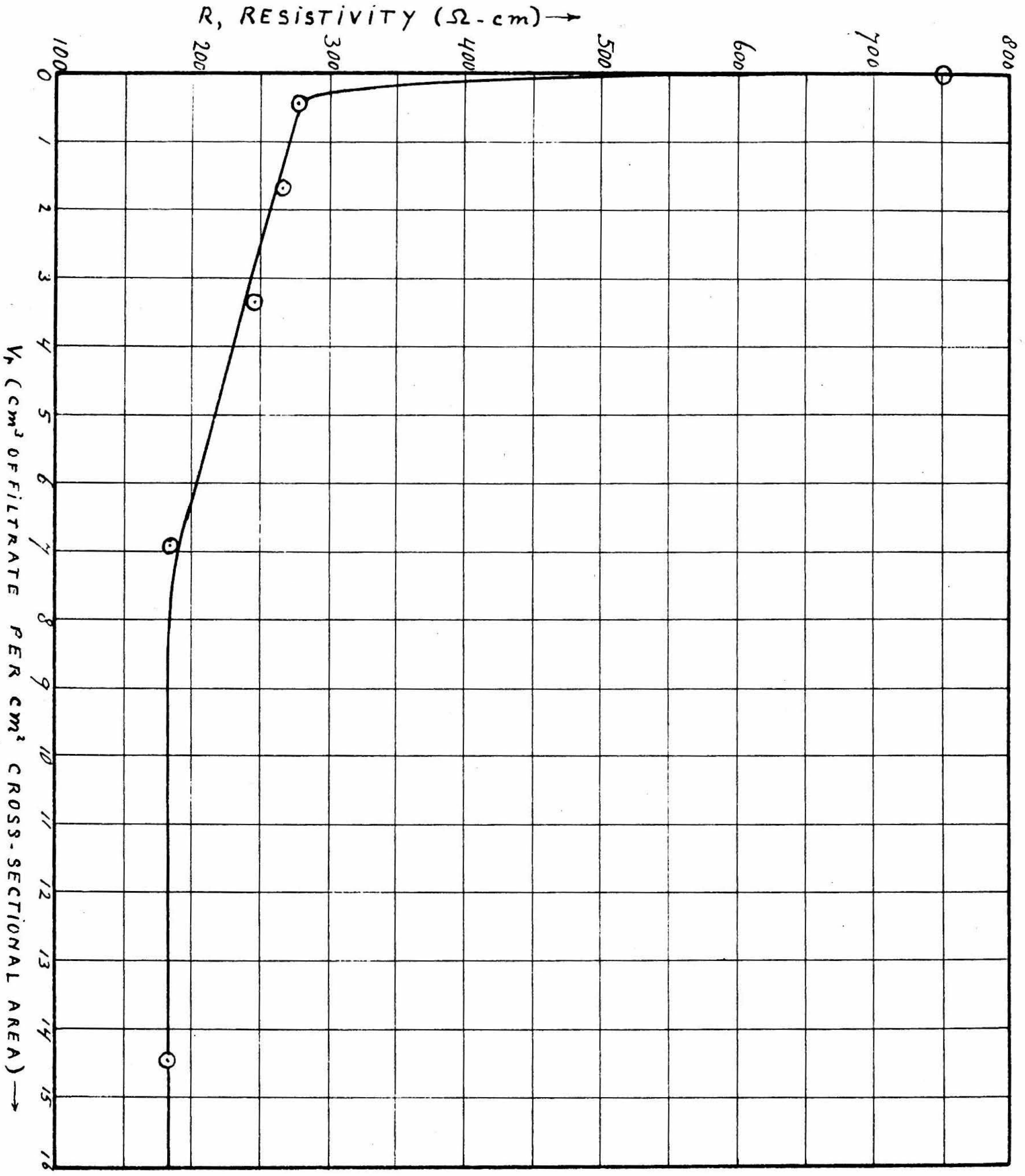
R, RESISTIVITY (Ω-cm) →
100
200
300
400
500
600
700
800
0
1
2
3
4
5
6
7
8
9
10
11
12
13
14
15
16
V_f (cm^3 OF FILTRATE PER cm^2 CROSS-SECTIONAL AREA) →

Fig. VII-16

Using the same procedure as described for the case of an oil sand with invading water resistivity equal to the connate water resistivity, the resistivity distribution in the invaded zone, as a function of the radial distance from the center of the borehole, is computed again. The result is shown in Fig. VII-17

We see that the resistivity is not constant, as was concluded from the relative permeability data, but varies with the radial distance, r.

The total magnitude of the variation however is small enough so that, approximation by a constant resistivity, R_i, may still be applied.

Other measurements were made using the same sample but different initial gas saturations.

It was found that the initial gas saturation for a given sample has little or no effect on the resulting saturation upon infiltration.

The water saturation in the invaded zone in this experiment varies from .81 to 1.00 with an average at approximately .90 .

We found that for oil of 17 cp viscosity the invaded zone of the Berea ss had a water saturation of approximately .48 . This illustrates clearly the influence of the viscosity of the nonwetting phase upon the resulting saturation of the invaded zones.

2) Relation between the water saturation of the invaded zone and of the undisturbed formation in oil and gas horizons

From computations based on resistivity log data, Tixier (19) showed that a relation exists between the amount of oil retained upon invasion of an oil sand and the amount of oil initially present in the sand.

That such relation should exist was explained in Part V of this thesis by the fact that the oil retained upon flushing depends upon the

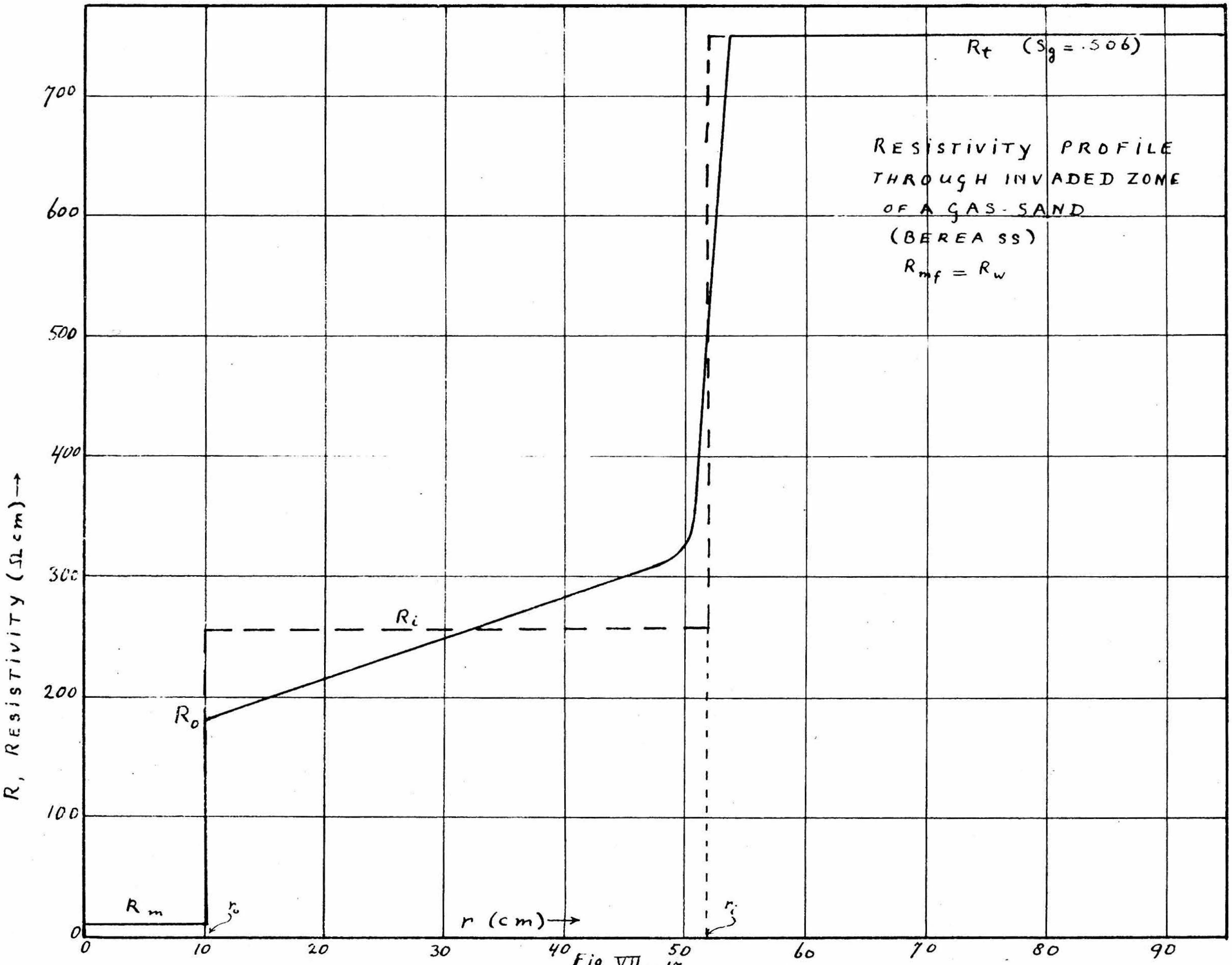
RESISTIVITY PROFILE
THROUGH INVADED ZONE
OF A GAS-SAND
(BEREA SS)
$R_{mf} = R_w$
R_t ($S_g = .506$)
R_i
R_o
R_m
r_c
r_i
R, RESISTIVITY (Ω cm) →
r (cm) →
0
100
200
300
400
500
600
700
0
10
20
30
40
50
60
70
80
90

Fig. VII - 17

relative permeability of the formation to oil and water at various saturations. The latter are related to the capillary characteristics of the rock and those in turn determine the bound water content or the initial oil saturation in the horizon in question.

Tixier found that the above relation could be approximated by $(S_W)_i^n = S_W$ with $n \approx 2$ where $(S_W)_i$ and S_W denote respectively the water saturation in the infiltrated zone and in the undisturbed formation.

In Part V we showed however that the saturations prevailing in the infiltrated zones depend upon the rate of flow of the invading fluid and the viscosity ratio of the oil and the water.

To obtain a quantitative estimate of the magnitude of the various factors involved, a series of experiments was carried out in which the effects of each factor were studied keeping all other factors constant. In all cases the bound water content was determined from the capillary pressure-saturation relationships. To facilitate the interpretation of the measurements, water of low resistivity was used and the infiltrating fluid was always identical to the initially present connate water. Under these conditions the water saturation upon flushing could be determined by measurement of the sample resistivities and application of Archie's formula.

The main series of experiments was carried out with oil of 30.2° A.P.I. gravity at approximately 70°F, having a viscosity of close to 17 centipoises.

The pressure gradient during the flushing was kept at approximately 2 psi/cm.

The average pressure gradients encountered during infiltration of porous horizons around drill holes are mostly smaller (0.1 - 1 psi/cm).

The relation between $(S_W)_i$ and (S_W) under the above conditions was investigated for four types of sandstone, namely a Saugus ss, a Berea ss and two types of Pico ss.

The relation is represented graphically in Fig. VII-18, graph I. We note that on a log-log scale the relation may be represented by a straight line, which for the particular conditions in question approaches very closely the graph for the relation $(S_W)_i{}^2 = S_W$ (graph II).

The effect of the pressure gradient during infiltration upon the invaded zone saturation was found by flushing a sample of Pico sandstone under various pressure gradients and computing the resulting values of $(S_W)_i$ from resistivity measurements. The applied gradients were respectively 0.1, 1 and 22 psi/inch. The results are shown by points 1, 2 and 3 respectively in Fig. VII-18.

On the assumption that for any pressure gradient the relation $(S_W)_i{}^n = S_W$ holds true, graphs have been drawn through points 1 and 3, to apply respectively to the cases where invasion took place under a gradient of 0.1 psi/inch and 22 psi/inch.

Unless specific information is at hand on permeabilities and rates of infiltration, the relation $(S_W)_i{}^2 = S_W$ will have to be used for the interpretation procedures as outlined in Part VI.

To find the effect of the viscosity of the non-wetting phase on the resulting infiltrated zone saturations, $(S_W)_i$ was determined for a Pico sandstone sample saturated with kerosene (45° A.P.I. gravity, viscosity 3 centipoises). The following results were obtained:

$R_W = 20.5\ \Omega$ cm $\qquad$ $R_o = 318.3\ \Omega$ cm.

After saturation with kerosene under a capillary pressure of 25 psi, the resistivity was found to be 3244 Ω cm. Using Archie's formula this gives $S_w = .313$. (By volumetric measurement we found $S_w = .28$).

After flushing with 500 cm of water, identical to the interstitial water (water resistivity = 20.5 Ω cm) under a pressure gradient of 2 psi/cm, the resistivity of the sample was found to be 593 Ω cm. Using again Archie's formula we obtain $(S_w)_i = \left(\frac{318.3}{593}\right)^{\frac{1}{2}} = .732$.

The corresponding point is plotted in Fig. VII-18. Assuming again that the relation $(S_w)_i^n = S_w$ applies also in this case, graph III is drawn to represent the relation between $(S_w)_i$ and S_w for $\mu_o/\mu_w = 3$. (Here μ_o and μ_w denote respectively the viscosity of the oil and that of the water).

For graph III we find $n \approx 4$. We see that the variation of n with the value of μ_o/μ_w is quite large. Lack of knowledge of the viscosity ratio under reservoir conditions may therefore introduce considerable errors in computations of water saturations of formations based on assumed values of n.

It is realised that the data presented in Fig. VII-18 are too few to be relied upon for precise evaluation of the combined effects of viscosity ratios and pressure gradients on the invaded zone saturations.

Taking into account the lowering of oil viscosity with temperature and amount of dissolved gas and the lowering of the water viscosity with temperature as described by Beal (21) it seems reasonable to use the relation $(S_w)_i^n = S_w$ with n = 2 in regions where the surface gravity of the oil is smaller than 30° A.P.I., and to use n = 3 where the surface gravity of the oil is larger than 30° A.P.I.

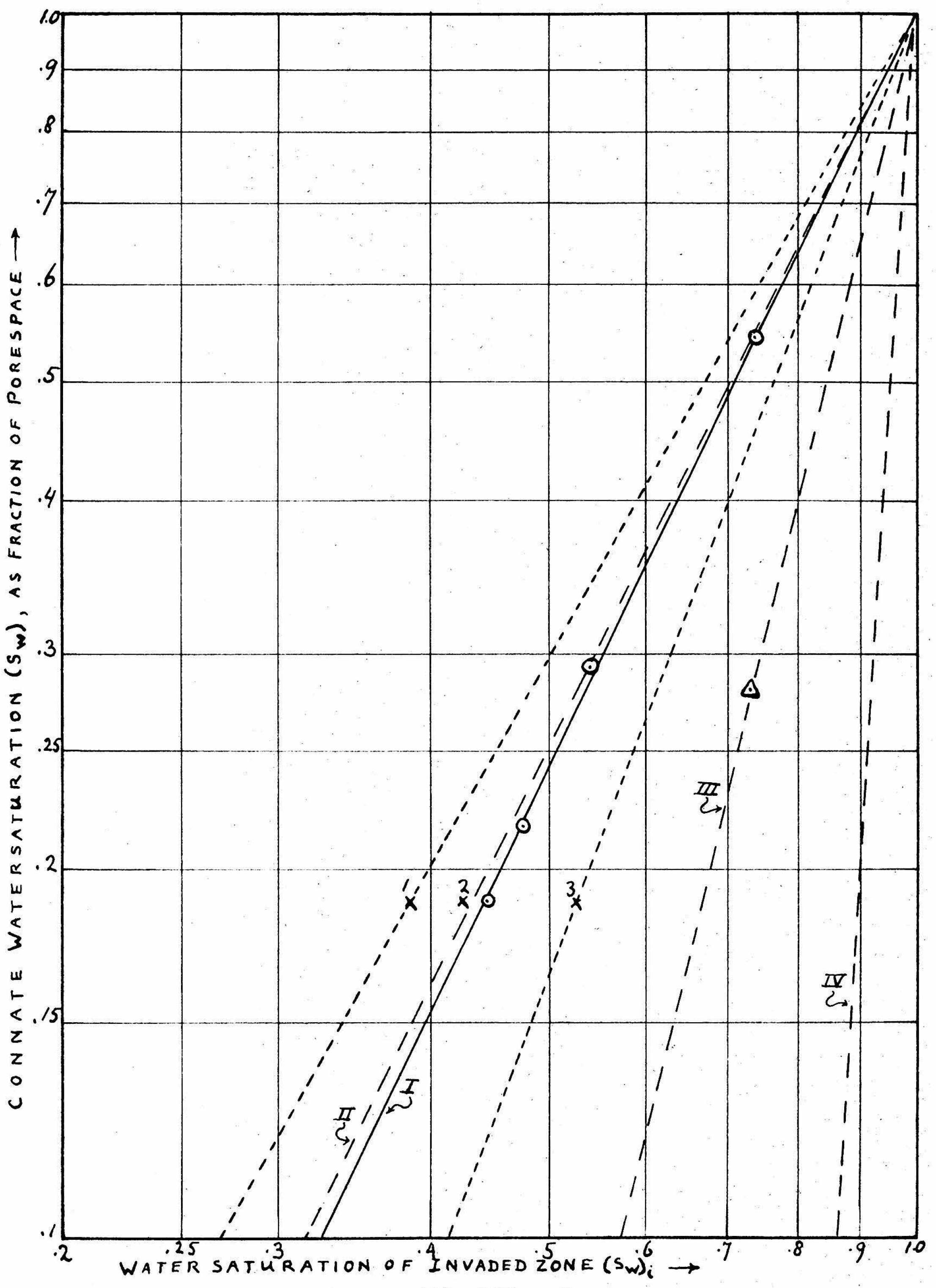

1.0
.9
.8
.7
.6
.5
.4
.3
.25
.2
.15
.1
CONNATE WATER SATURATION (S_w), AS FRACTION OF PORESPACE →
.2
.25
.3
.4
.5
.6
.7
.8
.9
1.0
WATER SATURATION OF INVADED ZONE $(S_w)_i$ →
I
II
III
IV
2
3

Fig. VII - 18

As described in the section on the resistivity profiles through invaded zones of gas sands, the water saturation in such zones varies continuously with the radial distance from the boreface. For gas sands we have to use therefore the concept of average invaded zone saturation. Based on the data obtained in the preceding section for the Berea sandstone, graph IV of Fig. VII-18 has been drawn to represent roughly the relation between the water saturation of the invaded zones and those of the undisturbed formations, for gas sands.

REFERENCES

1. W. R. Smythe: Static and Dynamic Electricity, New York, McGraw-Hill Book Co., Inc., 1939, 169.
2. W. R. Smythe: loc. cit. (1) p. 195.
3. V. A. Fock: Theory of the Determination of the Resistivity of Beds by Electrologging. State Technical Theoretical edition USSR (1933).
4. L. M. Alpin: A Theory of Electrical Well Logging, USSR (1938).
5. V. N. Dakhov: Well-logging, Interpretation of Logs, Moscow (1941), reprinted in 1945.
6. H. G. Doll, J. C. Legrand, E. F. Stratton: True Resistivity Determination from the Electric Log - Its Application to Log Analysis. Oil and Gas Fournal, September 20, 1947, 297.
7. Schlumberger Well Surveying Corporation, Houston, Texas, Resistivity Departure Curves, (1947).
8. H. Guyod: Electric Log Interpretation. Oil Weekly, December 17, 1945.
9. Drilling Mud (National Lead Company publication) May, 1940, p.4.
10. L. de Witte: Factors Governing Accumulation of Oil and Gas in Stratigraphic Traps. Thesis - California Institute of Technology,1950.
11. G. F. Tagg: The Earth Resistivity Method of Geophysical Prospecting - Some Theoretical Considerations. The Mining Magazine, 43, (1930), 150.
12. W. E. Bergman, P. G. Carpenter, H. B. Fisher: The Preparation of Drilling Muds for Laboratory Investigations. Oil and Gas Journal, (August, 1943), 196.
13. S. E. Buckley and M. C. Leverett: Mechanism of Fluid Displacements in Sands. A.I.M.E. Transactions 146 (1942), 107 - 116.

14. R. D. Wyckoff and H. G. Botset: The Flow of Gas-Liquid Mixtures through Unconsolidated Sands. Physics 7 (1936), 325.

15. M. C. Leverett: Flow of Oil-Water Mixtures through Unconsolidated Sands. A.I.M.E. Transactions 132 (1939), 149.

16. H. G. Botset: Flow of Gas-Liquid Mixtures through Consolidated Sands. A.I.M.E. Transactions 136 (1940), 91.

17. M. C. Leverett and W. B. Lewis: Steady Flow of Gas-Oil-Water Mixtures through Unconsolidated Sands. A.I.M.E. Transactions 142 (1941), 107.

18. W. Rose: Theoretical Generalizations Leading to the Evaluation of Relative Permeability. Petroleum Technology, May 1949, 111.

19. M. P. Tixier: Electric Log Analysis in the Rocky Mountains. Oil and Gas Journal, June 23, 1949.

20. E. R. Brownscombe, R. L. Slobod and B. H. Caudle: Relative Permeability of Cores, Desaturated by Capillary Pressure Method. A.P.I. Division of Production, Los Angeles Meeting, May 13 - 14, 1949.

21. C. Beal: The Viscosity of Air, Water, Natural Gas, Crude Oil and its Associated Gases at Oil Field Temperatures and Pressures. A.I.M.E. Transactions, 165, (1946), 94 - 115.
See also M. Muskat: Physical Principles of Oil Production. p. 97, fig. 248. McGraw-Hill, 1949.

22. W. Rose and W. A. Bruce: Evaluation of Capillary Character in Petroleum Reservoir Rock. Journal of Petroleum Technology, May 1949, 127.

23. M. Williams: Radial Filtration of Drilling Muds. A.I.M.E. Transactions 136 (1940), 57.

24. M. C. Leverett, Op. cit. (18) fig. 7, curves a anc c, pg. 159.

25. M. Williams, Op. cit., fig. 8.

26. F. Morgan, M. Muskat and R. C. Russell: Some Experiments on the Mobility of Interstitial Waters. A.I.M.E. Transactions 170 (1947), 51.

27. H. W. Patnode and M. R. J. Wyllie: The Presence of Conductive Solids as a Factor in Electric Log Interpretation. Journal of Petroleum Technology, February, 1950, pg. 47.

28. H. W. Patnode: Relationship Between Mud Resistivity and Mud Filtrate Resistivity. Journal of Petroleum Technology, January, 1949.

29. G. E. Archie: Electrical Resistivity Log as an Aid in Determining some Reservoir Characteristics. A.I.M.E. Transaction 164 (1945), 322.

30. H. Guyod: Electrical Logging Developments in the U.S.S.R. World Oil, August 1948, pg. 120.

31. C. R. Bailey, H. L. Bilharty, H. F. Dunlap and E. Shuler: The Relation between Electrical Resistivity and Brine Saturation in Reservoir Rocks. Petroleum Technology (October, 1949), 259.

32. L. de Witte: Experimental Studies on the Characteristics of Electrochemical Potentials Encountered in Drill Holes. Thesis - California Institute of Technology, Pasadena, 1950.

APPENDIX

A) Derivation of the Expression for the Inverse Distance from the Origin in Terms of Modified Bessel functions.

By substitution we can prove that

$$R = \int_0^\infty e^{-v \cosh \varphi} \, d\varphi$$

is a solution of the modified Bessel equation

$$\frac{d^2 R}{d v^2} + \frac{1}{v} \frac{d R}{d v} - \left(1 + \frac{n^2}{v^2}\right) R = 0$$

Substitution gives (for $n = 0$):

$$\int_0^\infty \cosh^2 \varphi \, e^{-v \cosh \varphi} \, d\varphi - 1/v \int_0^\infty \cosh \varphi \, e^{-v \cosh \varphi} \, d\varphi$$
$$- \int_0^\infty e^{-v \cosh \varphi} \, d\varphi = 0 \qquad \text{(A-1)}$$

Using $\cosh^2 \varphi - \sinh^2 \varphi = 1$ or $\cosh^2 \varphi - 1 = \sinh^2 \varphi$ and combining the first and third terms gives:

$$\int_0^\infty \left[\sinh \varphi \, e^{-v \cosh \varphi} \, d \cosh \varphi \right] = \text{(by partial integration)}$$
$$= \left| - \frac{\sinh \varphi}{v} e^{-v \cosh \varphi} \right|_0^\infty + \frac{1}{v} \int_0^\infty \cosh \varphi \, e^{-v \cosh \varphi} \, d\varphi$$

of which the first part equals zero and the second part equals the second term of (A-1) except for the negative sign. This makes the left hand member of (A-1) equal zero and proves that

$\int_0^\infty e^{-v \cosh \varphi} \, d\varphi$ is a solution of the modified Bessel equation of zero order.

However, any such solution must be of the form $R = A\, I_0\,(v) + B\, K_0\,(v)$ and since the integral is zero when $v = \infty$ it cannot contain $I_0(v)$ and it must be of the form $B\, K_0\,(v)$, so that we have:

$$B\, K_0\,(v) = \int_0^\infty e^{-v \cosh \varphi}\, d\varphi$$

Let $v = k\,r$, multiply both sides by $\frac{2}{\pi} \cos k\,z$ and integrate from $k = 0$ to $k = \infty$.

$$\frac{2}{\pi} B \int_0^\infty \cos k\,z\, K_0\,(kr)\, d\,k = \frac{2}{\pi} \int_0^\infty \cos kz \left(\int_0^\infty e^{-kr \cosh \varphi} d\varphi \right) d\,k$$

We integrate the right hand side first with respect to k using:

$$\int_0^\infty e^{ax} \cos px\, dx = \left| \frac{e^{ax}\,(a \cos px - p \sin px)}{a^2 + p^2} \right|_0^\infty = \frac{-a}{a^2 + p^2} \;;$$

with $a = -r \cosh \varphi$ and $p = z$

This gives: $\frac{2}{\pi} \int_0^\infty \frac{r \cosh \varphi}{z^2 + r^2 \cosh^2 \varphi}\, d\varphi$ and as $\frac{d \cosh^2 \varphi}{d\varphi} = 2 \cosh \varphi \sinh \varphi$

we may write:

$$\frac{2}{\pi} \int_0^\infty \frac{r \cosh \varphi\, d\varphi}{z^2 + r^2 \cosh^2 \varphi} = \frac{1}{\pi r} \int_0^\infty \frac{d\,(\cosh^2 \varphi\,)}{(\cosh^2 \varphi - 1)^{\frac{1}{2}}\,(\,z^2/r^2 + \cosh^2 \varphi\,)}$$

$$= \frac{1}{\pi r} \int_{(1+z^2/r^2)}^\infty \frac{d\,(\cosh^2 \varphi + z^2/r^2)}{\left[\cosh^2 \varphi + z^2/r^2 - (1 + z^2/r^2)\right]^{\frac{1}{2}}\,(z^2/r^2 + \cosh^2 \varphi)}$$

Using

$$\int_p^\infty \frac{dx}{x\,(c + bx)^{\frac{1}{2}}} = \left[\frac{2}{(-c)^{\frac{1}{2}}} \tan^{-1} \left(\frac{c + bx}{-c}\right)^{\frac{1}{2}} \right]_p^\infty =$$

$$= \frac{2}{(-c)^{\frac{1}{2}}} \left\{ \frac{\pi}{2} - \tan^{-1} \left(\frac{c + bp}{-c}\right)^{\frac{1}{2}} \right\}$$

with $b = 1$ and $a = -\,(1 + z^2/r^2)$, the above expression becomes:

$$\frac{2}{(1 + z^2/r^2)^{\frac{1}{2}}} \times \frac{1}{\pi r} \left\{ \frac{\pi}{2} - \tan^{-1} \left(\frac{- (1 + z^2/r^2) + (1 + z^2/r^2)}{1 + z^2/r^2} \right)^{\frac{1}{2}} \right\} =$$

$$= \frac{2}{\pi r} \times \frac{\pi}{2} \times \frac{1}{(1 + z^2/r^2)^{\frac{1}{2}}} = \frac{1}{(r^2 + z^2)^{\frac{1}{2}}} = \frac{1}{\bar{r}}$$

So we have:

$$\frac{1}{\bar{r}} = \frac{2}{\pi} B \int_0^\infty \cos(k\, z) K_0\, (k\, r)\, d\, k$$

where $\bar{r}$ is the inverse distance from the origin.

To evaluate B, we differentiate both sides with respect to z, multiply by r and integrate from $r = 0$ to $r = \infty$. This gives after rearranging:

$$- \frac{2B}{\pi} \int_0^\infty \frac{\sin kz}{k} \int_0^\infty k\, r\, K_0\, (k\, r)\, d\, (k\, r)\, d\, k = - \int_0^\infty \frac{z\, r\, d\, r}{(z^2 + r^2)^{3/2}}$$

and as $\int_0^v v\, K_0\, (v)\, d\, v = - v\, K_1\, (v)$ and $K_0' = - K$

this becomes:

$$\frac{2B}{\pi} \int_0^\infty \frac{\sin k\, z}{k} \Big| k\, r\, K_0'\, (k\, r) \Big|_0^\infty d\, k = \left| \frac{z}{(z^2 + r^2)^{\frac{1}{2}}} \right|_0^\infty$$

The limits for $k\, r\, K_0'\, (k\, r)$ are evaluated as follows:

From $K_0\, (v) = A \int_0^\infty e^{-v \cosh \varphi} d\, \varphi$ we have

$$K_0'\, (v) = \frac{d\, K_0\, (v)}{d\, v} = - A \int_0^\infty \cosh \varphi\;\; e^{-v \cosh \varphi} d\, \varphi$$

This is zero for $v = \infty$ because v appears in the integrand in the form $v\, e^{-av}$ with $a > 1$. For the other limit we use an expression derived from the definitions of K, I, Y and J:

$$K_0(v) = - 1/\beta\; Y_0\, (j\, v) + j\; \pi/2\; J_0\, (j\, v)$$

or

$$K_0(v) = - I_0\, (v) \ln (\alpha v) + v^2/2^2 + \frac{v^4}{2^4\, (2!)^2} (1 + \tfrac{1}{2}) +$$

$$+ \frac{v^6}{2^6\, (3!)^2} (1 + 1/2 + 1/3) + \cdots$$

Upon differentiating we find that the only term in $v\,K_0'\,(v)$ that does not contain the factor v is $I_0\,(v)$ and as $I_0\,(v) = 1$ for $v = 0$, also $v\,K_0'\,(v) = 1$ for $v = 0$ as all other terms vanish. We have therefore: $v\,K_0'\,(v) = 0$ for $v = \infty$ and $v\,K_0'\,(v) = 1$ for $v = 0$.

Hence $\Big|\, k\,r\,K_0'\,k\,r \,\Big|_0^\infty = -1$ and our equation becomes:

$$\frac{2\,B}{2\,\pi}\int_0^\infty \frac{\sin k\,z}{k}\,d\,k = 1 \quad \text{or} \quad \frac{2\,B}{\pi}\cdot\frac{\pi}{2} = 1 \quad \text{which gives } B = 1\,.$$

This means that the final formula for the inverse distance from the origin is:

$$\frac{1}{r} = \frac{2}{\pi}\int_0^\infty \cos\,(k\,z)\;K_0\,(k\,r)\;d\,k$$

B) Specifications of the Input Transformer and Computation of its Primary Inductance.

Specification No. 4088H

Primary and secondary balanced and each consisting of two turns in series having 3000 windings. (This means 6000 windings each for primary and secondary).

Core: #44 Alleghany Ludlum mu metal (initial permeability 15,000).

Lamination No. ei-21; $\frac{1}{2}$" lamination stack.

Cross section $\frac{1}{2}$" x $\frac{1}{2}$" Stacking factor .90 .

Shielding: 4 copper and 4 mu metal shields. Steel outer case; electrostatic shield between primary and secondary.

The impedance of the primary with open secondary is computed as follows:

The induced voltage due to a sinusoidal varying flux, $\varphi = \varphi_0 \sin 2\pi f t$, is:

$$e = 10^{-8} \frac{N\,d\varphi}{d\,t} = 2\pi f N \varphi_0 10^{-8} \cos 2\pi f t.$$

Here N is the number of windings and f is the frequency. The rms value of the voltage is: $E = \frac{2\pi}{2} f N \varphi_0 10^{-8} = 4.44 f N \varphi_0 10^{-8}$ Volts. In the primary coil, the impressed and induced voltage are equal if we neglect the resistance and core losses, and the flux can be found from the impressed voltage:

$$\varphi_0 = \frac{10^8 E}{4.44 f N} \qquad \text{where } f = 1000 \text{ cycles.}$$

With E between 0.1 and 0.01 volts and N = 6000 we have

$$\varphi_0 = \frac{10 E}{4.44 \times 6000 \times 1000} = 0.038 \text{ to } 0.38 \text{ maxwells.}$$

The corresponding flux density is found from $B = \varphi/A$ gauss, where A equals the cross sectional area of the core in cm^2 times the stacking factor: $A = .90 \times 1/4 \times (2.54)^2 = 1.45$

This gives: $B = .0262$ to $.262$ gauss.

From the normal magnetization chart for mu metal (from the Allegheny Ludlum catalogue) we find that for these flux densities, the permeability μ equals 15,000 cgs units.

By definition $L = 10^{-8} N \frac{d\varphi}{dI}$ where I is the current.

We had $\varphi = BA = \mu HA$ where H is the magnetising force which equals $\frac{F}{\ell}$ oersteds, with ℓ denoting the equivalent flux path. F, the magnetomotive force is given in cgs units by $F = \frac{4\pi N I}{10}$ gilberts.

This gives us $= \frac{4\pi N I}{10} \frac{\mu A}{\ell}$

Substituting this in the above expression for L we have:

$$L = \frac{0.4 \pi N^2 \mu A}{\ell \times 10^8}$$

For the ei-21 lamination the equivalent flux path is 8.26 cm.

$$L = \frac{1.26 \times (6000)^2 \times 15.00 \times 1.45}{8.26 \times 10^8} = 1188 \text{ Henrys}$$

The value found experimentally in the transformer engineers' laboratory was $L_p = 1170$ H.